Ⅳ．研究成果の刊行物・別刷

The FASEB Journal article fj.13-245522. Published online January 3, 2014.

Noninvasive and quantitative live imaging reveals a potential stress-responsive enhancer in the failing heart

Ken Matsuoka,[*,†] Yoshihiro Asano,[*,†,1] Shuichiro Higo,[*,†] Osamu Tsukamoto,[†] Yi Yan,[†] Satoru Yamazaki,[§] Takashi Matsuzaki,[*] Hidetaka Kioka,[*,†] Hisakazu Kato,[†] Yoshihiro Uno,[‡] Masanori Asakura, Hiroshi Asanuma,[¶] Tetsuo Minamino,[*] Hiroyuki Aburatani,[#] Masafumi Kitakaze, Issei Komuro,[*] and Seiji Takashima[*,†]

[*]Department of Cardiovascular Medicine and [†]Department of Medical Biochemistry and [‡]Laboratory of Reproductive Engineering, Institute of Experimental Animal Sciences, Osaka University Graduate School of Medicine, Suita, Japan; [§]Department of Cell Biology and Department of Clinical Research and Development, National Cerebral and Cardiovascular Center Research Institute, Suita, Japan; [¶]Department of Cardiovascular Science and Technology, Kyoto Prefectural University School of Medicine, Kyoto, Japan; and [#]Genome Science Division, Research Center for Advanced Science and Technology, University of Tokyo, Tokyo, Japan

ABSTRACT **Recent advances in genome analysis have enabled the identification of numerous distal enhancers that regulate gene expression in various conditions. However, the enhancers involved in pathological conditions are largely unknown because of the lack of *in vivo* quantitative assessment of enhancer activity in live animals. Here, we established a noninvasive and quantitative live imaging system for monitoring transcriptional activity and identified a novel stress-responsive enhancer of *Nppa* and *Nppb*, the most common markers of heart failure. The enhancer is a 650-bp fragment within 50 kb of the *Nppa* and *Nppb* loci. A chromosome conformation capture (3C) assay revealed that this distal enhancer directly interacts with the 5′-flanking regions of *Nppa* and *Nppb*. To monitor the enhancer activity in a live heart, we established an imaging system using the firefly luciferase reporter. Using this imaging system, we observed that the novel enhancer activated the reporter gene in pressure overload-induced failing hearts (failing hearts: 5.7±1.3-fold; sham-surgery hearts: 1.0±0.2-fold; $P<0.001$, repeated-measures ANOVA). This method will be particularly useful for identifying enhancers that function only during pathological conditions.—Matsuoka, K., Asano, Y., Higo, S., Tsukamoto, O., Yan, Y., Yamazaki, S., Matsuzaki, T., Kioka, H., Kato, H., Uno, Y., Asakura, M., Asanuma, H., Minamino, T., Aburatani, H., Kitakaze, M., Komuro, I., and Takashima, S. Noninvasive and quantitative live imaging reveals a potential stress-responsive enhancer in the failing heart. *FASEB J.* 28, 000–000 (2014). www.fasebj.org**

Key Words: natriuretic peptide · transcriptional regulation · in vivo *assessment*

Gene expression is regulated through the integrated action of many *cis*-regulatory elements, including core promoters, proximal promoters, distant enhancers, and insulators (1). Several methods have been used to explore the function of *cis*-regulatory elements during a variety of developmental stages (2, 3). However, the identification of gene regulatory elements with pathophysiological roles has been technically difficult because there are few appropriate models for monitoring transcriptional activity in live animals under pathological conditions.

Here, we focused on the regulatory elements that are responsive to heart failure. The natriuretic peptides, atrial natriuretic peptide (ANP) and brain natriuretic peptide (BNP), encoded by the neighboring genes *Nppa* and *Nppb* are activated in the embryonic heart, down-regulated after birth, and then reactivated during heart failure. Both peptides are well-known biomarkers that are strongly induced during heart failure and represent its severity. Cardiologists frequently use these peptides as natriuretic and vasorelaxant agents to treat various clinical conditions (4–8). Many studies have tried to elucidate the mechanisms of their transcriptional regulation because factors that regulate these

Abbreviations: 3C, chromosome conformation capture; ANP, atrial natriuretic peptide; BNP, brain natriuretic peptide; ChIP-seq, chromatin immunoprecipitation sequencing; CMV, cytomegalovirus; CR, conserved region; CTCF, CCCTC-binding factor; H3K4me1, histone H3 monomethylated at lysine 4; H3K4me3, histone H3 trimethylated at lysine 4; PE, phenylephrine; TAC, transverse aortic constriction

[1] Correspondence: Osaka University Graduate School of Medicine, 2-2 Yamadaoka, Suita, Osaka 565–0871, Japan. E-mail: asano@cardiology.med.osaka-u.ac.jp

doi: 10.1096/fj.13-245522

This article includes supplemental data. Please visit *http://www.fasebj.org* to obtain this information.

natriuretic peptides are potential therapeutic targets for heart disease (9–14).

Mice transgenic for various loci, including the 5′-flanking regions of the natriuretic peptide genes, have been used to identify the regulatory elements required for transcriptional activation either during heart development or in the diseased heart. These studies reported that the 5′-flanking regions of the natriuretic peptide genes regulated their expression during heart development (9, 10, 13); however, the 5′-flanking regions were not responsible for their specific reactivation in the diseased heart (11, 12). A recent study identified the distal enhancer elements regulating the natriuretic peptide genes in the developing heart by examining cardiac-specific transcription factor binding sites; however, these enhancer elements did not respond to heart failure (14). Therefore, the stress-responsive regulatory elements that function during heart failure have not yet been identified and are potentially located outside the 5′-flanking regions.

In this study, we aimed to identify the novel stress-responsive enhancer elements of the *Nppa* and *Nppb* genes in the failing heart. Furthermore, we established a noninvasive and quantitative live imaging assay to monitor the transcriptional activity of candidate enhancers in the failing heart. *In vivo* live imaging of the firefly luciferase reporter in a single mouse enabled us to analyze the sequential changes in enhancer activity during the progression of heart failure. Combined with a fine mapping technique using epigenetic markers, we identified a 650-bp stress-responsive enhancer that was strongly activated by cardiac hypertrophy and heart failure.

MATERIALS AND METHODS

Animals

All procedures were performed according to the U.S. National Institutes of Health (NIH) Guide for the Care and Use of Laboratory Animals (NIH publication no. 85-23, revised 1996) and were approved by the Animal Experiments Committee, Osaka University (approval no. 21-78-10).

Reagents and antibodies

Phenylephrine (PE) was purchased from Sigma-Aldrich (St. Louis, MO, USA). The anti-RNA polymerase II and anti-histone H3 trimethylated at lysine 4 (H3K4me3) antibodies used for chromatin immunoprecipitation sequencing (ChIP-seq) were kind gifts from Dr. H. Kimura (Graduate School of Frontier Biosciences, Osaka University).

Primary culture of neonatal rat cardiomyocytes

Ventricular myocytes obtained from 1- or 2-d-old Wistar rats were prepared and cultured overnight in Dulbecco's modified Eagle's medium (Sigma-Aldrich) containing 10% FBS, as described previously (15).

Comparative genomics

Genome-wide multiple alignments of the genomic sequences containing the *Nppa* and *Nppb* genes were performed using the University of California Santa Cruz (UCSC) Genome Browser (16); 8 vertebrate species were compared, including mouse (mm9, July 2007), rat (m4, Nov. 2004), human (hg18, Mar. 2006), orangutan (ponAbe2, July 2007), dog (canFam2, May 2005), horse (equCab1, Jan. 2007), opossum (monDom4, Jan. 2006), and chicken (galGal3, May 2006). We used vertebrate Multiz alignment of DNA sequences (17) to analyze the homology of DNA sequences among mouse and other species. We used the Placental Mammal Basewise Conservation assessed by PhyloP (18) to assess the degree of mammalian conservation. Next, we identified discrete conserved fragments. The transcribed sequences within the conserved set were filtered out using known genes, spliced ESTs, and mRNA annotations obtained from the UCSC genome browser. Finally, we manually curated the data set to remove any additional false positives by visual examination of the UCSC genomic data. We defined the noncoding conserved regions (CRs) that were homologous at least in the human and mouse genomes and at least 1 kb away from the transcription start sites as the enhancer candidates.

ChIP sequencing on mouse heart tissues

Whole hearts were isolated from 8-wk-old C57BL6 mice, perfused rapidly with cold PBS, flash-frozen in liquid nitrogen, homogenized using a sterile tissue grinder, and cross-linked with 0.3% paraformaldehyde. Subsequently, chromatin isolation, sonication, and immunoprecipitation using an anti-RNA polymerase II antibody and an anti-H3K4me3 antibody were performed. The ChIP DNA and input samples were sheared by sonication, end-repaired, ligated to the sequencing adapters, and amplified. The purified ChIP DNA library samples were sequenced using the Illumina Genome Analyzer II (Illumina, Inc., San Diego, CA, USA). Unfiltered sequence reads were aligned to the mouse reference genome [U.S. National Center for Biotechnology Information (NCBI) build 37, mm9] using Bowtie. RNA polymerase II- and H3K4me3-enriched regions were identified using MACS (19) with the default parameters.

Lentiviral enhancer assay

Eleven CRs were PCR amplified from the mouse BAC clone containing the *Nppa* and *Nppb* loci (clone RP23-128E8; BACPAC Resources Center, Children's Hospital Oakland, Oakland, CA, USA; primers and probes are listed in Supplemental Table S1). The PCR fragments were subcloned into the pCR-Blunt II-TOPO vector (Invitrogen, Carlsbad, CA, USA) and recombined into a lentiviral vector encoding the firefly luciferase reporter (pGreenFire Transcriptional Reporter Lentivector; System Biosciences, Mountain View, CA, USA). The lentiviral particles were produced by transfection of 293T cells with the 3 lentiviral packaging plasmids (*i.e.*, pMDLg/pRRE, pRSV-Rev, and pMD2.VSV.G) using Lipofectamine 2000 (Invitrogen). The supernatant from 293T cells containing the lentiviral particles was collected 48 h after transfection, sterilized using a 0.45-μm cellulose acetate filter, and concentrated by centrifugation (Peg-it Virus Precipitation Solution, System Biosciences).

Rat neonatal cardiomyocytes isolated as described above were plated in 96-well plates. The next day, the medium was replaced with a serum-free medium containing the lentiviral vector, and the cells were incubated for 12 h. Subsequently, the cardiomyocytes were exposed to 100 μM PE for 48 h prior to the luciferase assay.

RNA extraction and quantitative RT-PCR

The total RNA was prepared from rat cardiomyocytes, rat cardiac fibroblasts, murine hearts, and murine brains using the RNA-Bee RNA isolation reagent (Tel-Test, Friendswood, TX, USA) and then converted to cDNA using the high-capacity cDNA reverse transcription kit (Applied Biosystems, Foster City, CA, USA), according to the manufacturer's instructions. The quantitative RT-PCR was performed using the TaqMan technology and the StepOnePlus real-time PCR System (Applied Biosystems). All samples were processed in duplicate. The level of each transcript was quantified according to the threshold cycle (C_t) method using GAPDH as an internal control. Inventoried TaqMan gene expression assays were used: *Nppa*, Rn0056661, Mm01255748; *Nppb*, Rn00580641, Mm01255770; *Gapdh*, rodent GAPDH control reagent.

3C analysis

The whole hearts of the mice were isolated, perfused rapidly with cold PBS, flash-frozen in liquid nitrogen, homogenized using a sterile tissue grinder, and fixed with 1% paraformaldehyde. The cross-linked tissues utilized for 3C experiments were subjected to digestion with *Bam*HI following standard protocols (20, 21). The mouse BAC DNA containing *Nppa* and *Nppb* (clone RP23-128E8) was used as a control. The TaqMan real-time PCR was performed using probes near the restriction sites; the primers and probes are listed in Supplemental Table S2.

Transgenic mouse enhancer assay

The candidate enhancer regions were cloned into a vector encoding the minimal CMV promoter driving the luciferase gene as described above. Transgenic mouse embryos were generated by pronuclear injection into the zygotes of BDF1 mice using standard methods. Because black fur attenuates light transmission, albino mice were generated by crossing the transgenic founders to ICR albino mice.

In vivo bioluminescence imaging

Prior to *in vivo* imaging, the mice were anesthetized using isoflurane, and the black mice were shaved from the neck to the lower torso to allow the optimal visualization of fluorescence without interference from the black fur. A d-luciferin solution was injected intraperitoneally (150 mg/kg i.p.) or intravenously (75 mg/kg i.v.). The mice were imaged using an *in vivo* live imaging system (IVIS Lumina II; Caliper Life Sciences, Waltham, MA, USA). For quantification, the bioluminescence light intensity was measured at the region of interest and expressed in relative light units (RLU/min) using Living Image 4.0 (Caliper Life Sciences). To calculate the enhancer activity in the heart, we defined the ratio of heart to brain luciferase intensities as the cardiac-specific enhancer activity.

Transverse aortic constriction (TAC)

Transgenic mice aged 8 wk and weighing 20–25 g were subjected to pressure overload, as described previously (22). Briefly, the chest was entered *via* the second intercostal space at the upper left sternal border. After the arch of the aorta was isolated, a TAC was created using a 7-0 suture tied twice around a 27-gauge needle and the aortic arch, between the innominate and left common carotid arteries. After the suture was tied, the needle was gently removed, yielding 60–80% constriction of the aorta.

PE-induced hypertrophy

Transgenic mice aged 8 wk and weighing 20–25 g were treated with PE (75 mg/kg/d) using an osmotic minipump (Alzet, Cupertino, CA, USA) to induce cardiac hypertrophy, as previously reported (23, 24).

Statistical analysis

Data are expressed as means ± se. The 2-tailed Student's *t* test and repeated ANOVA were used to analyze differences between the groups. Values of $P < 0.05$ were considered to represent a significant difference.

RESULTS

Identification of candidate enhancers near the *Nppa-Nppb* locus using comparative genomics and ChIP-seq

To identify potential enhancers, we performed a comparative analysis of the genomic sequences of mouse and divergent species and identified CRs that may function as common regulatory sequences (25–27). We defined CRs that were homologous at least in the human and mouse genomes and at least 1 kb away from the transcription start sites of *Nppa* and *Nppb* as the candidate enhancers. First, we analyzed the 50-kb *Nppa-Nppb* locus bounded by the binding sites of 2 CCCTC-binding factors (CTCFs), which can function as insulators (28, 29). Using a genome database (30), we identified 11 CRs, including the *Nppa* and *Nppb* introns in the 50-kb region **(Fig. 1)**.

Next, we performed a ChIP-seq analysis on RNA polymerase II and H3K4me3 in the adult mouse heart. We analyzed the epigenetic modifications near the *Nppa* and *Nppb* genes combined with the ChIP-seq analysis using a public database of the adult mouse heart (30). We hypothesized that the normal heart would have activated epigenetic marks because *Nppa* and *Nppb* are expressed, albeit at low levels, in normal conditions. Recent genome-wide studies have determined that enhancers can be defined as DNA sequences bound by the RNA polymerase II and transcriptional coactivator protein p300, and where histone H3 monomethylated at lysine 4 (H3K4me1) accumulates instead of H3K4me3 (31–34). Among the 11 CRs identified, only CR9 coincided with the binding sites of RNA polymerase II and p300, and overlapped with the gene areas modified by H3K4me1, and filled all criteria for the enhancer (Fig. 1). In addition, H3K4me1 modifications in CR9 were only observed in the heart but not in the other organs (Fig. 1 and Supplemental Fig. S1). Therefore, we analyzed the 11 CRs, including CR9, as the most likely distal candidate enhancers for the stress-responsive regulatory regions of the natriuretic peptide genes.

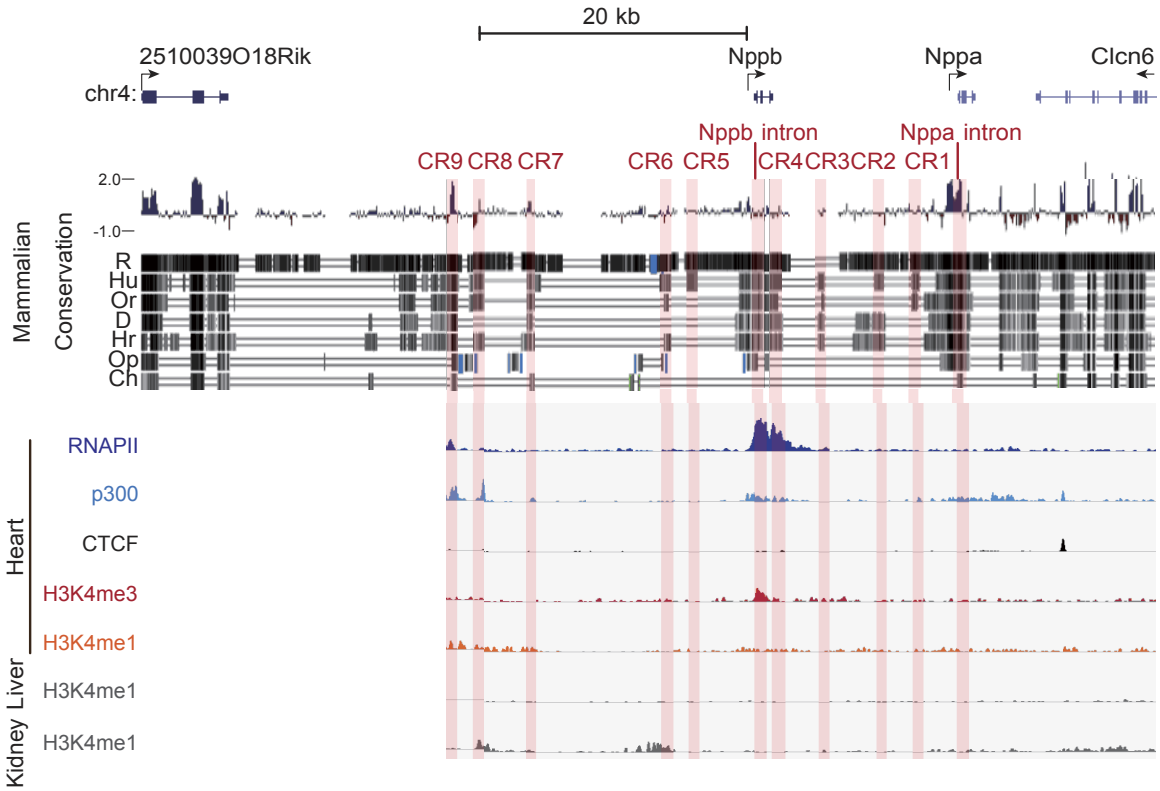

Figure 1. Mammalian evolutionarily conserved regions and ChIP-seq data surrounding the murine *Nppa* and *Nppb* loci. We used an open database on the University of California Santa Cruz (UCSC) Genome Browser to assess the degree of DNA sequence conservation around *Nppa* and *Nppb* gene loci. Blue and red vertical lines, the Placental Mammal Basewise Conservation assessed by PhyloP; black vertical lines, the vertebrate Multiz alignment of DNA sequences among mice and 7 other species (rats, humans, orangutans, dogs, horses, opossums, and chickens). We defined noncoding conserved regions (CRs) that were homologous at least in the human and mouse genomes and at least 1 kb away from the transcription start sites of *Nppa* and *Nppb* as the candidate enhancers. CRs are highlighted as light red vertical bars (CR1-9, *Nppa* intron, and *Nppb* intron). ChIP-seq data for H3K4me1, p300, and CTCF were obtained from an open database of the adult mouse heart. Some CRs coincided with the peaks for H3K4me1, RNA polymerase II, and the transcriptional coactivator protein p300. R, rat; Hu, human; Or, orangutan; D, dog; Hr, horse; Op, opossum; Ch, chicken.

Identification of a distal enhancer element responsive to an a_1-adrenergic receptor agonist

We screened the candidate enhancers for potential stress-responsive regulatory regions. We analyzed the enhancer activity of these 11 CRs after treatment with PE, an a_1-adrenergic receptor agonist, which mimics cardiac overload and induces *Nppa* and *Nppb* expression in cardiomyocytes (35). We confirmed that PE induced the expression of endogenous *Nppa* and *Nppb* specifically in cardiomyocytes but not in cardiac fibroblasts (**Fig. 2*A***). Then, we introduced the 11 CRs with a minimum human cytomegalovirus (CMV) promoter and the luciferase gene into rat cardiomyocytes using a lentiviral vector system.

Among the 11 CRs tested, only CR9, which is located 22 kb upstream from the *Nppb* transcription start site and shows high mammalian conservation score in the Placental Mammal Basewise Conservation by PhyloP (Fig. 2*B*), reproducibly increased the PE-induced luciferase activity by ~5-fold compared to the minimal CMV promoter alone (Fig. 2*C*). However, CR9 did not respond to PE in cardiac fibroblasts (Fig. 2*C*). These results suggest that CR9 is the regulatory element that is responsive to PE specifically in cardiomyocytes.

Long-range physical interaction between the distal enhancer element and the proximal promoters of the *Nppa* and *Nppb* genes

Confirming the looping interactions between distal elements and promoters is one way to demonstrate the transcriptional regulatory activity of distal elements. We performed a 3C assay (20) to comprehensively investigate whether the genomic region containing CR9 moved closer to the *Nppa* or *Nppb* promoter in an adult murine heart treated with a continuous infusion of PE *in vivo*.

The ligation frequencies were quantified by TaqMan real-time PCR using specific primers and probes and were compared to the ligation frequency of noncross-linked *Bam*HI-digested BAC DNA containing the *Nppa-Nppb* locus. We observed that CR9 interacts with both the *Nppa* and *Nppb* promoter regions at a higher frequency relative to other gene areas (Fig. 2*D*); furthermore, PE treatment strengthened these interac-

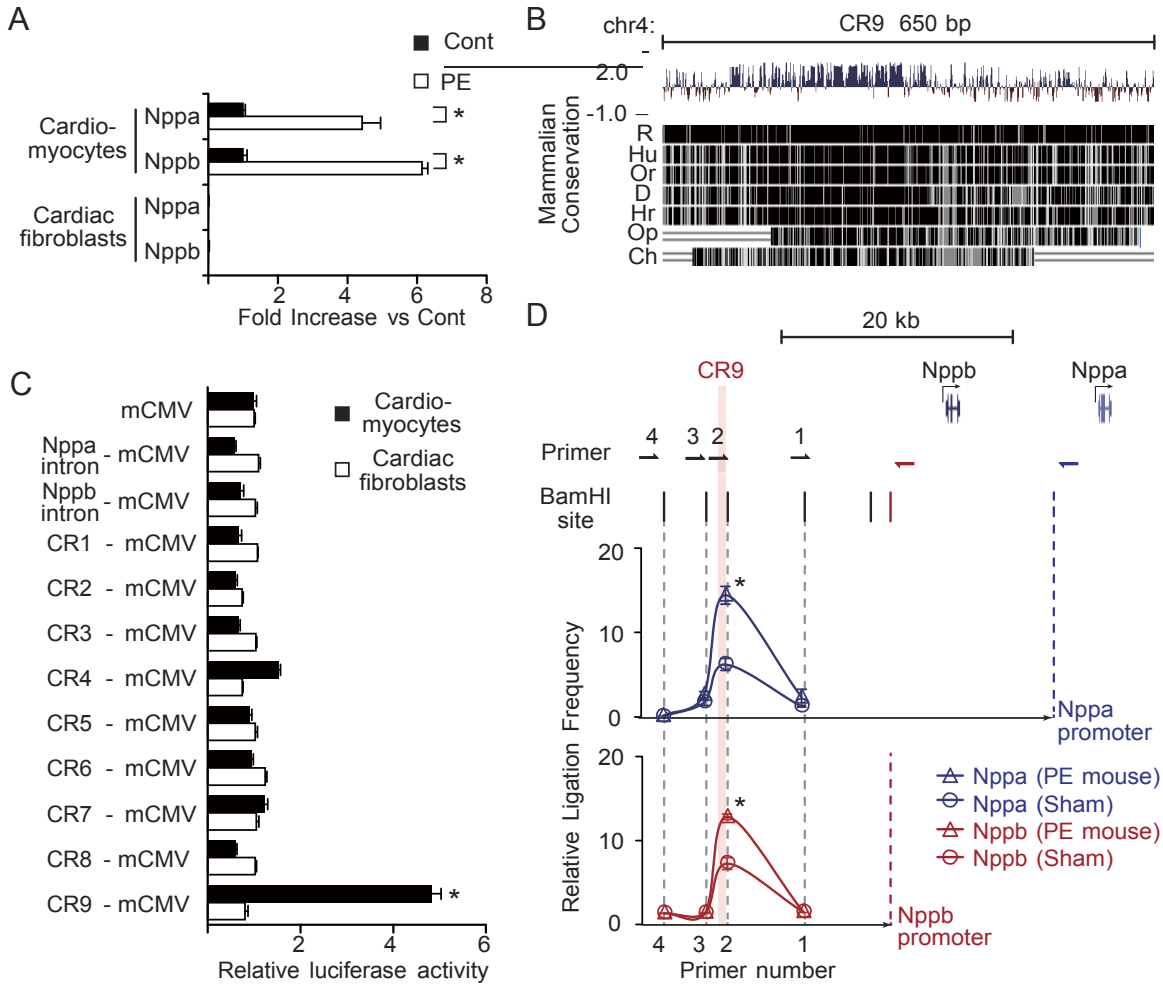

Figure 2. Identification of a distal enhancer element that is responsive to an a_1-adrenergic receptor agonist. *A*) Relative transcript levels of *Nppa* and *Nppb* in rat neonatal cardiomyocytes and cardiac fibroblasts 48 h after treatment with PE (100 μM). Values are means ± se (n=3 cultures). *P < 0.01 *vs.* control; *t* test. *B*) CR9 is a highly conserved genomic region in vertebrates. *C*) Relative luciferase reporter activities of CRs in rat neonatal cardiomyocytes and cardiac fibroblasts 48 h after treatment with PE (100 μM). PE-induced luciferase activity driven by the mCMV promoter was defined as 1. Values are means ± se (n=5 cultures). *P < 0.001 *vs.* mCMV alone; *t* test. *D*) *In vivo* 3C analysis of the murine *Nppa* and *Nppb* loci, showing relative ligation frequencies of each primer to the *Nppa* promoter (blue triangle, mouse with PE treatment; blue circle, mouse without PE) and the *Nppb* promoter (red triangle, mouse with PE treatment; red circle, mouse without PE). Vertical bars and arrows show the positions of *Bam*HI sites and primers. Data were normalized to the amplification value of a *Bam*HI-digested and religated BAC clone, which included the *Nppa* and *Nppb* loci (means ± se; n=2 hearts). R, rat; Hu, human; Or, orangutan; D, dog; Hr, horse; Op, opossum; Ch, chicken. *P < 0.05 *vs.* control; *t* test.

tions (Fig. 2*D*). These results suggest that there is a close proximity between the distal genomic region containing CR9 and the proximal promoters of the *Nppa* and *Nppb* genes in the PE-induced hypertrophic heart.

Establishment of an *in vivo* live imaging system for gene expression in a murine model of heart disease

We confirmed the activity of the newly identified enhancer CR9 in the heart *in vivo*. The conventional histological evaluation of LacZ reporter expression in the heart only provides data at a single time point; therefore, this method cannot be employed for kinetic assessments or time course analyses of reporter expression in a live heart.

To overcome this difficulty, we established a noninvasive and quantitative live imaging system that allowed real-time monitoring of the firefly luciferase reporter. We generated 3 transgenic mouse lines (Tg-line1, Tg-line2, and Tg-line3) in which the CR9 enhancer element and a minimal CMV promoter driving the luciferase reporter gene were introduced into the germline. The live-imaging system detected luciferase expression in the heart, brain, and intestine of the Tg-line1 **(Fig. 3*A*)**, in the heart, salivary glands, and skin of the Tg-line2 (Supplemental Fig. S2*A*), and in the heart of the Tg-line3 (Supplemental Fig. S2*E*).

To identify the organs in which CR9 functioned as a stress-responsive enhancer, we examined the luciferase reporter expression in each organ by quantitative PCR. Continuous infusion of PE increased the blood pressure and resulted in cardiac hypertrophy (24, 36). The

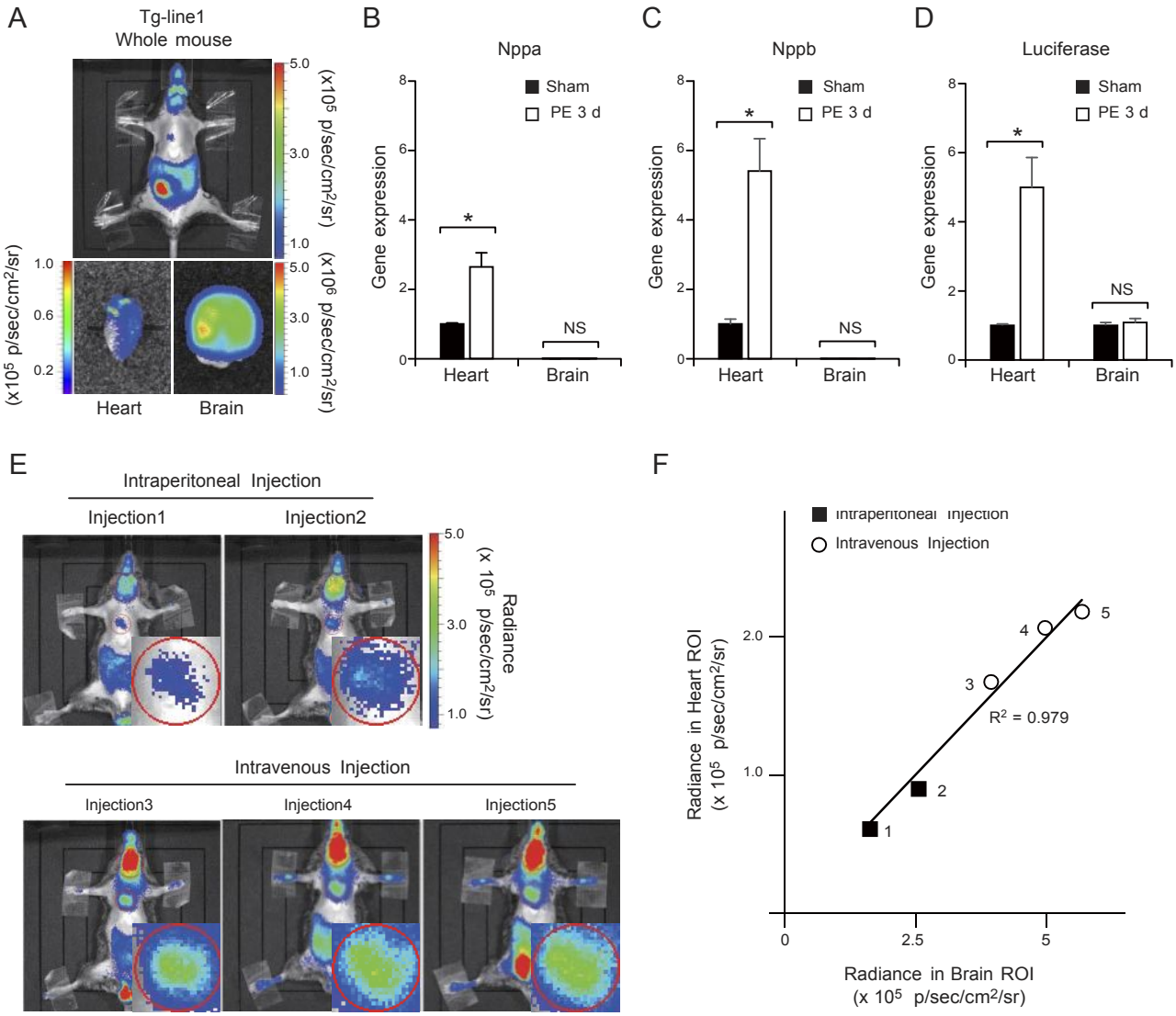

Figure 3. Establishment of an *in vivo* live imaging system for enhancer activity. *A*) Chemiluminescence imaging of CR9 in a mouse of Tg-line1. Top panel: result from whole-animal *in vivo* live imaging. Bottom panels: chemiluminescence images of the heart and brain in the same mouse. *B, C*) Relative transcript levels of *Nppa* and *Nppb* in the ventricular myocardium and brain of CR9 Tg-line1 mice treated with continuous infusion of PE for 3 d. Average transcript level in the ventricular myocardium of preinfused mice was defined as 1 (means ± se; n=5 hearts). *$P < 0.01$ *vs.* sham-infused mice; *t* test. *D*) Relative transcript levels of luciferase reporter in the ventricular myocardium and brain of the CR9 Tg-line1 mice continuously infused with PE for 3 d. Average transcript level in the ventricular myocardium and brain of preinfused mice was defined as 1. (means ± se; n=5 hearts). *$P < 0.01$ *vs.* sham-infused mice; *t* test. *E*) Comparison of the chemiluminescence intensities obtained using different luciferin injection methods in a Tg-line1 mouse; injections 1 and 2, intraperitoneal injections (top panels), injections 3, 4, and 5, intravenous injections (bottom panels). Injections were performed >4 h apart to eliminate the effect of the previous injection. Inset in each panel shows a magnified image of the heart. *F*) Scatterplots of the chemiluminescence intensities in the heart and brain. Plots indicate the independent experiments shown in each panel in *E*. There is a linear relationship between the expression in the heart and the brain, $R^2 = 0.979$.

expression of endogenous *Nppa* and *Nppb* mRNA increased 3 d after the PE infusion began (Fig. 3*B*, *C* and Supplemental Fig. S2*B*, *C*, *F*, *G*). Concomitantly, the quantitative PCR analysis of the CR9 luciferase mRNA expression showed enhanced expression in the ventricular myocardium 3 d after the PE infusion (Fig. 3*D* and Supplemental Fig. S2*D*, *H*). On the other hand, in the brain and the salivary glands where neither *Nppa* nor *Nppb* is highly expressed, the CR9-driven luciferase mRNA expression did not respond to PE (Fig. 3*B–D* and Supplemental Fig. S2*B–D*, *F–H*). Therefore, the patterns of PE-induced luciferase expression suggest that CR9 is almost exclusively active in the heart. Because the integration sites were random in these three lines, the patterns of luciferase expression depend on CR9 or other enhancers near the integrated sites. The expression of luciferase in the brain of Tg-line1 and salivary glands of Tg-line2, both of which express neither *Nppa* nor *Nppb,* might be driven by other enhancers near the integrated sites.

To evaluate the accuracy and reproducibility of this method, we measured the luminescence in the heart of

a mouse from Tg-line1. In this transgenic line, the brain, intestine, and testis expressed the reporter protein due to positional effects of the insertion site and most likely not due to CR9 activity. Because the luciferase mRNA expression in the brain remained unchanged after PE treatment (Fig. 3*D*), we used the reporter activity in the brain as a control. The absolute luminescence values of the heart were affected by the injection method and the amount of luciferase substrate injected (Fig. 3*E*). However, using brain luminescence as a control, we successfully eliminated the signal variations caused by these differences. The ratio of the luminescence in the heart and brain remained constant within each mouse, independent of the injection method (Fig. 3*F*). Therefore, we defined the ratio of heart to brain luciferase intensities as the cardiac-specific enhancer activity.

Distal enhancer element was activated in the murine model of heart failure

To examine whether the CR9 enhancer was also responsible for gene expression in other pathological conditions, we subjected Tg-line1 mice to heart failure induced by TAC and compared them with sham-surgery mice. This model mimics the heart condition of patients with hypertension who suffer a continuous pressure overload on the heart. The pressure overload by TAC caused potent cardiac hypertrophy at 2 wk postsurgery and reduced cardiac contractility at 3 wk postsurgery (**Fig. 4*A*, *B***), as previously reported (22). The endogenous *Nppa* and *Nppb* expression increased severalfold in the ventricular myocardium 3 wk after the TAC surgery (Fig. 4*C*). The heart to brain luciferase intensity ratio also increased severalfold 3 wk following the TAC surgery (Fig. 4*D*, *E* and Supplemental Fig. S3). However, the heart to brain luciferase intensity ratio of sham-surgery mice did not change after the surgery (Fig. 4*D*, *E* and Supplemental Fig. S3; 3 wk after TAC surgery: 5.7±1.3 fold; 3 wk after sham surgery: 1.0±0.2 fold; $P < 0.001$, repeated ANOVA). These results suggest that CR9 increases transcriptional activity during mechanical pressure overload-induced hypertrophy and subsequent heart failure.

DISCUSSION

Here, we focused on the stress-responsive regulatory elements of *Nppa* and *Nppb* in heart failure. By screening the evolutionarily conserved and epigenetically modified regions around the *Nppa* and *Nppb* gene loci, we identified a 650-bp transcriptional enhancer that was responsive to an α_1-adrenergic receptor agonist *in vitro*. Furthermore, *in vivo* 3C analysis revealed that this distal enhancer directly interacted with the 5′-flanking regions of both *Nppa* and *Nppb*. Using *in vivo* live imaging of luciferase reporter gene expression, we observed that this 650-bp enhancer caused cardiac-specific activation of reporter gene expression during the progression of pressure overload-induced heart failure. Notably, this is the first study to provide a time series analysis for monitoring enhancer activity under pathological conditions in an individual live mouse.

Although numerous approaches have been used to explore the stress-responsive regulatory elements driving gene transcription during heart failure (11, 12, 14), these elements have not yet been identified due to the technical difficulty involved. To detect the elements that are responsive to pathological conditions such as heart failure, it is essential to confirm the activity of the responsive element using a beating heart that remains connected to the systemic cardiovascular system. Therefore, it would be beneficial to establish transgenic mouse lines carrying a reporter plasmid to assess the responsive elements driving the expression of specific genes. However, the creation of multiple stable adult mouse lines to identify these elements is time-consuming.

In this study, we utilized two improved methods for reporter analysis and successfully identified a novel potent enhancer.

First, by performing an enhancer analysis using a lentiviral vector, we accurately identified candidate enhancers in cardiomyocytes and subsequently generated transgenic reporter mice. Previous promoter analyses used electroporation or lipofection to transfect cultured cardiomyocytes with plasmids (37, 38), but the transfection efficiency of these methods in primary cardiomyocytes is too low to accurately measure reporter activity during the stress response. In this study, greater than 90% transduction efficiency of cardiomyocytes was achieved using a lentiviral vector, which enabled us to accurately identify a specific enhancer fragment. Using this method, we efficiently minimized the number of reporter plasmids to be subsequently integrated into the mouse genome to screen for potential enhancers.

Second, by sequentially measuring the enhancer activity in a single live mouse, we collected robust data to assess enhancer activity in the heart *in vivo*. LacZ is not a suitable reporter for this purpose because LacZ activity can only be assessed after animal euthanization. Therefore, we overcame this limitation using the luciferase reporter plasmid. Recent advances in high-sensitivity luminescence imaging have made it possible to evaluate enhancer-driven luciferase activity without operating on the mice. Therefore, we sequentially assessed reporter activity and hemodynamic changes in the same mouse throughout the time course of the development of heart failure. These data were highly reproducible and enabled us to identify an enhancer element that was activated by cardiac overload. Because this method can be applied to any organ, the *in vivo* luciferase reporter assay may be used for assessing the *in vivo* enhancer or promoter activities responsible for clinically important diseases. The noninvasive nature of this method also enabled us to simultaneously assess the hemodynamic and metabolic parameters *in vivo* along with reporter activity. Specifically, the Tg-line1

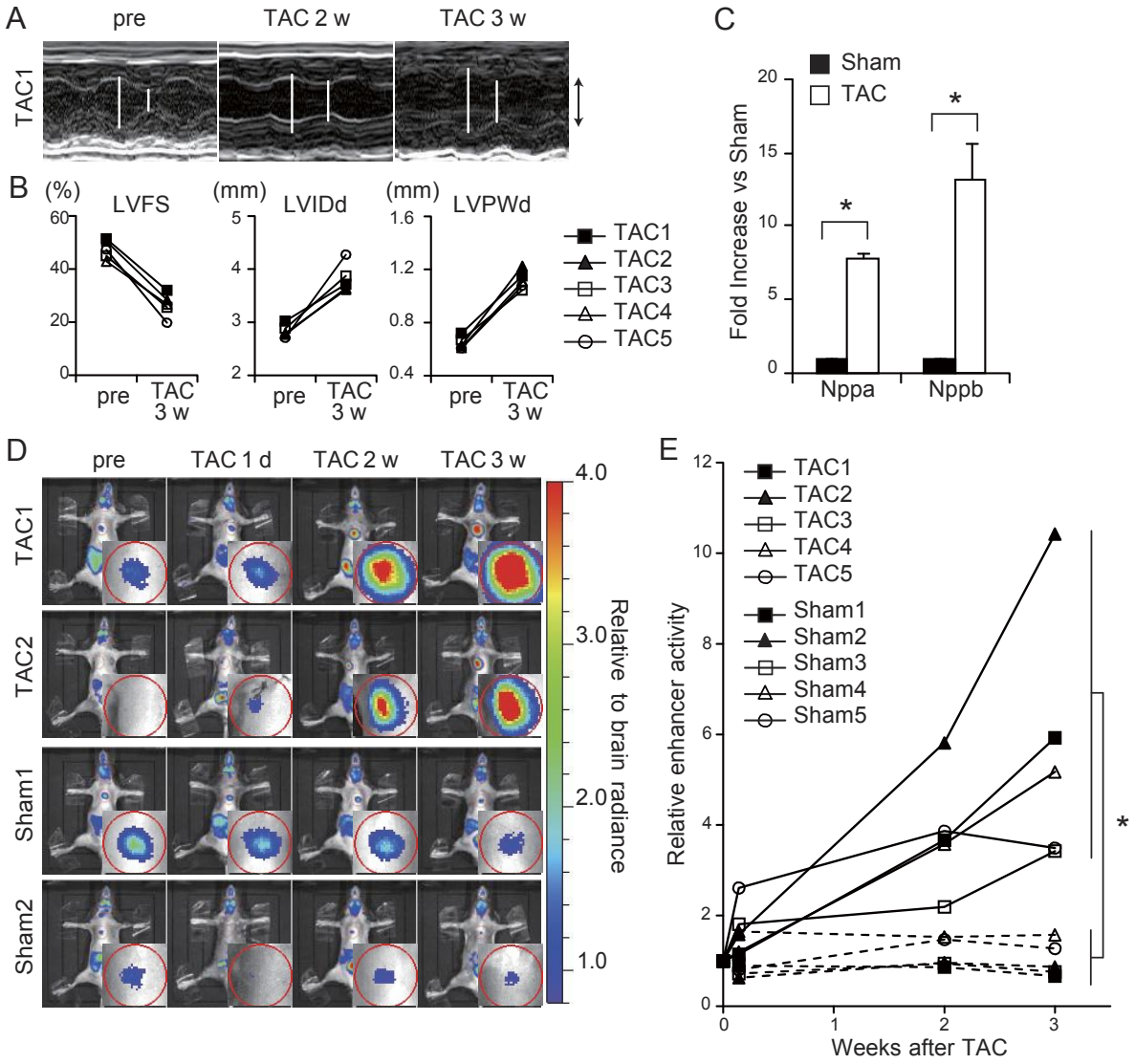

Figure 4. Distal enhancer element is reactivated in the murine model of heart failure. *A*) Representative M-mode echocardiograms in a mouse of Tg-line1 (TAC1) before and after TAC. Open bars indicate maximal left ventricular internal dimension in diastole (LVIDd) and maximal left ventricular internal dimension in systole (LVIDs). Up and down arrows represent 3 mm. *B)* Echocardiographic changes in left ventricular fractional shortening (LVFS), LVIDd, and left ventricular posterior wall thickness in diastole (LVPWd) in 5 mice of Tg-line1 (TAC1-5) before and after TAC. ***C*)** Relative *Nppa* and *Nppb* transcript levels in the ventricular myocardium 3 wk after the TAC procedure (means ± se; n=3 hearts). *P < 0.05 *vs.* sham-surgery mice; *t* test. *D*) Sequential *in vivo* live imaging of 4 representative Tg-line1 mice before and after TAC or sham surgery at each time point. Top 2 and bottom 2 panels represent sequential imaging data of TAC and sham-surgery mice, respectively. Sequential imaging of the 6 other surgically treated mice is shown in Supplemental Fig. S3. Insets in images show magnified images of the heart. Color scale depends on the ratio relative to brain intensity. *E*) Cardiac-specific enhancer activity plots of 10 Tg-line1 mice (TAC1, TAC2, and Sham1, Sham2, shown in *D*) and TAC3–5 and Sham3–5 shown in Supplemental Fig. S3). Heart to brain luciferase intensity ratio represents the cardiac-specific enhancer activity; enhancer activity in presurgery mice was defined as 1. 3 wk after TAC surgery: 5.7 ± 1.3 fold; 3 wk after sham surgery: 1.0 ± 0.2 fold; means ± se; n = 5. *P < 0.001, repeated ANOVA.

mice enabled us to accurately quantify the expression level of the natriuretic peptides. These mice are useful tools for repeatedly assessing the degree of heart failure to screen various cardiovascular drugs.

The integration of activities from multiple enhancers could confer specificity and robustness to transcriptional regulation (1). Warren *et al.* (14) identified the *Nppa* enhancer in the embryonic heart by examining Nkx2-5 binding regions around the *Nppa* locus, but the enhancer did not respond to heart failure. This enhancer does not overlap with CR9 and might regulate *Nppa* expression only during the embryonic stage (14). On the other hand, Horsthuis *et al.* (11) showed that the regulatory region from −27 to +58 kb relative to the transcription start site of *Nppa* was sufficient for *Nppa* gene expression in the failing heart, similar to CR9. However, because this 85-kb regulatory region does not include CR9, *Nppa* may have multiple enhanc-

ers that regulate its expression during heart failure. Furthermore, the length of the 85-kb region poses a challenge for understanding its specific biological role.

This is the first study to provide a time course imaging analysis of enhancer activity using an individual live diseased mouse model. Using this new method, we identified a novel heart enhancer. This method can be widely used for identifying enhancers that regulate transcriptional activity only under pathological conditions. FJ

This research was supported by the Japan Society for the Promotion of Science (JSPS) through the Funding Program for Next Generation World-Leading Researchers (NEXT Program), which was initiated by the Council for Science and Technology Policy (CSTP); grants-in-aid from the Ministry of Health, Labor, and Welfare of Japan; grants-in-aid from the Ministry of Education, Culture, Sports, Science, and Technology of Japan; and grants-in-aid from the Japan Society for the Promotion of Science. This research was also supported by grants from the Japan Heart Foundation, the Japan Cardiovascular Research Foundation, the Japan Medical Association, the Japan Intractable Diseases Research Foundation, the Uehara Memorial Foundation, the Takeda Science Foundation, the Ichiro Kanehara Foundation, the Inoue Foundation for Science, the Mochida Memorial Foundation, a Heart Foundation/Novartis Grant for Research Award on Molecular and Cellular Cardiology, the Japan Foundation of Applied Enzymology, the Naito Foundation, the Banyu Foundation, and Showa Houkoukai. The authors thank Hiroshi Kimura for antibodies, Seitaro Nomura for the ChIP-seq analysis, Saori Ikezawa and Eri Takata for technical assistance, and Yuko Okada and Hiromi Fujii for secretarial support.

REFERENCES

1. Spitz, F., and Furlong, E. E. (2012) Transcription factors: from enhancer binding to developmental control. *Nat. Rev. Genet.* **13,** 613–626
2. Chien, K. R., Domian, I. J., and Parker, K. K. (2008) Cardiogenesis and the complex biology of regenerative cardiovascular medicine. *Science* **322,** 1494–1497
3. Olson, E. N. (2006) Gene regulatory networks in the evolution and development of the heart. *Science* **313,** 1922–1927
4. Burley, D. S., and Baxter, G. F. (2007) B-type natriuretic peptide at early reperfusion limits infarct size in the rat isolated heart. *Basic Res. Cardiol.* **102,** 529–541
5. Holtwick, R., van Eickels, M., Skryabin, B. V., Baba, H. A., Bubikat, A., Begrow, F., Schneider, M. D., Garbers, D. L., and Kuhn, M. (2003) Pressure-independent cardiac hypertrophy in mice with cardiomyocyte-restricted inactivation of the atrial natriuretic peptide receptor guanylyl cyclase-A. *J. Clin. Invest.* **111,** 1399–1407
6. Kitakaze, M., Asakura, M., Kim, J., Shintani, Y., Asanuma, H., Hamasaki, T., Seguchi, O., Myoishi, M., Minamino, T., Ohara, T., Nagai, Y., Nanto, S., Watanabe, K., Fukuzawa, S., Hirayama, A., Nakamura, N., Kimura, K., Fujii, K., Ishihara, M., Saito, Y., Tomoike, H., and Kitamura, S. (2007) Human atrial natriuretic peptide and nicorandil as adjuncts to reperfusion treatment for acute myocardial infarction (J-WIND): two randomised trials. *Lancet* **370,** 1483–1493
7. Li, P., Wang, D., Lucas, J., Oparil, S., Xing, D., Cao, X., Novak, L., Renfrow, M. B., and Chen, Y. F. (2008) Atrial natriuretic peptide inhibits transforming growth factor beta-induced Smad signaling and myofibroblast transformation in mouse cardiac fibroblasts. *Circ. Res.* **102,** 185–192
8. Tamura, N., Ogawa, Y., Chusho, H., Nakamura, K., Nakao, K., Suda, M., Kasahara, M., Hashimoto, R., Katsuura, G., Mukoyama, M., Itoh, H., Saito, Y., Tanaka, I., Otani, H., and Katsuki, M. (2000) Cardiac fibrosis in mice lacking brain natriuretic peptide. *Proc. Natl. Acad. Sci. U. S. A.* **97,** 4239–4244
9. De Lange, F. J., Moorman, A. F., and Christoffels, V. M. (2003) Atrial cardiomyocyte-specific expression of Cre recombinase driven by an Nppa gene fragment. *Genesis* **37,** 1–4
10. Habets, P. E., Moorman, A. F., Clout, D. E., van Roon, M. A., Lingbeek, M., van Lohuizen, M., Campione, M., and Christoffels, V. M. (2002) Cooperative action of Tbx2 and Nkx2.5 inhibits ANF expression in the atrioventricular canal: implications for cardiac chamber formation. *Genes Dev.* **16,** 1234–1246
11. Horsthuis, T., Houweling, A. C., Habets, P. E., de Lange, F. J., el Azzouzi, H., Clout, D. E., Moorman, A. F., and Christoffels, V. M. (2008) Distinct regulation of developmental and heart disease-induced atrial natriuretic factor expression by two separate distal sequences. *Circ. Res.* **102,** 849–859
12. Knowlton, K. U., Rockman, H. A., Itani, M., Vovan, A., Seidman, C. E., and Chien, K. R. (1995) Divergent pathways mediate the induction of ANF transgenes in neonatal and hypertrophic ventricular myocardium. *J. Clin. Invest.* **96,** 1311–1318
13. Small, E. M., and Krieg, P. A. (2003) Transgenic analysis of the atrialnatriuretic factor (ANF) promoter: Nkx2-5 and GATA-4 binding sites are required for atrial specific expression of ANF. *Dev. Biol.* **261,** 116–131
14. Warren, S. A., Terada, R., Briggs, L. E., Cole-Jeffrey, C. T., Chien, W. M., Seki, T., Weinberg, E. O., Yang, T. P., Chin, M. T., Bungert, J., and Kasahara, H. (2011) Differential role of Nkx2-5 in activation of the atrial natriuretic factor gene in the developing versus failing heart. *Mol. Cell. Biol.* **31,** 4633–4645
15. Simpson, P., McGrath, A., and Savion, S. (1982) Myocyte hypertrophy in neonatal rat heart cultures and its regulation by serum and by catecholamines. *Circ. Res.* **51,** 787–801
16. Siepel, A., Bejerano, G., Pedersen, J. S., Hinrichs, A. S., Hou, M., Rosenbloom, K., Clawson, H., Spieth, J., Hillier, L. W., Richards, S., Weinstock, G. M., Wilson, R. K., Gibbs, R. A., Kent, W. J., Miller, W., and Haussler, D. (2005) Evolutionarily conserved elements in vertebrate, insect, worm, and yeast genomes. *Genome Res.* **15,** 1034–1050
17. Blanchette, M., Kent, W. J., Riemer, C., Elnitski, L., Smit, A. F., Roskin, K. M., Baertsch, R., Rosenbloom, K., Clawson, H., Green, E. D., Haussler, D., and Miller, W. (2004) Aligning multiple genomic sequences with the threaded blockset aligner. *Genome Res.* **14,** 708–715
18. Pollard, K. S., Hubisz, M. J., Rosenbloom, K. R., and Siepel, A. (2010) Detection of nonneutral substitution rates on mammalian phylogenies. *Genome Res.* **20,** 110–121
19. Zhang, Y., Liu, T., Meyer, C. A., Eeckhoute, J., Johnson, D. S., Bernstein, B. E., Nusbaum, C., Myers, R. M., Brown, M., Li, W., and Liu, X. S. (2008) Model-based analysis of ChIP-Seq (MACS). *Genome Biol.* **9,** R137
20. Dekker, J., Rippe, K., Dekker, M., and Kleckner, N. (2002) Capturing chromosome conformation. *Science* **295,** 1306–1311
21. Hagege, H., Klous, P., Braem, C., Splinter, E., Dekker, J., Cathala, G., de Laat, W., and Forne, T. (2007) Quantitative analysis of chromosome conformation capture assays (3C-qPCR). *Nat. Protoc.* **2,** 1722–1733
22. Liao, Y., Ishikura, F., Beppu, S., Asakura, M., Takashima, S., Asanuma, H., Sanada, S., Kim, J., Ogita, H., Kuzuya, T., Node, K., Kitakaze, M., and Hori, M. (2002) Echocardiographic assessment of LV hypertrophy and function in aortic-banded mice: necropsy validation. *Am. J. Physiol. Heart Circ. Physiol.* **282,** H1703–H1708
23. Saadane, N., Alpert, L., and Chalifour, L. E. (1999) Expression of immediate early genes, GATA-4, and Nkx-2.5 in adrenergic-induced cardiac hypertrophy and during regression in adult mice. *Brit. J. Pharmacol.* **127,** 1165–1176
24. Vecchione, C., Fratta, L., Rizzoni, D., Notte, A., Poulet, R., Porteri, E., Frati, G., Guelfi, D., Trimarco, V., Mulvany, M. J., Agabiti-Rosei, E., Trimarco, B., Cotecchia, S., and Lembo, G. (2002) Cardiovascular influences of a1j3-adrenergic receptor defect in mice. *Circulation* **105,** 1700–1707
25. Nobrega, M. A., Ovcharenko, I., Afzal, V., and Rubin, E. M. (2003) Scanning human gene deserts for long-range enhancers. *Science* **302,** 413
26. Thomas, J. W., Touchman, J. W., Blakesley, R. W., Bouffard, G. G., Beckstrom-Sternberg, S. M., Margulies, E. H., Blanchette, M., Siepel, A. C., Thomas, P. J., McDowell, J. C., Maskeri, B., Hansen, N. F., Schwartz, M. S., Weber, R. J., Kent, W. J.,

Karolchik, D., Bruen, T. C., Bevan, R., Cutler, D. J., Schwartz, S., Elnitski, L., Idol, J. R., Prasad, A. B., Lee-Lin, S. Q., Maduro, V. V., Summers, T. J., Portnoy, M. E., Dietrich, N. L., Akhter, N., Ayele, K., Benjamin, B., Cariaga, K., Brinkley, C. P., Brooks, S. Y., Granite, S., Guan, X., Gupta, J., Haghighi, P., Ho, S. L., Huang, M. C., Karlins, E., Laric, P. L., Legaspi, R., Lim, M. J., Maduro, Q. L., Masiello, C. A., Mastrian, S. D., McCloskey, J. C., Pearson, R., Stantripop, S., Tiongson, E. E., Tran, J. T., Tsurgeon, C., Vogt, J. L., Walker, M. A., Wetherby, K. D., Wiggins, L. S., Young, A. C., Zhang, L. H., Osoegawa, K., Zhu, B., Zhao, B., Shu, C. L., De Jong, P. J., Lawrence, C. E., Smit, A. F., Chakravarti, A., Haussler, D., Green, P., Miller, W., and Green, E. D. (2003) Comparative analyses of multi-species sequences from targeted genomic regions. *Nature* **424,** 788–793

27. Woolfe, A., Goodson, M., Goode, D. K., Snell, P., McEwen, G. K., Vavouri, T., Smith, S. F., North, P., Callaway, H., Kelly, K., Walter, K., Abnizova, I., Gilks, W., Edwards, Y. J., Cooke, J. E., and Elgar, G. (2005) Highly conserved non-coding sequences are associated with vertebrate development. *PLoS Biol.* **3,** e7
28. Bell, A. C., West, A. G., and Felsenfeld, G. (1999) The protein CTCF is required for the enhancer blocking activity of vertebrate insulators. *Cell* **98,** 387–396
29. Felsenfeld, G., Burgess-Beusse, B., Farrell, C., Gaszner, M., Ghirlando, R., Huang, S., Jin, C., Litt, M., Magdinier, F., Mutskov, V., Nakatani, Y., Tagami, H., West, A., and Yusufzai, T. (2004) Chromatin boundaries and chromatin domains. *Cold Spring Harb. Symp. Quant. Biol.* **69,** 245–250
30. Shen, Y., Yue, F., McCleary, D. F., Ye, Z., Edsall, L., Kuan, S., Wagner, U., Dixon, J., Lee, L., Lobanenkov, V. V., and Ren, B. (2012) A map of the cis-regulatory sequences in the mouse genome. *Nature* **488,** 116–120
31. Birney, E., Stamatoyannopoulos, J. A., Dutta, A., Guigo, R., Gingeras, T. R., Margulies, E. H., Weng, Z., Snyder, M., Dermitzakis, E. T., Thurman, R. E., Kuehn, M. S., Taylor, C. M., Neph, S., Koch, C. M., Asthana, S., Malhotra, A., Adzhubei, I., Greenbaum, J. A., Andrews, R. M., Flicek, P., Boyle, P. J., Cao, H., Carter, N. P., Clelland, G. K., Davis, S., Day, N., Dhami, P., Dillon, S. C., Dorschner, M. O., Fiegler, H., Giresi, P. G., Goldy, J., Hawrylycz, M., Haydock, A., Humbert, R., James, K. D., Johnson, B. E., Johnson, E. M., Frum, T. T., Rosenzweig, E. R., Karnani, N., Lee, K., Lefebvre, G. C., Navas, P. A., Neri, F., Parker, S. C., Sabo, P. J., Sandstrom, R., Shafer, A., Vetrie, D., Weaver, M., Wilcox, S., Yu, M., Collins, F. S., Dekker, J., Lieb, J. D., Tullius, T. D., Crawford, G. E., Sunyaev, S., Noble, W. S., Dunham, I., Denoeud, F., Reymond, A., Kapranov, P., Rozowsky, J., Zheng, D., Castelo, R., Frankish, A., Harrow, J., Ghosh, S., Sandelin, A., Hofacker, I. L., Baertsch, R., Keefe, D., Dike, S., Cheng, J., Hirsch, H. A., Sekinger, E. A., Lagarde, J., Abril, J. F., Shahab, A., Flamm, C., Fried, C., Hackermuller, J., Hertel, J., Lindemeyer, M., Missal, K., Tanzer, A., Washietl, S., Korbel, J., Emanuelsson, O., Pedersen, J. S., Holroyd, N., Taylor, R., Swarbreck, D., Matthews, N., Dickson, M. C., Thomas, D. J., Weirauch, M. T., Gilbert, J., Drenkow, J., Bell, I., Zhao, X., Srinivasan, K. G., Sung, W. K., Ooi, H. S., Chiu, K. P., Foissac, S., Alioto, T., Brent, M., Pachter, L., Tress, M. L., Valencia, A., Choo, S. W., Choo, C. Y., Ucla, C., Manzano, C., Wyss, C., Cheung, E., Clark, T. G., Brown, J. B., Ganesh, M., Patel, S., Tammana, H., Chrast, J., Henrichsen, C. N., Kai, C., Kawai, J., Nagalakshmi, U., Wu, J., Lian, Z., Lian, J., Newburger, P., Zhang, X., Bickel, P., Mattick, J. S., Carninci, P., Hayashizaki, Y., Weissman, S., Hubbard, T., Myers, R. M., Rogers, J., Stadler, P. F., Lowe, T. M., Wei, C. L., Ruan, Y., Struhl, K., Gerstein, M., Antonarakis, S. E., Fu, Y., Green, E. D., Karaoz, U., Siepel, A., Taylor, J., Liefer, L. A., Wetterstrand, K. A., Good, P. J., Feingold, E. A., Guyer, M. S., Cooper, G. M., Asimenos, G., Dewey, C. N., Hou, M., Nikolaev, S., Montoya-Burgos, J. I., Loytynoja, A., Whelan, S., Pardi, F., Massingham, T., Huang, H., Zhang, N. R., Holmes, I., Mullikin, J. C., Ureta-Vidal, A., Paten, B., Seringhaus, M., Church, D., Rosenbloom, K., Kent, W. J., Stone, E. A., Batzoglou, S., Goldman, N., Hardison, R. C., Haussler, D., Miller, W., Sidow, A., Trinklein, N. D., Zhang, Z. D., Barrera, L., Stuart, R., King, D. C., Ameur, A., Enroth, S., Bieda, M. C., Kim, J., Bhinge, A. A., Jiang, N., Liu, J., Yao, F., Vega, V. B., Lee, C. W., Ng, P., Shahab, A., Yang, A., Moqtaderi, Z., Zhu, Z., Xu, X., Squazzo, S., Oberley, M. J., Inman, D., Singer, M. A., Richmond, T. A., Munn, K. J., Rada-Iglesias, A., Wallerman, O., Komorowski, J., Fowler, J. C., Couttet, P., Bruce, A. W., Dovey, O. M., Ellis, P. D., Langford, C. F., Nix, D. A., Euskirchen, G., Hartman, S., Urban, A. E., Kraus, P., Van Calcar, S., Heintzman, N., Kim, T. H., Wang, K., Qu, C., Hon, G., Luna, R., Glass, C. K., Rosenfeld, M. G., Aldred, S. F., Cooper, S. J., Halees, A., Lin, J. M., Shulha, H. P., Zhang, X., Xu, M., Haidar, J. N., Yu, Y., Ruan, Y., Iyer, V. R., Green, R. D., Wadelius, C., Farnham, P. J., Ren, B., Harte, R. A., Hinrichs, A. S., Trumbower, H., Clawson, H., Hillman-Jackson, J., Zweig, A. S., Smith, K., Thakkapallayil, A., Barber, G., Kuhn, R. M., Karolchik, D., Armengol, L., Bird, C. P., de Bakker, P. I., Kern, A. D., Lopez-Bigas, N., Martin, J. D., Stranger, B. E., Woodroffe, A., Davydov, E., Dimas, A., Eyras, E., Hallgrimsdottir, I. B., Huppert, J., Zody, M. C., Abecasis, G. R., Estivill, X., Bouffard, G. G., Guan, X., Hansen, N. F., Idol, J. R., Maduro, V. V., Maskeri, B., McDowell, J. C., Park, M., Thomas, P. J., Young, A. C., Blakesley, R. W., Muzny, D. M., Sodergren, E., Wheeler, D. A., Worley, K. C., Jiang, H., Weinstock, G. M., Gibbs, R. A., Graves, T., Fulton, R., Mardis, E. R., Wilson, R. K., Clamp, M., Cuff, J., Gnerre, S., Jaffe, D. B., Chang, J. L., Lindblad-Toh, K., Lander, E. S., Koriabine, M., Nefedov, M., Osoegawa, K., Yoshinaga, Y., Zhu, B., and de Jong, P. J. (2007) Identification and analysis of functional elements in 1% of the human genome by the ENCODE pilot project. *Nature* **447,** 799–816
32. Blow, M. J., McCulley, D. J., Li, Z., Zhang, T., Akiyama, J. A., Holt, A., Plajzer-Frick, I., Shoukry, M., Wright, C., Chen, F., Afzal, V., Bristow, J., Ren, B., Black, B. L., Rubin, E. M., Visel, A., and Pennacchio, L. A. (2010) ChIP-Seq identification of weakly conserved heart enhancers. *Nat. Genet.* **42,** 806–810
33. Koch, F., Jourquin, F., Ferrier, P., and Andrau, J. C. (2008) Genome-wide RNA polymerase II: not genes only!. *Trends Biochem. Sci.* **33,** 265–273
34. Szutorisz, H., Dillon, N., and Tora, L. (2005) The role of enhancers as centres for general transcription factor recruitment. *Trends Biochem. Sci.* **30,** 593–599
35. Sei, C. A., Irons, C. E., Sprenkle, A. B., McDonough, P. M., Brown, J. H., and Glembotski, C. C. (1991) The a-adrenergic stimulation of atrial natriuretic factor expression in cardiac myocytes requires calcium influx, protein kinase C, and calmodulin-regulated pathways. *J. Biol. Chem.* **266,** 15910–15916
36. Iaccarino, G., Dolber, P. C., Lefkowitz, R. J., and Koch, W. J. (1999) Bj3-adrenergic receptor kinase-1 levels in catecholamine-induced myocardial hypertrophy: regulation by beta- but not alpha1-adrenergic stimulation. *Hypertension* **33,** 396–401
37. Seidman, C. E., Wong, D. W., Jarcho, J. A., Bloch, K. D., and Seidman, J. G. (1988) *Cis*-acting sequences that modulate atrial natriuretic factor gene expression. *Proc. Natl. Acad. Sci. U. S. A.* **85,** 4104–4108
38. Thuerauf, D. J., and Glembotski, C. C. (1997) Differential effects of protein kinase C, Ras, and Raf-1 kinase on the induction of the cardiac B-type natriuretic peptide gene through a critical promoter-proximal M-CAT element. *J. Biol. Chem.* **272,** 7464–7472

Received for publication November 12, 2013.
Accepted for publication January 2, 2014.

Evaluation of intramitochondrial ATP levels identifies G0/G1 switch gene 2 as a positive regulator of oxidative phosphorylation

Hidetaka Kioka[a,b,1], Hisakazu Kato[a,1], Makoto Fujikawa[c], Osamu Tsukamoto[a], Toshiharu Suzuki[d,e], Hiromi Imamura[f], Atsushi Nakano[a,g], Shuichiro Higo[a,b], Satoru Yamazaki[h], Takashi Matsuzaki[b], Kazuaki Takafuji[i], Hiroshi Asanuma[j], Masanori Asakura[g], Tetsuo Minamino[b], Yasunori Shintani[a], Masasuke Yoshida[e], Hiroyuki Noji[k], Masafumi Kitakaze[g], Issei Komuro[b,l], Yoshihiro Asano[a,b,2], and Seiji Takashima[a,2]

Departments of [a]Medical Biochemistry and [b]Cardiovascular Medicine and [i]Center for Research Education, Osaka University Graduate School of Medicine, Osaka 565-0871, Japan; [c]Department of Biochemistry, Faculty of Pharmaceutical Science, Tokyo University of Science, Chiba 278-8510, Japan; [d]Chemical Resources Laboratory, Tokyo Institute of Technology, Yokohama 226-8503, Japan; [e]Department of Molecular Bioscience, Kyoto Sangyo University, Kyoto 603-8555, Japan; [f]The Hakubi Center for Advanced Research and Graduate School of Biostudies, Kyoto University, Kyoto 606-8501, Japan; Departments of [g]Clinical Research and Development and [h]Cell Biology, National Cerebral and Cardiovascular Center Research Institute, Osaka 565-8565, Japan; [j]Department of Cardiovascular Science and Technology, Kyoto Prefectural University School of Medicine, Kyoto 602-8566, Japan; and [k]Department of Applied Chemistry, School of Engineering and [l]Department of Cardiovascular Medicine, Graduate School of Medicine, University of Tokyo, Tokyo 113-8656, Japan

Edited by Gottfried Schatz, University of Basel, Reinach, Switzerland, and approved November 19, 2013 (received for review October 7, 2013)

The oxidative phosphorylation (OXPHOS) system generates most of the ATP in respiring cells. ATP-depleting conditions, such as hypoxia, trigger responses that promote ATP production. However, how OXPHOS is regulated during hypoxia has yet to be elucidated. In this study, selective measurement of intramitochondrial ATP levels identified the hypoxia-inducible protein G0/G1 switch gene 2 (G0s2) as a positive regulator of OXPHOS. A mitochondria-targeted, FRET-based ATP biosensor enabled us to assess OXPHOS activity in living cells. Mitochondria-targeted, FRET-based ATP biosensor and ATP production assay in a semi-intact cell system revealed that G0s2 increases mitochondrial ATP production. The expression of G0s2 was rapidly and transiently induced by hypoxic stimuli, and G0s2 interacts with OXPHOS complex V (F_oF_1-ATP synthase). Furthermore, physiological enhancement of G0s2 expression prevented cells from ATP depletion and induced a cellular tolerance for hypoxic stress. These results show that G0s2 positively regulates OXPHOS activity by interacting with F_oF_1-ATP synthase, which causes an increase in ATP production in response to hypoxic stress and protects cells from a critical energy crisis. These findings contribute to the understanding of a unique stress response to energy depletion. Additionally, this study shows the importance of assessing intramitochondrial ATP levels to evaluate OXPHOS activity in living cells.

energy metabolism | live-cell imaging

Maintaining cellular homeostasis and activities requires a stable energy supply. Most eukaryotic cells generate ATP as their energy currency mainly through the mitochondrial oxidative phosphorylation (OXPHOS) system. The OXPHOS system consists of five large protein complex units (i.e., complexes I–V), comprising more than 100 proteins. In this system, oxygen (O_2) is essential as the terminal electron acceptor for complex IV to finally produce the proton-motive force that drives the ATP-generating molecular motor complex V (F_oF_1-ATP synthase).

Hypoxia causes the depletion of intracellular ATP and triggers adaptive cellular responses to help maintain intracellular ATP levels and minimize any deleterious effects of energy depletion. Although the metabolic switch from mitochondrial respiration to anaerobic glycolysis is widely recognized (1–4), several recent reports have shown that hypoxic stimuli unexpectedly increase OXPHOS efficiency as well (5–7). In other words, cells have adaptive mechanisms to maintain intracellular ATP levels by enhancing OXPHOS, particularly in the early phase of hypoxia, in which the O_2 supply is limited but still remains. However, the mechanism by which OXPHOS is regulated during this early hypoxic phase is still not fully understood.

Revealing the mechanism of this fine-tuned regulation of OXPHOS requires accurate and noninvasive measurements of OXPHOS activity. Although researchers have established methods to measure OXPHOS activity, precise measurement, especially in living cells, is still difficult. Measuring the intracellular ATP concentration is one of the most commonly used methods for evaluating OXPHOS activity. However, there are two major problems with this method. First, the intracellular ATP concentration does not always accurately reflect OXPHOS activity, because it can also be affected by glycolytic ATP production, cytosolic ATPases, and ATP buffering enzymes, such as creatine kinase and adenylate kinase (8). Second, because measurements of the ATP concentration by chromatography (9), MS (10), NMR (11), or luciferase assays (12) are based on cell extract analysis, these methods cannot be used to measure the serial ATP concentration changes in living cells in real time.

In this study, we overcame these problems by the selective measurement of the intramitochondrial matrix ATP concentration ($[ATP]_{mito}$) in living cells. In the final step of OXPHOS, ATP is produced not in the cytosol but in the mitochondrial matrix. Therefore, we hypothesized that a selectively measuring $[ATP]_{mito}$ is suitable for the highly sensitive evaluation of cellular ATP production by OXPHOS. In fact, real-time evaluation of both $[ATP]_{mito}$ and the cytosolic ATP concentration ($[ATP]_{cyto}$) in living cells revealed that $[ATP]_{mito}$ reflected OXPHOS activity with far more sensitivity than $[ATP]_{cyto}$. Using this fine method, we found that G0/G1 switch gene 2 (G0s2), a hypoxia-induced

Significance

We developed a sensitive method to assess the activity of oxidative phosphorylation in living cells using a FRET-based ATP biosensor. We then revealed that G0/G1 switch gene 2, a protein rapidly induced by hypoxia, increases mitochondrial ATP production by interacting with F_oF_1-ATP synthase and protects cells from a critical energy crisis.

Author contributions: Y.A. and S.T. designed research; H. Kioka, H. Kato, O.T., and A.N. performed research; M.F., T.S., H.I., S.H., S.Y., T. Matsuzaki, K.T., H.A., M.A., T. Minamino, Y.S., M.Y., H.N., M.K., and I.K. contributed new reagents/analytic tools; H. Kioka and H. Kato analyzed data; and Y.A. and S.T. wrote the paper.

The authors declare no conflict of interest.

This article is a PNAS Direct Submission.

[1]H. Kioka and H. Kato contributed equally to this work.

[2]To whom correspondence may be addressed. E-mail: asano@cardiology.med.osaka-u.ac.jp or takasima@cardiology.med.osaka-u.ac.jp.

This article contains supporting information online at www.pnas.org/lookup/suppl/doi:10.1073/pnas.1318547111/-/DCSupplemental.

protein in cardiomyocytes, increases OXPHOS activity. G0s2 interacted with F_oF_1-ATP synthase and increased the ATP production rate. Our results suggest that hypoxia-induced protein G0s2 is a positive regulator of OXPHOS and protects cells by preserving ATP production, even under hypoxic conditions.

Results

Establishment of a Sensitive Method to Assess OXPHOS Activity in Living Cells. To elucidate the mechanism by which OXPHOS is regulated under hypoxia, it is essential to establish a sensitive method for assessing OXPHOS activity in living cells. For this purpose, we used an ATP indicator based on ε-subunit for analytical measurements (ATeam), which is an ATP-sensing FRET-based indicator (13). We introduced this ATP biosensor into cardiomyocytes that possess an abundance of mitochondria and produce the highest levels of ATP among all primary cells (14, 15). The ATeam assay can measure both $[ATP]_{cyto}$ (i.e., the Cyto-ATeam assay) and $[ATP]_{mito}$ when a duplex of the mitochondrial targeting signal of cytochrome c oxidase subunit VIII is attached to the indicator (i.e., the Mit-ATeam assay). In this case, the YFP/CFP emission ratio of the ATeam fluorescence represents the ATP concentration in each compartment. Interestingly, the Mit-ATeam assay was a far more sensitive method than the Cyto-ATeam assay in determining OXPHOS activity in living cells. For example, a very low dose of oligomycin A (0.01 μg/mL), a specific OXPHOS complex V (F_oF_1-ATP synthase) inhibitor, greatly reduced the YFP/CFP emission ratio of the Mit-ATeam fluorescence that represents $[ATP]_{mito}$ within 10 min (Fig. 1 A, Upper and B and Movie S1). In contrast, the same dose of oligomycin A resulted in a slight and slow decline of the YFP/CFP emission ratio of Cyto-ATeam fluorescence (Fig. 1 A, Lower and B and Movie S1). The same phenomenon was observed when the cells were exposed to hypoxia, which suppresses the activity of OXPHOS complex IV (cytochrome c oxidase). Again, $[ATP]_{mito}$ decreased more markedly than $[ATP]_{cyto}$ during 2.5 h of hypoxia (Fig. 1 C and D and Movie S2). These results indicate that the Mit-ATeam assay is far more sensitive for measuring the activity of OXPHOS than the Cyto-ATeam assay. In addition, OXPHOS inhibition decreased the YFP/CFP emission ratio of the Mit-ATeam fluorescence of HeLa cells as well as cardiomyocytes (Fig. S1), suggesting the broad applicability of this assay. Therefore, we used Mit-ATeam for the assessment of the OXPHOS activity in living cells.

Hypoxia-Induced Gene G0s2 Affects the Intramitochondrial ATP Concentration. The expression of genes involved in OXPHOS regulation is considered to be up-regulated in the early phase of hypoxia. Thus, to find unique OXPHOS regulators, we focused on the rapidly induced genes in response to hypoxic stimulation. We compared the gene expression profiles of cultured rat cardiomyocytes at three different time points during hypoxic conditions (0, 2, and 12 h) (Fig. S2A). The expression of well-known hypoxia-induced genes, such as VEGF-α and hexokinase 2 mRNA (16, 17), was slightly up-regulated at 2 h and further enhanced at 12 h of hypoxia. In contrast, three other genes (Adamts1, Cdkn3, and G0s2) underwent rapid increases in expression at 2 h but declined at 12 h of sustained hypoxia (Fig. S2 B and C). This rapid and transient time course of expression implies that these three genes may play distinct regulatory roles, especially in the early hypoxic phase, in which oxygen is limited but still available. To examine whether these genes are involved in the regulation of OXPHOS activity, we knocked down these genes by shRNA (see Fig. S7A) and examined $[ATP]_{mito}$ using the Mit-ATeam assay. In this experiment, $[ATP]_{mito}$ in cardiomyocytes treated with shRNA for G0s2 clearly declined within 24 h compared with the control cardiomyocytes (Fig. 2A and Movie S3). In addition, the time course of ATP decline was in agreement with the time course of G0s2 depletion (Fig. 2A and Fig. S3A). Importantly, the overexpression of G0s2 restored normal ATP levels (Fig. 2 B and C), and again, the Cyto-ATeam assay could not detect a significant effect of G0s2 knockdown within this time frame (Fig. S3B and Movie S4). These findings imply that mitochondrial ATP production through OXPHOS was inhibited by G0s2 ablation. We confirmed that the mRNA and protein levels of G0s2 both increased after 2–6 h of hypoxia and then declined after 12 h of hypoxia (Fig. 2 D and E). G0s2 was first reported as a gene with

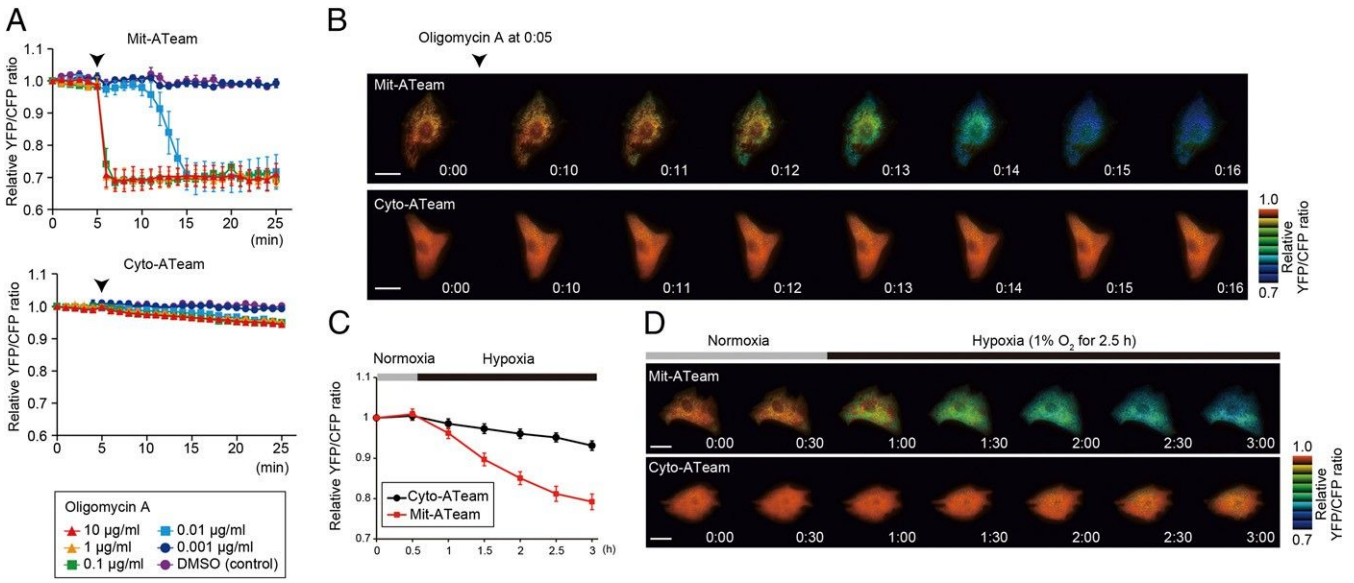

Fig. 1. Establishment of a sensitive method to assess OXPHOS activity in living cells. (A) YFP/CFP emission ratio plots of (Upper) Mit-ATeam and (Lower) Cyto-ATeam fluorescence in cardiomyocytes. Various concentrations (0.001, 0.01, 0.1, 1, and 10 μg/mL) of oligomycin A or DMSO (control) were added at 5 min (arrowhead; n = 3). (B) Representative sequential YFP/CFP ratiometric pseudocolored images of (Upper) Mit-ATeam and (Lower) Cyto-ATeam in cardiomyocytes. Oligomycin A (0.01 μg/mL) was added at 5 min. (Scale bars: 20 μm.) (C) YFP/CFP emission ratio plots of Mit-ATeam and Cyto-ATeam fluorescence in cardiomyocytes (n = 10). (D) Representative sequential YFP/CFP ratiometric pseudocolored images of (Upper) Mit-ATeam and (Lower) Cyto-ATeam in cardiomyocytes. Cells were exposed to 1% hypoxia from the time point 30 min. All of the measurements were normalized to the YFP/CFP emission ratio at 0 min. Data are represented as the means ± SEMs. (Scale bars: 20 μm.)

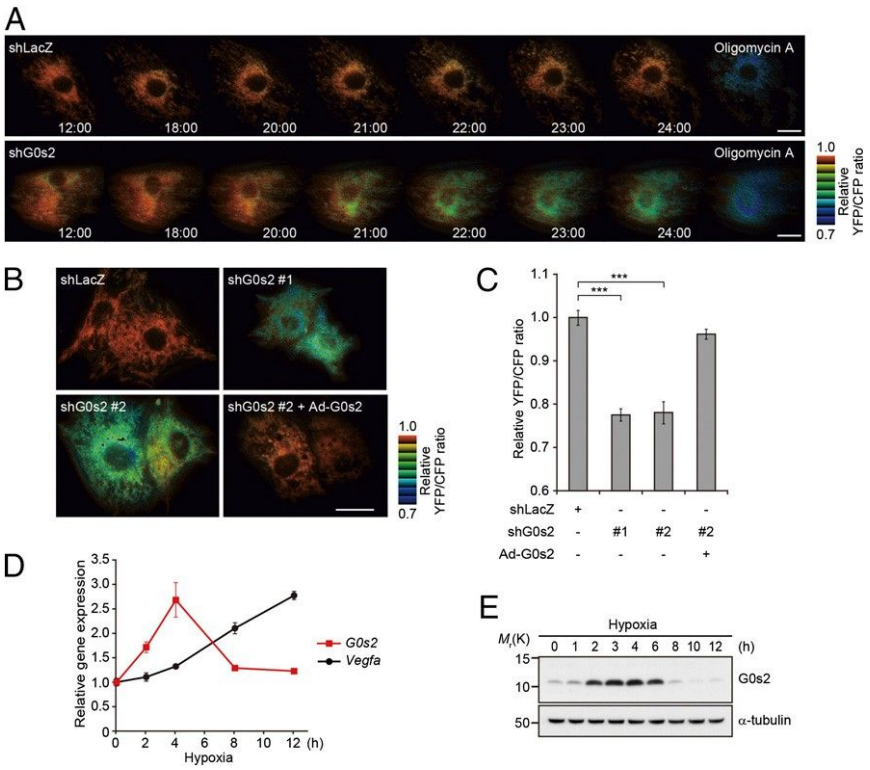

Fig. 2. G0s2, a hypoxia-inducible protein, affects intramitochondrial ATP concentration in cardiomyocytes. (A) Sequential YFP/CFP ratiometric pseudocolored images of Mit-ATeam fluorescence in cardiomyocytes expressing (Upper) shRNAs for LacZ (shLacZ) or (Lower) G0s2 (shG0s2). Oligomycin A (1 μg/mL) was added at the end of the time-lapse imaging to completely inhibit ATP synthesis. The indicated time represents the period after adenovirus infection. (B) Representative YFP/CFP ratiometric pseudocolored images of Mit-ATeam fluorescence in cardiomyocytes expressing the indicated adenovirus for 24 h. (Scale bar: A and B, 20 μm.) (C) The bar graph shows the mean YFP/CFP emission ratio of Mit-ATeam fluorescence in cardiomyocytes expressing shLacZ (n = 30), shG0s2 #1 (n = 30), shG0s2 #2 (n = 29), and shG0s2 #2 + G0s2 WT (n = 32) for 24 h. All of the measurements were normalized to the average of the control cells (shLacZ). ***P < 0.001. (D) Gene expression value plots of G0s2 (red line) and VEGF-α (Vegfa; black line) levels in cardiomyocytes under hypoxic conditions (1% O_2). Each value was compared with the level of Actb expression (n = 3). Values represent the means ± SEMs. (E) Immunoblotting of the G0s2 expression in cardiomyocytes under hypoxic conditions (1% O_2).

expression that was induced during the cell cycle switch from G0 to G1 phase (18). G0s2 is expressed in many tissues and especially abundant in heart, skeletal muscle, liver, kidney, brain, and adipose tissue (19). Although G0s2 may play a role in cell cycle progression (20), the function of G0s2 in the hypoxic response remains unknown.

G0s2 Rescues the Decline of ATP Production During Hypoxia. We next tested whether the overexpression of the G0s2 before hypoxic stress could prevent hypoxia-induced ATP depletion. We prepared cardiomyocytes overexpressing G0s2 and control cardiomyocytes. During sustained hypoxia, $[ATP]_{mito}$ gradually declined in control cardiomyocytes as measured by the Mit-ATeam assay. Notably, the overexpression of G0s2 before the onset of hypoxia reduced this decline in $[ATP]_{mito}$, which allowed the cardiomyocytes to promptly recover to baseline levels of $[ATP]_{mito}$ after reoxygenation (Fig. 3 A and B and Movie S5). In addition, the prehypoxia overexpression of G0s2 preserved cell viability during sustained hypoxia (Fig. 3C). These results suggest that G0s2 can preserve mitochondrial ATP production even under hypoxia and protect cells from the energy crisis under hypoxia.

G0s2 Binds to F_oF_1-ATP Synthase but Not Other OXPHOS Protein Complexes. To reveal the mechanism by which G0s2 affects $[ATP]_{mito}$, we sought to identify the biochemical targets of G0s2. We screened for G0s2 binding proteins by immunoaffinity purification of cell lysates from cardiomyocytes expressing C-terminally Flag-tagged G0s2 (G0s2-Flag). G0s2-Flag is expressed in cardiomyocytes localized to the mitochondria (Fig. S4A). MS analysis revealed that multiple F_oF_1-ATP synthase subunits, but no other mitochondrial respiratory chain complex subunits, were coimmunoprecipitated with G0s2-Flag (Fig. S4B and Table S1). F_oF_1-ATP synthase is a well-known ATP-producing enzyme composed of a protein complex that contains an extramembranous F_1 and an intramembranous F_o domain linked by a peripheral and a central stalk (21–24). The binding of F_oF_1-ATP synthase to G0s2-Flag was confirmed by immunoblotting with antibodies against several subunits of F_oF_1-ATP synthase (Fig. 4A).

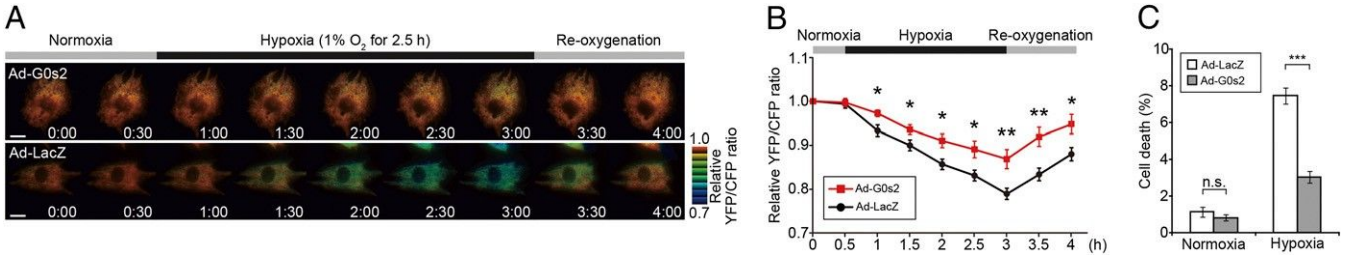

Fig. 3. Overexpression of G0s2 before hypoxia rescues the decline of mitochondrial ATP production during hypoxia. (A) Sequential YFP/CFP ratiometric pseudocolored images of Mit-ATeam fluorescence in cardiomyocytes expressing (Upper) G0s2 WT or (Lower) LacZ during hypoxia and reoxygenation. (Scale bar: 20 μm.) (B) YFP/CFP emission ratio plots of Mit-ATeam fluorescence in cardiomyocytes expressing G0s2 WT (n = 20) or LacZ (n = 19) during hypoxia and reoxygenation. All of the measurements were normalized to the ratio at time 0 and compared between cardiomyocytes with G0s2 WT and LacZ at each time point. (C) The bar graph shows the cell viability of cardiomyocytes overexpressing G0s2 under hypoxic conditions. Cardiomyocytes expressing either LacZ or G0s2 WT were cultured under normoxic or hypoxic conditions for 18 h (n = 8). The asterisks denote statistical significance comparing G0s2 with LacZ. Data are represented as the means ± SEMs. n.s., not significant. *P < 0.05; **P < 0.01; ***P < 0.001.

Conversely, G0s2-Flag was coimmunoprecipitated with F_oF_1-ATP synthase (Fig. S4C). G0s2-Flag was also found to be associated with the F_oF_1-ATP synthase in 293T and HeLa cells (Fig. S4C). Both coimmunoprecipitation using an anti-G0s2 antibody and a reciprocal immunoprecipitation revealed that endogenous G0s2 interacts with F_oF_1-ATP synthase, whereas none of the proteins in complexes I–IV or adenine nucleotide translocase 1 (ANT1; also referred to as ADP/ATP carrier) were coimmunoprecipitated with G0s2 (Fig. 4 B and C).

Given that the G0s2 protein contains an evolutionarily conserved amino terminus and one hydrophobic domain (HD) (19), we created three G0s2 partial deletion mutants to identify the domain in G0s2 that is important for binding to F_oF_1-ATP synthase (Fig. S4D). Among these mutants, G0s2 ΔC and G0s2 ΔN but not G0s2 ΔHD bound to the F_oF_1-ATP synthase complex (Fig. 4D and Fig. S4 E and F). Furthermore, we confirmed that G0s2 directly interacts with F_oF_1-ATP synthase in an in vitro pull-down assay using a recombinant maltose-binding protein–fused G0s2 protein and purified F_oF_1-ATP synthase from bovine heart mitochondria (Fig. S5). Immunocytochemical analysis revealed that endogenous G0s2 colocalized with the β-subunit of F_oF_1-ATP synthase (Fig. 4E). The knockdown of G0s2 expression by shRNA abolished G0s2 staining (Figs. S6 and S7A), indicating that both antibodies used for immunostaining specifically recognize G0s2. These data suggest that G0s2 interacts with the F_oF_1-ATP synthase complex through its HD in mitochondria and regulates OXPHOS activity.

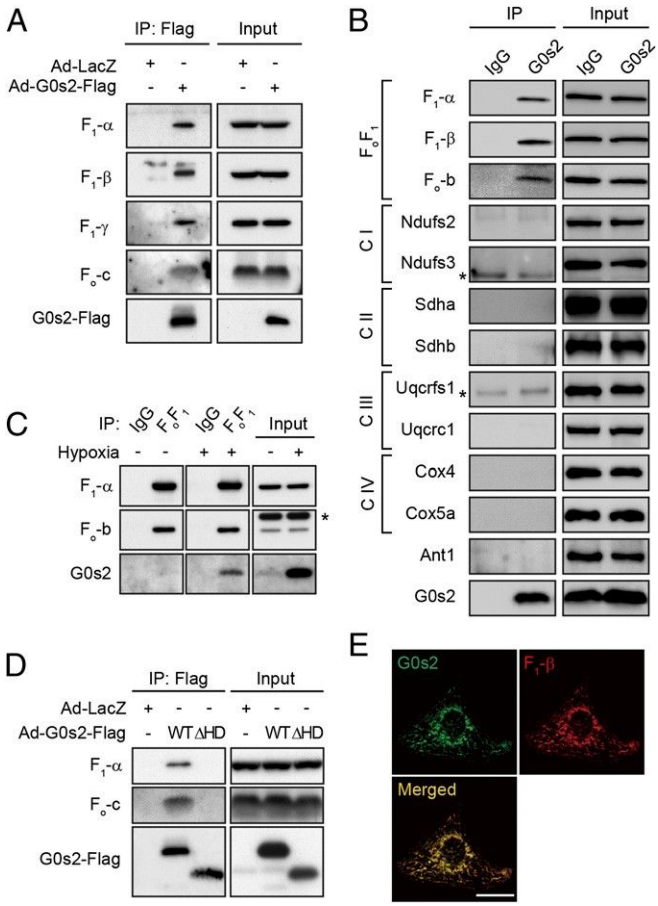

Fig. 4. G0s2 interacts with the F_oF_1-ATP synthase in mitochondria. (A) Immunoprecipitation (IP) of G0s2-Flag in cardiomyocytes. Cell lysates from cardiomyocytes expressing G0s2-Flag or LacZ were immunoprecipitated with an anti-Flag antibody. (B) IP of endogenous G0s2 in cardiomyocytes. Endogenous G0s2 was induced by hypoxia and immunoprecipitated using an anti-G0s2 antibody. C, OXPHOS complex; F_oF_1, F_oF_1-ATP synthase. *IgG light chain. (C) IP of F_oF_1-ATP synthase in cardiomyocytes under normoxic or hypoxic conditions. Cell lysates from cardiomyocytes cultured under normoxia or hypoxia for 4 h were immunoprecipitated with an antibody against the whole F_oF_1-ATP synthase complex or a control IgG. *Nonspecific band. (D) IP of G0s2 mutants expressed in cardiomyocytes. Cell lysates were immunoprecipitated with an anti-Flag antibody. (E) Immunostained images of hypoxia-stimulated (4 h) cardiomyocytes with anti-G0s2 (green) and anti–F_oF_1-ATP synthase β-subunit (red) antibodies. (Scale bars: 20 μm.)

G0s2 Increases Mitochondrial ATP Production Rate. $[ATP]_{mito}$ is mainly determined by the rate of ATP synthesis by F_oF_1-ATP synthase and ATP/ADP exchange by the ATP/ADP translocase ANT1. This theory means that the increased $[ATP]_{mito}$ observed in the G0s2-overexpressing cells may result from the increased ATP synthesis and/or decreased ATP/ADP exchange, although G0s2 did not interact with ANT1 (Fig. 4B). To resolve this issue and directly measure the rate of ATP production in mitochondria, we used a semiintact cell system called the mitochondrial activity of streptolysin O permeabilized cells (MASC) assay (25). In this assay, we permeabilized the plasma membrane to wash out any cytosolic components, such as creatine and glycolytic substrates, but left the mitochondria intact. Furthermore, we treated the cells with P^1, P^5-di(adenosine-5′) pentaphosphate to inhibit the activity of adenylate kinase. These steps allowed us to measure the ATP production rate mostly from OXPHOS, with a minimal contribution of ATP buffering systems in the cytosol. The MASC assay was suitable for accurate measurement of mitochondrial ATP production rate, because mitochondria in this semiintact cell system suffered much smaller damage than the isolated mitochondria in the conventional method. Surprisingly, in the MASC assay, the ATP production rate markedly increased when G0s2 was expressed in HeLa cells that lacked endogenous G0s2 (Fig. 5A). In cardiomyocytes, shRNA-mediated G0s2 knockdown decreased the ATP production rate in mitochondria, and the expression of G0s2 WT but not G0s2 ΔHD could restore the ATP production rate (Fig. 5B and Fig. S7A). In both cells, complete inhibition of ATP production by oligomycin A indicated that the observed ATP synthesis was catalyzed by OXPHOS but not other metabolism (Fig. 5 A and B).

Next, to evaluate the physiological role of G0s2, we examined whether endogenous G0s2 induced by hypoxia could enhance the ATP production rate. Cardiomyocytes were pretreated with hypoxia for 4 h, during which G0s2 expression was largely induced. We then evaluated the ATP production rate of both hypoxia-pretreated and nontreated cardiomyocytes under room air conditions. Even under these equivalent normoxic conditions, hypoxia-pretreated cardiomyocytes produced ATP faster than nontreated control cardiomyocytes (Fig. 5C and Fig. S7B). G0s2 knockdown attenuated this increase in the rate of ATP production, indicating that the enhanced ATP production rate resulting from hypoxia pretreatment primarily depends on endogenous G0s2 induction. This increased G0s2 expression was essential for cell survival, because G0s2-depleted cells died earlier than control cells under conditions of hypoxic stress (Fig. 5D)

Furthermore, to assess the effect of G0s2 on cellular respiration, we continuously measured the oxygen consumption rate (OCR) using an XF96 Extracellular Flux Analyzer. G0s2 knockdown decreased the basal OCR of cardiomyocytes, most likely because of the decreased activity of ATP synthesis (Fig. 5 E and F). In contrast, the proton leakage of the mitochondrial inner membrane and the maximum respiratory capacity of OXPHOS complexes I–IV were unaffected by G0s2 ablation (Fig. 5 E and F). These data show that G0s2 knockdown reduced respiration caused by ATP synthesis without affecting respiration caused by proton leakage, nonmitochondrial respiration, or the maximal respiration capacity.

All these findings indicate that G0s2 enhances the mitochondrial ATP production rate by increasing the activity of F_oF_1-ATP synthase.

Discussion

In this study, we showed that G0s2 kinetically increased OXPHOS activity through direct binding to F_oF_1-ATP synthase. Our previous

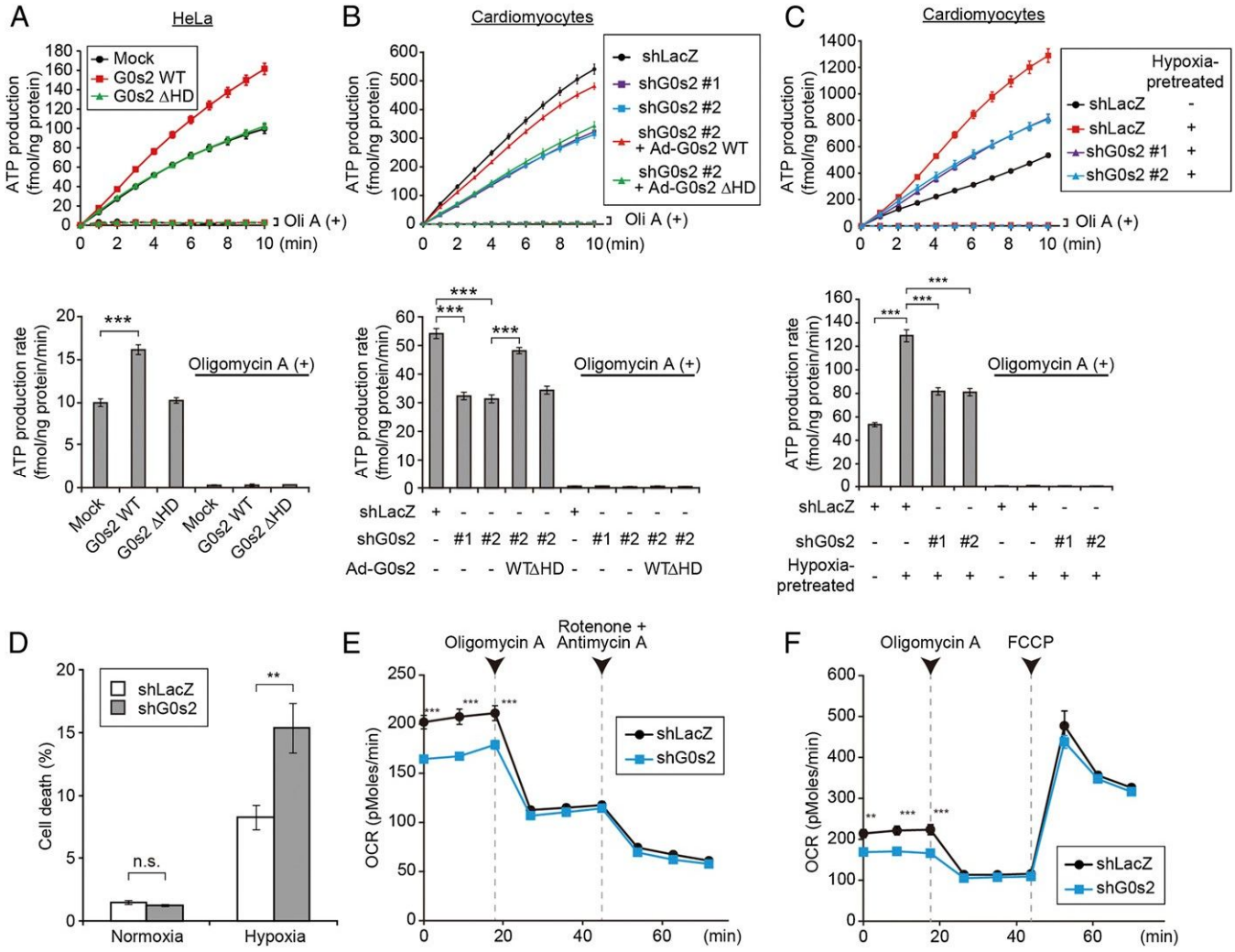

Fig. 5. G0s2 enhances the mitochondrial ATP production rate. (A and B) MASC assay of (A) permeabilized HeLa cells expressing the indicated plasmids or (B) cardiomyocytes expressing the indicated adenovirus in the presence (dotted lines) or absence (solid lines) of 1 μg/mL oligomycin A (Oli A). Upper shows the ATP production plots, and Lower shows the mean ATP production rates between 0 and 10 min. (A) n = 12. (B) Solid lines, n = 12; dotted lines, n = 8. (C) MASC assay of permeabilized cardiomyocytes pretreated with hypoxia. Cells expressing the indicated adenovirus were pretreated with or without hypoxia for 4 h. After the pretreatment, the cells were permeabilized under room air conditions followed by MASC assay in the presence (dotted lines; n = 8) or absence (solid lines; n = 12) of 1 μg/mL Oli A. Upper shows the ATP production plot, and Lower shows the mean ATP production rate between 0 and 10 min. (D) The bar graph represents the cell viability of G0s2-depleted cardiomyocytes under hypoxic conditions. Cardiomyocytes expressing shLacZ or shG0s2 (#2) were cultured under normoxic or hypoxic conditions for 18 h. (E and F) The OCR in cardiomyocytes expressing shLacZ and shG0s2 (#2) under basal conditions and in response to the indicated mitochondrial inhibitors (n = 8). FCCP, carbonyl cyanide-4-(trifluoromethoxy)-phenylhydrazone. Data are represented as the means ± SEMs. n.s., not significant. **P < 0.01; ***P < 0.001.

studies of F_oF_1-ATP synthase have revealed that this enzyme has a specific structure that connects two molecular nanomotors that synchronize with each other to produce ATP (26–30). These physically distinct structures suggest that a specific activating factor for F_oF_1-ATP synthase must exist. Combined with the findings from this study, we hypothesize that G0s2 may lower the activation barrier of the F_oF_1-ATP synthase nanomotor and enhance the ATP production rate with the equivalent proton motive driving force (PMF; i.e., the sum of the membrane potential and the pH gradient). Activation barriers might be generated by various factors, such as friction between the stator and rotor of F_oF_1-ATP synthase, physical and electrical resistance to proton transport through the channel, and the existence of rotary blockers such as the bacterial e-subunit and cyclophilin D (31). The increased ATP production rate caused by G0s2 overexpression observed in the MASC assay supports this hypothesis, because the PMF in the initial phase of this assay should be the same. If this hypothesis is true, even with reduced PMF, cells that express G0s2 should produce ATP faster than cells that express little or no G0s2. In fact, G0s2 overexpression attenuated the decline of $[ATP]_{mito}$ under hypoxic conditions that reduced the PMF. Precise real-time measurement of the PMF is currently difficult, but these hypotheses might be proven in future studies. Kinetically faster ATP production should accompany greater consumption of both O_2 and PMF; however, our results suggest that preserving ATP production is more beneficial than preserving PMF for cell viability, particularly when the O_2 supply is restricted but still exists. The transience of endogenous G0s2 expression induced by hypoxia might serve to protect tissues in the early phase of energy crisis. There may be specific mechanisms to decrease G0s2 expression under prolonged ischemia that have yet to be identified. Another possible mechanism by which G0s2 could increase the ATP production rate is that G0s2 increases the F_o-F_1 coupling efficiency of F_oF_1-ATP synthase. However, this hypothesis is less likely, because G0s2 altered the oxygen consumption rate to increase the ATP production rate. Although this uncoupling phenomenon has rarely been reported for mammalian mitochondrial F_oF_1-ATP synthase, we cannot completely eliminate the possibility that intrinsically

uncoupled F_oF_1-ATP synthase exists, because we could not accurately measure the amount of uncoupled F_oF_1-ATP synthase in intact cells.

G0s2 was first identified in cultured monocytes during the drug-induced cell cycle transition from G0 to G1 phase (18, 32). A limited number of studies have implied that G0s2 is involved in cell proliferation (33), differentiation (19), apoptosis (34), inflammation (35), and lipid metabolism (36) in various cellular settings. Moreover, G0s2 was reported to localize to the cytosol (33), endoplasmic reticulum (19), mitochondria (34), or the surface of lipid droplets (36). How G0s2 distinguishes these multiple functions is still not clear. In our hands, G0s2 is always localized to mitochondria, which was shown by immunostaining with two antibodies against different epitopes of G0s2 (Fig. S6). Complete depletion of mitochondrial staining by G0s2 knockdown strongly suggests the specific localization of G0s2 to mitochondria. We also showed that G0s2 specifically bound to mitochondrial F_oF_1-ATP synthase but not other OXPHOS protein complexes and functionally regulated OXPHOS activity. Together, these data suggest that G0s2 acts in the mitochondria. However, different cellular conditions may change the localization and role of G0s2. Additionally, G0s2-mediated changes in ATP metabolism may possibly affect the lipid metabolism or cellular proliferation. Additional studies will reveal the functional mechanisms by which G0s2 exerts these multiple functions in different cellular conditions.

In this study, we evaluated $[ATP]_{mito}$ and $[ATP]_{cyto}$ separately using FRET-based ATP biosensors in living cells. This dual evaluation revealed that $[ATP]_{mito}$ reflected mitochondrial ATP production with much greater sensitivity than $[ATP]_{cyto}$ (Fig. 1 and Movies S1 and S2). Because $[ATP]_{cyto}$ is strongly influenced by the activity of various cytosolic ATP hydrolytic enzymes and ATP buffering enzymes, $[ATP]_{cyto}$ does not always reflect the ATP availability that determines cellular function.

Taken together, our results indicate that G0s2 is a positive regulator of OXPHOS that works to increase the mitochondrial ATP production rate even under hypoxic conditions. Therefore, enhancing the level and function of G0s2 could be beneficial for hypoxia- and mitochondria-related disorders, such as ischemic diseases, metabolic diseases, and cancer.

Materials and Methods

Cells were infected with adenovirus encoding FRET-based ATP indicators AT1.03 or mit-AT1.03 to measure changes in cytosolic or mitochondrial ATP concentrations, respectively. Image acquisitions and FRET analyses were performed as described previously with some modifications (13). For the control of oxygen concentration during time-lapse imaging, digital gas mixer for stage-top incubator GM8000 (Tokai Hit) was used to create hypoxic (1% O_2) or normoxic (20% O_2) condition. Additional methods are found in SI Materials and Methods.

ACKNOWLEDGMENTS. We thank M. Murata for helpful discussions and advice, H. Miyagi (Olympus Co. Ltd.) for technical advice regarding microscopy, T. Miyazaki (Cyclex Co. Ltd.) for making antibodies, S. Ikezawa and A. Ogai for technical assistance, K. Tanaka for help with the purification of bovine F_oF_1-ATP synthase, and Y. Okada and H. Fujii for secretarial support. This research was supported by the Japan Society for the Promotion of Science through the Funding Program for Next Generation World-Leading Researchers (NEXT Program) initiated by the Council for Science and Technology Policy; grants-in-aid from the Ministry of Health, Labor, and Welfare–Japan; and grants-in-aid from the Ministry of Education, Culture, Sports, Science, and Technology–Japan. This research was also supported by grants from Takeda Science Foundation, Japan Heart Foundation, Japan Cardiovascular Research Foundation, Japan Intractable Diseases Research Foundation, Japan Foundation of Applied Enzymology, Japan Medical Association, Uehara Memorial Foundation, Mochida Memorial Foundation, Banyu Foundation, Naito Foundation, Inoue Foundation for Science, Osaka Medical Research foundation for Intractable Diseases, Ichiro Kanehara Foundation, and Showa Houkoukai.

1. Kim JW, Tchernyshyov I, Semenza GL, Dang CV (2006) HIF-1-mediated expression of pyruvate dehydrogenase kinase: A metabolic switch required for cellular adaptation to hypoxia. Cell Metab 3(3):177–185.
2. Papandreou I, Cairns RA, Fontana L, Lim AL, Denko NC (2006) HIF-1 mediates adaptation to hypoxia by actively downregulating mitochondrial oxygen consumption. Cell Metab 3(3): 187–197.
3. Semenza GL (2012) Hypoxia-inducible factors in physiology and medicine. Cell 148(3): 399–408.
4. Semenza GL, et al. (1996) Hypoxia response elements in the aldolase A, enolase 1, and lactate dehydrogenase A gene promoters contain essential binding sites for hypoxia-inducible factor 1. J Biol Chem 271(51):32529–32537.
5. Chen YC, et al. (2012) Identification of a protein mediating respiratory supercomplex stability. Cell Metab 15(3):348–360.
6. Fukuda R, et al. (2007) HIF-1 regulates cytochrome oxidase subunits to optimize efficiency of respiration in hypoxic cells. Cell 129(1):111–122.
7. Strogolova V, Furness A, Robb-McGrath M, Garlich J, Stuart RA (2012) Rcf1 and Rcf2, members of the hypoxia-induced gene 1 protein family, are critical components of the mitochondrial cytochrome bc1-cytochrome c oxidase supercomplex. Mol Cell Biol 32(8):1363–1373.
8. Saks V, et al. (2006) Cardiac system bioenergetics: Metabolic basis of the Frank-Starling law. J Physiol 571(Pt 2):253–273.
9. Smolenski RT, Lachno DR, Ledingham SJ, Yacoub MH (1990) Determination of sixteen nucleotides, nucleosides and bases using high-performance liquid chromatography and its application to the study of purine metabolism in hearts for transplantation. J Chromatogr A 527(2):414–420.
10. Shimura D, et al. (2013) Metabolomic profiling analysis reveals chamber-dependent metabolite patterns in the mouse heart. Am J Physiol Heart Circ Physiol 305(4):H494–H505.
11. Kemp GJ, Meyerspeer M, Moser E (2007) Absolute quantification of phosphorus metabolite concentrations in human muscle in vivo by 31P MRS: A quantitative review. NMR Biomed 20(6):555–565.
12. Ford SR, et al. (1996) Use of firefly luciferase for ATP measurement: Other nucleotides enhance turnover. J Biolumin Chemilumin 11(3):149–167.
13. Imamura H, et al. (2009) Visualization of ATP levels inside single living cells with fluorescence resonance energy transfer-based genetically encoded indicators. Proc Natl Acad Sci USA 106(37):15651–15656.
14. Lopaschuk GD, Kelly DP (2008) Signalling in cardiac metabolism. Cardiovasc Res 79(2): 205–207.
15. Hattori F, et al. (2010) Nongenetic method for purifying stem cell-derived cardiomyocytes. Nat Methods 7(1):61–66.
16. Forsythe JA, et al. (1996) Activation of vascular endothelial growth factor gene transcription by hypoxia-inducible factor 1. Mol Cell Biol 16(9):4604–4613.
17. Wolf A, et al. (2011) Hexokinase 2 is a key mediator of aerobic glycolysis and promotes tumor growth in human glioblastoma multiforme. J Exp Med 208(2):313–326.
18. Russell L, Forsdyke DR (1991) A human putative lymphocyte G0/G1 switch gene containing a CpG-rich island encodes a small basic protein with the potential to be phosphorylated. DNA Cell Biol 10(8):581–591.
19. Zandbergen F, et al. (2005) The G0/G1 switch gene 2 is a novel PPAR target gene. Biochem J 392(Pt 2):313–324.
20. Heckmann BL, Zhang X, Xie X, Liu J (2013) The G0/G1 switch gene 2 (G0S2): Regulating metabolism and beyond. Biochim Biophys Acta 1831(2):276–281.
21. Dimroth P, von Ballmoos C, Meier T (2006) Catalytic and mechanical cycles in F-ATP synthases. Fourth in the Cycles Review Series. EMBO Rep 7(3):276–282.
22. Senior AE (2007) ATP synthase: Motoring to the finish line. Cell 130(2):220–221.
23. Walker JE (1998) ATP synthesis by rotary catalysis (Nobel Lecture). Angew Chem Int Ed 37:5000–5011.
24. Yoshida M, Muneyuki E, Hisabori T (2001) ATP synthase—a marvellous rotary engine of the cell. Nat Rev Mol Cell Biol 2(9):669–677.
25. Fujikawa M, Yoshida M (2010) A sensitive, simple assay of mitochondrial ATP synthesis of cultured mammalian cells suitable for high-throughput analysis. Biochem Biophys Res Commun 401(4):538–543.
26. Adachi K, et al. (2007) Coupling of rotation and catalysis in F(1)-ATPase revealed by single-molecule imaging and manipulation. Cell 130(2):309–321.
27. Itoh H, et al. (2004) Mechanically driven ATP synthesis by F1-ATPase. Nature 427(6973):465–468.
28. Noji H, Yasuda R, Yoshida M, Kinosita K, Jr. (1997) Direct observation of the rotation of F1-ATPase. Nature 386(6622):299–302.
29. Rondelez Y, et al. (2005) Highly coupled ATP synthesis by F1-ATPase single molecules. Nature 433(7027):773–777.
30. Uchihashi T, Iino R, Ando T, Noji H (2011) High-speed atomic force microscopy reveals rotary catalysis of rotorless F_1-ATPase. Science 333(6043):755–758.
31. Giorgio V, et al. (2009) Cyclophilin D modulates mitochondrial F0F1-ATP synthase by interacting with the lateral stalk of the complex. J Biol Chem 284(49):33982–33988.
32. Siderovski DP, Blum S, Forsdyke RE, Forsdyke DR (1990) A set of human putative lymphocyte G0/G1 switch genes includes genes homologous to rodent cytokine and zinc finger protein-encoding genes. DNA Cell Biol 9(8):579–587.
33. Yamada T, Park CS, Burns A, Nakada D, Lacorazza HD (2012) The cytosolic protein G0S2 maintains quiescence in hematopoietic stem cells. PLoS ONE 7(5):e38280.
34. Welch C, et al. (2009) Identification of a protein, G0S2, that lacks Bcl-2 homology domains and interacts with and antagonizes Bcl-2. Cancer Res 69(17):6782–6789.
35. Kobayashi S, et al. (2008) Expression profiling of PBMC-based diagnostic gene markers isolated from vasculitis patients. DNA Res 15(4):253–265.
36. Yang X, et al. (2010) The G(0)/G(1) switch gene 2 regulates adipose lipolysis through association with adipose triglyceride lipase. Cell Metab 11(3):194–205.

Atherosclerosis 227 (2013) 373e379

Contents lists available at SciVerse ScienceDirect

Atherosclerosis

journal homepage: www.elsevier.com/locate/atherosclerosis

Decreased mortality associated with statin treatment in patients with acute myocardial infarction and lymphotoxin-alpha C804A polymorphism

Shinichiro Suna [a,1], Yasuhiko Sakata [a,b,*,1], Daisaku Nakatani [a,1], Keiji Okuda [a,1], Masahiko Shimizu [a,1], Masaya Usami [a,1], Sen Matsumoto [a,1], Masahiko Hara [a,1], Kouichi Ozaki [c,1], Hiroya Mizuno [a,1], Tetsuo Minamino [a,1], Seiji Takashima [a,1], Masami Nishino [d,1], Yasushi Matsumura [e,1], Hiroshi Takeda [e,1], Toshihiro Tanaka [c,1], Hiroshi Sato [f,1], Masatsugu Hori [g,1], Issei Komuro [a,1]

[a] Department of Cardiovascular Medicine, Osaka University Graduate School of Medicine, Suita, Japan
[b] Department of Evidence-Based Cardiovascular Medicine, Tohoku University Graduate School of Medicine, Sendai, Japan
[c] Laboratory for Cardiovascular Diseases, SNP Research Center, RIKEN Center for Genomic Medicine, Yokohama, Japan
[d] Osaka Rosai Hospital, Sakai, Japan
[e] Department of Medical Information Science, Osaka University Graduate School of Medicine, Suita, Japan
[f] School of Human Welfare Studies, Kwansei Gakuin University, Nishinomiya, Japan
[g] Osaka Medical Center for Cancer and Cardiovascular Disease, Osaka, Japan

a r t i c l e i n f o

Article history:
Received 23 August 2012
Received in revised form
11 January 2013
Accepted 14 January 2013
Available online 25 January 2013

Keywords:
Lymphotoxin alpha
Myocardial infarction
Single nucleotide polymorphism
Statin

a b s t r a c t

Aims: We previously reported the association of single nucleotide polymorphisms in the lymphotoxin alpha (LTa) gene with susceptibility to acute myocardial infarction (AMI) and increased mortality after discharge. In the present study, we investigated whether the adverse effect of LTa C804A polymorphism on mortality could be pharmacologically modified by statin treatment after AMI.

Methods and results: We conducted a multicenter study that included 3486 post-AMI patients between 1998 and 2008. During a median follow-up period of 1775 days, 247 deaths were recorded. The mortality rate was significantly higher in LTa 804A allele carriers compared to non-804A allele carriers (7.9% vs. 5.7%, p ¼ 0.011). The LTa 804A allele was significantly associated with increased mortality for post-AMI patients not receiving statins (hazard ratio [HR]: 1.48, 95% confidence interval [CI]: 1.03e2.12, p ¼ 0.034), but not for those receiving statins (HR: 1.22, 95% CI: 0.70e2.10, p ¼ 0.486). In-vitro experimental analyses demonstrated that the LTa 804A polymorphic protein, 26Asn-LTa$_3$, induced monocyte-endothelial interaction and endoplasmic reticulum (ER) stress in cardiomyocytes more strongly than the LTa$_3$ 804C polymorphic protein 26Thr-LTa$_3$. However, the effects of both LTa$_3$ proteins were decreased and became comparable by the pretreatment of cells with pravastatin.

Conclusion: LTa C804A polymorphism was associated with an increased risk of mortality for AMI patients, although this effect was masked in patients treated with statins. This finding is supported by the observed attenuation of 26Asn-LTa$_3$-mediated monocyte-endothelial interaction and ER stress in cardiomyocytes treated with pravastatin. LTa C804A polymorphism may have potential as a novel therapeutic target for secondary prevention after AMI.

1. Introduction

Myocardial infarction (MI) is one of the major causes of death in developed countries. Although the implementation of evidence-based therapies has greatly reduced mortality [1,2], the long-term mortality rate after discharge for AMI remains high. Because personal risk after AMI survival dramatically varies demographically, the development of improved secondary prevention programs,

Abbreviations: AMI, acute myocardial infarction; Asn, asparagine; CI, confidence interval; ER, endoplasmic reticulum; GRP, glucose-regulated protein; HR, hazard ratio; HUVEC, human umbilical vein endothelial cells; LTa, lymphotoxin alpha; SNPs, single nucleotide polymorphisms; Thr, threonine; TNF, tumor necrosis factor; VCAM1, vascular cell adhesion molecules 1.

* Corresponding author. Department of Evidence-based Cardiovascular Medicine, Tohoku University Graduate School of Medicine, 1-1 Seiryo-machi, Aoba-ku, Sendai 980-8574, Japan. Tel.: þ81 22 717 7152; fax: þ81 22 717 7156.
E-mail address: sakatayk@cardio.med.tohoku.ac.jp (Y. Sakata).
[1] On behalf of the Osaka Acute Coronary Insufficiency Study.

0021-9150/$ e see front matter © 2013 Elsevier Ireland Ltd. All rights reserved.
http://dx.doi.org/10.1016/j.atherosclerosis.2013.01.020

including personalized therapy approaches is necessary to reduce post-AMI mortality. In particular, therapeutic approaches that take into account genetically determined risk may have great potential for personalized treatments that improve adverse outcomes after MI.

Recently, others and we identified that single nucleotide polymorphisms (SNPs) in the genes encoding lymphotoxin alpha (LTa) and its associated proteins are associated with AMI onset [3e8]. LTa is a proinflammatory cytokine with homology to inflammatory cytokine tumor necrosis factor (TNF)-a [9e11] and is related with the development of atherosclerotic lesions in coronary arteries [12,13]. Interestingly, SNPs in the LTa gene are associated with both increased susceptibility to AMI onset post-AMI mortality [14]. Based on the pro-inflammatory characteristics of LTa, we hypothesized that the adverse effects of LTa polymorphism could be mediated by statins, which are one of the most widely prescribed medicines with anti-inflammatory properties [15].

Here, we investigated the pharmacogenetic interactions between LTa C804A polymorphism and statins in post-AMI patients, and attempted to determine the underlying mechanisms through in-vitro analyses.

2. Materials and methods

2.1. Epidemiologic data regarding the impact of LTa C804A polymorphism

Among 10,076 consecutive Japanese AMI patients who were registered in the Osaka Acute Coronary Insufficiency Study (OACIS) between 1998 and 2008, we enrolled 3486 patients who were discharged alive and submitted samples for the genetic analysis performed in this study. Details of the OACIS and genotyping have been reported elsewhere [14,16]. All patients provided written informed consent, and the study protocol complied with the Guidelines for Genome/Genetic Research issued by the Japanese government and was approved by the ethics committee of each institution.

The patients were divided into two groups according to the presence (n ¼ 1390; statin(þ) group) or absence (n ¼ 2096; statin(−) group) of statin treatment at discharge. In each group, the incidence of all-cause mortality was compared between patients with the AA or CA genotype (A allele carriers) and those with the CC genotype (non-A allele carriers) of LTa C804A polymorphism. LTa C804A polymorphism (rs1041981) was determined using an automated fluorescent allele-specific DNA primer assay (Toyobo Gene Analysis, Tsuruga, Japan) [17].

2.2. Cell culture and materials

Human umbilical vein endothelial cells (HUVEC) were purchased from Clonetics (San Diego, CA, USA) and cultured in EGM-2 SingleQuots endothelial cell medium (Clonetics) at 37 °C in a humidified 5% CO_2 incubator. Cells from passages three to eight were used for experiments. THP1 cells, a human acute monocytic leukemia cell line, were purchased from ATCC (Manassas, VA, USA) and cultured in RPMI 1640 medium (Clonetics) containing 10% fetal calf serum, 2 mM glutamine, and 1% penicillin/streptomycin at 37 °C in a humidified 5% CO_2 incubator [12]. Recombinant 26Thr-LTa_3 and 26Asn-LTa_3 proteins were expressed in Escherichia coli using the pET29 system (Novagen, Madison, WI, USA) and purified as previously described [8]. Cytotoxic assays were conducted in the WEHI164s fibrosarcoma cell line (provided by the Institute of Development, Aging and Cancer, Tohoku University). Pravastatin was obtained from Daiichi-Sankyo (Tokyo, Japan).

2.3. Neonatal rat cardiomyocyte preparation

Primary ventricular myocytes were isolated from neonatal rats, purified by Percoll density gradient centrifugation, and pre-plated for 1 h to enrich for cardiac myocytes (95%). The obtained cells were plated at a density of 7.5×10^5 cells per well (3.5-cm diameter), and then cultured in Dulbecco's Modified Eagle Medium (Invitrogen, Camarillo, CA, USA) containing 10% fetal calf serum, 2 mM glutamine, and 1% penicillin/streptomycin at 37 °C in a humidified 5% CO_2 incubator [18].

2.4. Monocyte-endothelial cell adhesion assay

We previously reported that LTa_3 increases monocyte-endothelial interactions in vitro [12]. To investigate the effects of LTa C804A polymorphism and statin treatment on monocyte-endothelial cell interactions, cell adhesion assays involving THP1 cells and HUVEC were conducted. As LTa C804A polymorphism replaces threonine with asparagine at residue 26 (Thr26Asn) in the LTa_3 protein, recombinant 26Thr- and 26Asn-LTa_3 were compared. For the assay, HUVEC were first cultured in 96-well microplates (Asahi Techno Glass, Tokyo, Japan) for two days to form monolayers, and were then incubated with 1 ng/ml 26Thr-LTa_3 or 26Asn-LTa_3 for 5 h prior to performing the adhesion assay. The effects of pravastatin treatment on adhesion of THP1 cells to HUVEC were also examined by adding 10 mM pravastatin to HUVEC cultures 12 h before stimulation with LTa_3 [12]. Further details of this assay are shown in supplementary method.

2.5. Vascular cell adhesion molecule 1 (VCAM1) assay

To determine the influence of 26Thr-LTa_3 and 26Asn-LTa_3 on the expression of VCAM1, Western blot analysis was performed as previously described [12]. Briefly, total cellular protein (10e20 mg) was obtained from HUVEC after stimulation with 1 ng/ml 26Thr-LTa_3 or 26Asn-LTa_3 for 6 h. To evaluate whether the effects of 26Thr-LTa_3/26Asn-LTa_3 on VCAM1 expression were influenced by pravastatin treatment, 10 mM pravastatin was added 12 h before 26Thr-LTa_3/26Asn-LTa_3 stimulation of HUVEC cultures. VCAM1 and actin were detected using anti-VCAM1 and anti-actin antibodies, respectively (Santa Cruz Biotechnology, Santa Cruz, CA, USA).

2.6. Monocyte migration assay

The migration of monocytes to HUVEC was analyzed using a modified Boyden chamber method. Briefly, HUVEC were cultured in the lower compartments of 24-well Transwell® microplates (Corning, Acton, MA, USA) for two days to form a monolayer. To investigate the effects of LTa C804A polymorphism on the migration of THP1 cells to HUVEC, HUVEC were incubated with 1 ng/ml 26Thr-LTa_3 or 26Asn-LTa_3 for 5 h prior to performing the migration assay. We also examined the effects of pravastatin treatment on monocytes migration by adding 10 mM pravastatin to HUVEC cultures 12 h before stimulation with LTa_3. Further details of this assay are shown in Supplementary Methods.

2.7. Endoplasmic reticulum (ER) stress in rat neonatal cardiomyocytes

ER stress induced by LTa_3 on rat neonatal cardiomyocytes was evaluated by treating rat cardiomyocytes with either 10 ng/ml 26Thr-LTa_3 or 26Asn-LTa_3 for 24 h. The effects of pravastatin on 26Thr-LTa_3/26Asn-LTa_3-induced ER stress were evaluated by adding 10 mM pravastatin to cultures of rat cardiomyocytes 24 h before stimulation with LTa_3. For Western blot analysis, Glucose-regulated

protein 94 kDa (GRP94) and 78 kDa (GRP78) were detected using anti-GRP94 and anti-GRP78 antibodies, respectively (Assay Designs, Ann Arbor, MI, USA), and GAPDH was detected using anti-GAPDH antibody (Millipore, Billerica, MA, USA).

2.8. Statistical analysis

All statistical analyses were performed with either SPSS 11.0 software (SPSS Inc., Tokyo, Japan) or R software (http://www.R-project.org/). For epidemiologic analysis, discrete variables were expressed as counts or percentages, as indicated, and compared with the c^2-test. Continuous variables were expressed as the mean ± SD and compared using the unpaired Student's t-test. Survival curves were constructed using the KaplaneMeier method and differences in mortality rates were compared between groups with the Log-rank test. Cox regression analyses were used to determine whether LTa C804A polymorphism was an independent predictor of mortality. For experimental analysis, data are presented as the mean ± SE. Statistical significance was determined by the unpaired Student's t-test or one-way ANOVA followed by Bonferroni's correction, except for the analysis of GRP78/94, for which ManneWhitney's U test was used. All reported p values are two-sided, and statistical significance was defined as $p < 0.05$.

3. Results

3.1. Impact of LTa C804A polymorphism on mortality and statin treatment in post-AMI patients

Among 10,076 consecutive Japanese AMI patients who were registered in the Osaka Acute Coronary Insufficiency Study (OACIS) between 1998 and 2008, typing for this polymorphism was conducted for 3506 post AMI patients, and successful typing was obtained for 3486 patients, which denotes call rate was 99.4% (Suppl. Fig. 1). The prevalence of the C804A genotypes was as follows: CC 1333(38.2%), CA 1592(45.7%), AA 561(16.1%) (p ¼ 0.020 by HardyeWeinberg equilibrium test) (Suppl. Table 1).

After comparing the incidence of all-cause mortality among patients with the three genotypes of LTa C804A polymorphism, a similar trend of increasing mortality for patients with the AA and CA genotypes was detected (Suppl. Fig. 2). Therefore, we selected LTa C804A polymorphism as a dominant parameter and compared the incidence of all-cause mortality between patients with the AA or CA genotype (A allele carriers) and those with the CC genotype (non-A allele carriers). The baseline characteristics of all subjects and the two patient subgroups, consisting of those with (statin(þ)) and without (statin(−)) statin treatment at discharge, are shown in Table 1 and Suppl. Table 2. In both patient subgroups, no significant differences were detected in the baseline characteristics between LTa 804A allele carriers (AA þ CA genotypes) and non-804A allele carriers (CC genotypes), except for age and reperfusion therapy. Age was significantly younger and reperfusion rate was significantly higher in the former subgroup.

A total of 247 deaths were recorded during the median follow-up period of 1775 days. KaplaneMeier curves were constructed for patients based on LTa C804A polymorphism (Fig. 1A), revealing that 804A allele carriers had significantly higher all-cause mortality than that of non-804A allele carriers (7.9% vs. 5.7%, p ¼ 0.011). We also plotted KaplaneMeier curves for all-cause mortality among subgroups that were divided based on treatment with statins at discharge (Fig. 1B). For patients not receiving statin therapy (statin(−)), all-cause mortality was significantly higher in 804A carriers compared to non-804A carriers (9.8% vs. 6.8%, p ¼ 0.025), but did not differ among those receiving statin therapy (statin(þ))

Table 1
Patient demographics based on lymphotoxin alpha C804A polymorphism.

	LTA 804 polymorphism		p Value
	Non-A allele carrier (CC) N ¼ 1333	A allele carrier (AA þ AC) N ¼ 2153	
Age (y.o.)	64.7± 11.0	63.9± 11.4	0.035
Male (%)	77.8	78.1	0.853
BMI (kg/m^2)	23.9± 3.4	23.8± 3.4	0.686
DM (%)	31.0	34.2	0.053
HT (%)	58.9	59.2	0.869
HL (%)	48.5	47.0	0.404
Smoking (%)	64.6	65.3	0.691
OMI (%)	10.5	11.5	0.343
AP (%)	24.2	24.8	0.695
Admission < 24 h (%)	39.9	38.3	0.335
STEMI (%)	86.4	86.5	0.959
peak CK > 3000(%)	31.6	34.8	0.061
Killip > 1 at admission (%)	11.8	13.3	0.193
T-Cho (mg/dl) at admission	197.9± 42.9	195.6± 44.7	0.145
HDL-Cho (mg/dl)	46.8± 12.7	46.1± 12.3	0.093
Multi-vessel disease (%)	33.9	37.3	0.050
Reperfusion therapy (%)	89.5	91.8	0.023
Stent (%)	78.8	77.0	0.249
Thrombectomy (%)	39.1	39.4	0.883
Final TIMI3 (%)	89.2	88.1	0.338
ACEIs (%)	54.4	54.9	0.768
ARBs (%)	23.9	24.2	0.842
ACEIs or ARBs (%)	76.4	76.6	0.921
Beta blockers (%)	45.0	47.6	0.135
Ca blockers (%)	21.3	21.1	0.904
Statin (%)	41.4	38.9	0.145
Diuretics (%)	24.8	27.7	0.057
Anti-platelets (%)	98.3	98.2	0.800
Nitrates (%)	37.7	39.5	0.304
Anti-coagulants (%)	18.8	18.4	0.816
T-Cho (mg/dl) at discharge	186.9± 35.1	185.4± 36.4	0.339
HDL-Cho (mg/dl)	38.8± 10.7	38.0± 10.7	0.110

Patient characteristics between LTa 804A allele carriers (AA þ AC) and non-804A allele carriers (CC).
Discrete variables are expressed as counts or percentages, as indicated, and were compared with the c^2-test. Continuous variables are expressed as the mean ± SD, and were compared with the unpaired Student's t-test.
LTa ¼ lymphotoxin alpha; BMI ¼ body mass index; DM ¼ diabetes mellitus; HT ¼ hypertension; HL ¼ hyperlipidemia; OMI ¼ old myocardial infarction; AP ¼ angina pectoris; STEMI ¼ ST elevation myocardial infarction; CK ¼ creatinine kinase; T-Cho ¼ total cholesterol; HDL-Cho ¼ high density lipoprotein cholesterol; PCI ¼ percutaneous coronary intervention; emergent PCI ¼ PCI performed within 24 h after the onset of MI; Multi-vessel disease ¼ two or three vessel disease; Final TIMI3 ¼ final TIMI3 acquisition at reperfusion therapy; ACEI ¼ angiotensin converting enzyme inhibitor; ARB ¼ angiotensin II receptor blocker; Ca blockers ¼ calcium channel antagonists at discharge.

(5.0% vs. 4.2%, p ¼ 0.345), suggesting that the mortality effects of LTa C804A polymorphism are influenced by statin therapy.

Cox's proportional hazard analysis confirmed that the 804A allele was significantly associated with increased mortality (Table 2, adjusted HR 1.44, 95% CI: 1.06e1.95, p ¼ 0.018). Interestingly, this trend was evident for patients without statin treatment at discharge (adjusted HR 1.48, 95% CI: 1.03e2.12, p ¼ 0.034), but not for those who were treated with statins at discharge (adjusted HR: 1.22, 95% CI: 0.70e2.10, p ¼ 0.486) (Table 2).

3.2. LTa-induced adhesion of THP1 cells to endothelial cells is attenuated by pravastatin

As shown in Fig. 2A, both 26Thr-LTa_3 and 26Asn-LTa_3, corresponding to LTa 804C- and 804A-polymorphic proteins, respectively, increased the adhesion of THP1 cells to HUVEC monolayers when compared with controls ($p < 0.001$). Notably, exposure of HUVEC to 26Asn-LTa_3 led to greater increases in the adhesion rate

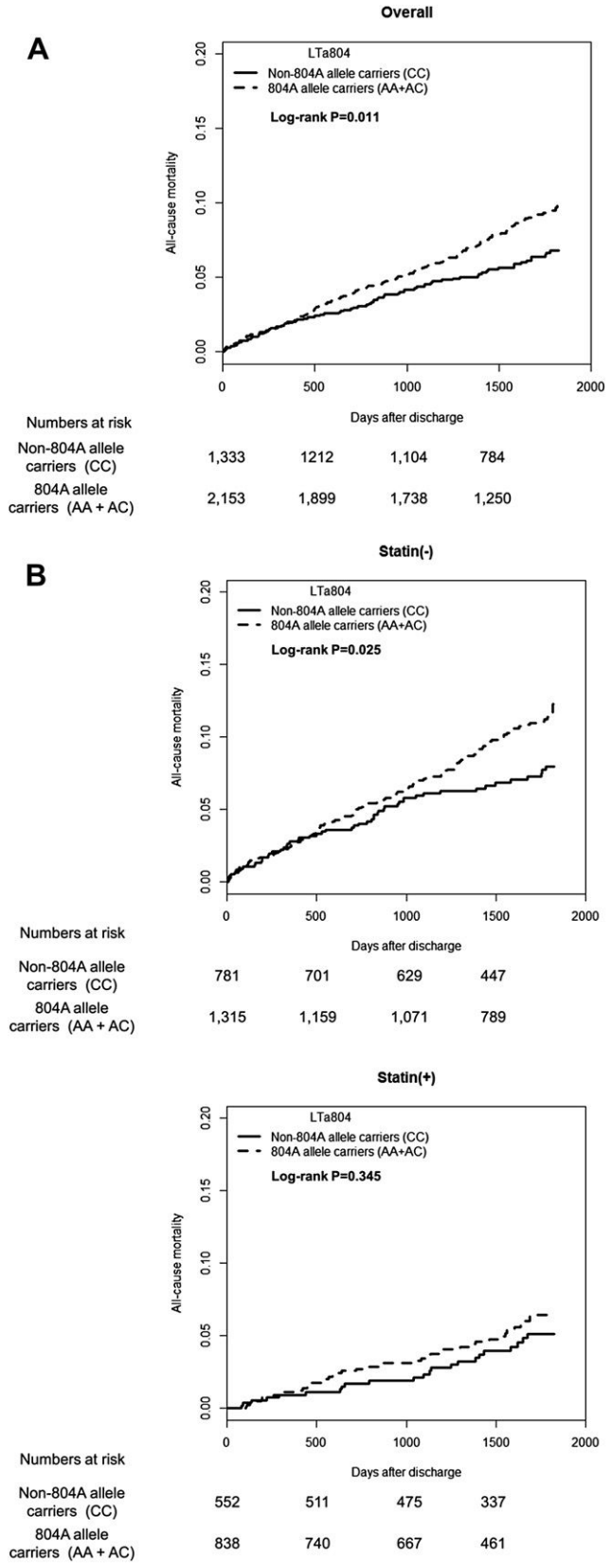

Fig. 1. All-cause mortality for AMI patients in relation to LTa C804A polymorphism and statin treatment. A. All-cause mortality rate was significantly higher in LTa 804A allele carriers (AA þ AC, N ¼ 2153) (dotted line) than in non-804A allele carriers (CC, N ¼ 1333) (solid line) (p ¼ 0.011 by the Log-rank test). B. All-cause mortality rate was significantly higher in LTa 804A allele carriers (AA þ AC) (dotted line) than in non-804A allele carriers (CC) (solid line) in the subgroup without statin therapy (statin(−)) (p ¼ 0.025 by the Log-rank test), whereas no difference was detected between the LTa C804A polymorphism groups for those that received statin therapy (statin(þ)) (p ¼ 0.345 by the Log-rank test).

Table 2
Hazard ratio for all-cause mortality among LTa 804A allele carriers in the presence or absence of statin prescription at discharge.

	Death	Total N	HR	95% CI	p Value
Model 1					
Overall	247	3486	1.42	1.08e1.86	0.011
Statin(−)	182	2096	1.44	1.04e1.98	0.026
Statin(þ)	65	1390	1.28	0.77e2.12	0.346
Model2					
Overall	247	3486	1.49	1.14e1.96	0.004
Statin(−)	182	2096	1.54	1.12e2.13	0.008
Statin(þ)	65	1390	1.33	0.80e2.20	0.278
Model 3					
Overall	199	3024	1.40	1.04e1.89	0.027
Statin(−)	144	1784	1.48	1.03e2.12	0.034
Statin(þ)	55	1240	1.22	0.70e2.10	0.486

Model 1. Hazard ratio of LTa 804A allele carriers (AA þ AC) for all-cause mortality (unadjusted).
Model 2. The hazard ratio of LTa 804A-allele carriers on all-cause mortality after being discharged alive was analyzed by Cox regression analysis. Covariates were age and sex.
Model 3. Model 2 þ diabetes mellitus, hypertension, hyperlipidemia, smoking history, peak CK 2: 3,000, multi-vessel disease, reperfusion therapy, and ACEI/ARBs, beta blockers at discharge.
Abbreviations are the same as those used in Table 1.

compared to that of 26Thr-LTa_3 (2.36 vs. 2.03 fold, respectively, compared with control; $p < 0.05$), although the rate decreased and was comparable between the groups (1.58 vs. 1.43 fold, respectively, p ¼ n.s.) after the pretreatment of HUVEC with pravastatin. Western blotting revealed that the expression level of VCAM1 on HUVEC was markedly increased by treatment with 26Asn-LTa_3 compared to that with 26Thr-LTa_3. However, both 26Asn- and 26Thr-LTa_3-induced VCAM1 expression was attenuated at similar levels by pravastatin (Fig. 2B).

3.3. LTa-induced monocyte migration is attenuated by pravastatin

In a two-chamber migration assay, the migration rate of THP1 towards the HUVEC-conditioned medium markedly increased by exposure to 26Thr-LTa_3 and 26Asn-LTa_3 when compared with controls ($p < 0.001$). In the absence of pravastatin pretreatment, the migration ratio displayed a larger increase for 26Asn-LTa_3 stimulation compared to 26Thr-LTa_3 (2.14 vs. 1.55 fold compared with control, $p < 0.05$), whereas the two LTa proteins displayed similar small effects in the presence of pravastatin (1.48 vs. 1.46 fold compared with control, p ¼ n.s.) (Fig. 2C).

3.4. LTa-induced ER stress in rat cardiomyocytes is attenuated by pravastatin

GRP78 expression levels in rat neonatal cardiomyocytes were increased by LTa_3 stimulation after 24 h when compared with controls ($p < 0.001$) (Fig. 3A and B). Exposure to 26Asn-LTa_3 led to greater GRP78 expression compared to that induced by 26Thr-LTa_3 (1.68 vs. 1.53 fold compared with control, $p < 0.05$ by Manne Whitney's U test), although no differences in expression were detected after the pretreatment of cardiomyocytes with 10 mM pravastatin (p ¼ n.s.). Similarly, GRP94 expression was also markedly increased following 26Asn-LTa_3 stimulation compared to exposure to 26Thr-LTa_3 (1.83 vs. 1.59 fold compared with control, $p < 0.05$ by ManneWhitney's U test) (Fig. 3C and D), and no

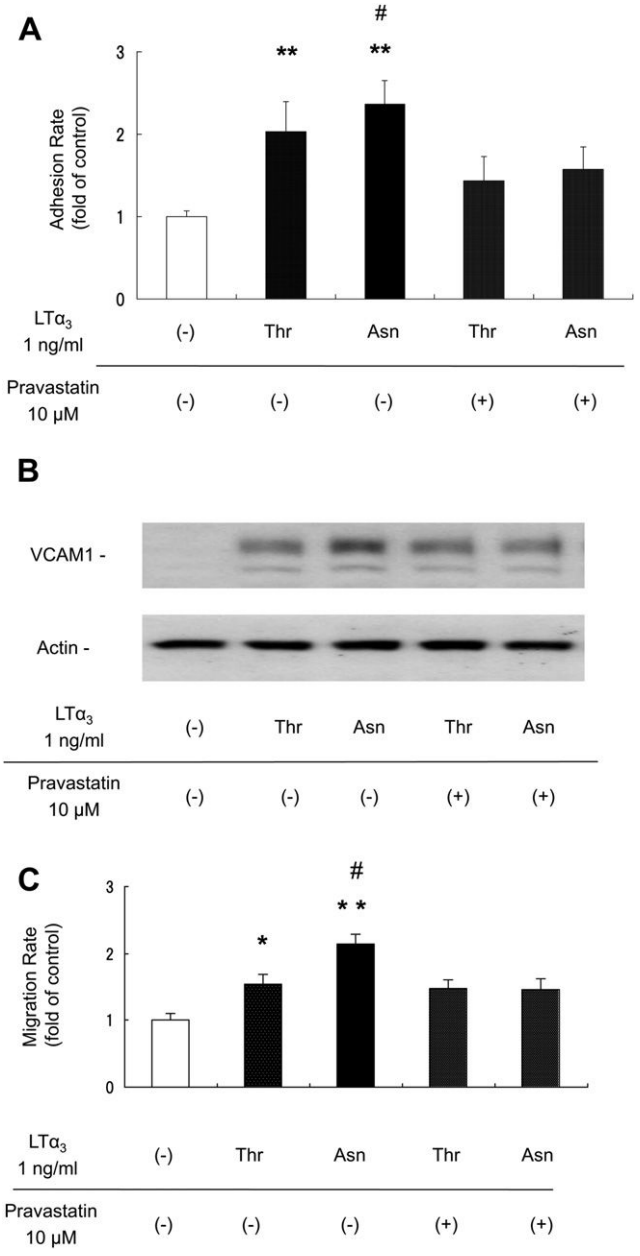

Fig. 2. Effects of LTa C804A polymorphism on monocyte-endothelial adhesion (A) and induction of VCAM1 expression (B) in the absence and presence of pravastatin treatment. Effect of LTa C804A polymorphism on THP1 cell migration rate (C). A. The adhesion rate of THP1 onto HUVEC was increased by both 26Thr-LTa$_3$ and 26Asn-LTa$_3$ stimulation of HUVEC. The adhesion rate was higher when cells were stimulated by 26Asn-LTa$_3$ than by 26Thr-LTa$_3$ (**p < 0.001 vs. control, #p < 0.05 vs. 26Thr-LTa$_3$ protein by the unpaired t-test), but the difference was reduced by the pretreatment of cells with 10 mM pravastatin. B. The expression levels of VCAM1 were increased by 26Thr-LTa$_3$ or 26Asn-LTa$_3$ stimulation in comparison with control. 26Asn-LTa$_3$ led to greater induction of VCAM1 expression compared to 26Thr-LTa$_3$, but VCAM1 was expressed at comparable levels for both proteins following the pretreatment of HUVEC with 10 mM pravastatin. A representative result among five independent experiments is shown. C. The migration rate of THP1 towards HUVEC was increased by both 26Thr-LTa$_3$ and 26Asn-LTa$_3$, although the rate was higher for cells stimulated with 26Asn-LTa$_3$ (2.14 vs. 1.55 fold when compared with control, **p < 0.001 vs. control, *p < 0.01 vs. control, and #p < 0.05 vs. 26Thr-LTa$_3$ by the unpaired t-test). However, no significant differences were detected between the two proteins following the pretreatment of HUVEC with 10 mM pravastatin (1.48 vs. 1.46 fold when compared with control by the unpaired t-test).

differences in expression were detected after pravastatin pretreatment (p ¼ n.s.).

4. Discussion

We previously reported the clinical impacts of polymorphisms in the genes encoding LTa and its related proteins on susceptibility to AMI and increased post-AMI mortality. The results of the present study further underline the importance of the LTa cascade in the pathogenesis of cardiovascular diseases by showing that a functional SNP in the LTa gene at C804A, which replaces threonine with asparagine at residue 26 (Thr26Asn), is associated with increased all-cause mortality after AMI. Furthermore, our findings suggest that LTa gene polymorphism has clinical significance as a therapeutic target, because a reduction of 26Asn-associated mortality risk by statin treatment was suggested in the cohort of post-AMI patients, as well as in the in-vitro experimental studies.

We found that LTa C804A polymorphism is also associated with increased mortality among AMI patients registered in OACIS, a prospective observational study of AMI being conducted in Osaka, Japan. However, this result was not entirely unexpected, as we previously reported that A252G polymorphism in the LTa gene, which has a strong linkage disequilibrium with C804A, is associated with increased post-AMI mortality [14]. Therefore, the most important finding of the present study was the demonstration of the pharmacological modification of the C804A-related mortality risk with statin treatment in the secondary prevention setting of post-AMI. Our findings also suggest that the pharmacological modification mediated by statin might be attributable to decreased monocyte-endothelial interaction and ER stress in cardiomyocytes.

The growth of atherosclerotic lesions involves the inflammatory response and is characterized by the adhesion of monocytes onto endothelial cells, migration of monocytes into intima, scavenging of lipoprotein particles, followed by the formation of foam cells and secretion of various pro-inflammatory cytokines [19]. We recently demonstrated that LTa$_3$ stimulation induces the expression of various genes involved in inflammation and cell adhesion, including VCAM1, which is a key player in the binding of monocytes to endothelial cells [20], in HUVEC and human coronary arterial endothelial cells [12,21]. In the present study, the stimulation of HUVEC with LTa 804A polymorphic protein (26Asn-LTa$_3$) markedly increased both the adhesion and the migration of monocytes to endothelial cells in comparison with LTa 804C polymorphic protein (26Thr-LTa$_3$). Notably, the differences between 26Asn- and 26Thr-LTa$_3$ were attenuated by the pretreatment of cells with pravastatin, a result that is consistent with our epidemiologic data. Additionally, we performed the experiments to elucidate whether or not LTa$_3$ could alter the transformation of monocytes into macrophages by the observation of morphological change with microscopy and by using fluorescent-labeled oxidized low-density lipoprotein (DiI-Ox-LDL, Biomedical Technologies Inc. Stoughton, MA, USA) followed by fluorescence activated cell sorting (FACS). However, we observed no transformation of monocytes into macrophages after LTa$_3$ stimulus, whereas Phorbol 12-myristate 13-acetate (PMA) stimulus induced the transformation.

Several reports have described the role of LTa in inflammation and atherosclerosis. Although the LTa signaling pathway is considered to be similar in part to that of TNFa, LTa appears to play a dominant role in the regulation of atherosclerotic lesion growth. Schreyer et al. [13] showed that TNFa deficiency did not alter lesion development in mice fed an atherogenic diet, whereas the loss of LTa resulted in a three-fold decrease in the amount of lesions. In addition, we previously revealed that LTa is expressed in the atherosclerotic plaques of patients with coronary artery disease [8]. The present data suggest that the increased risk of mortality

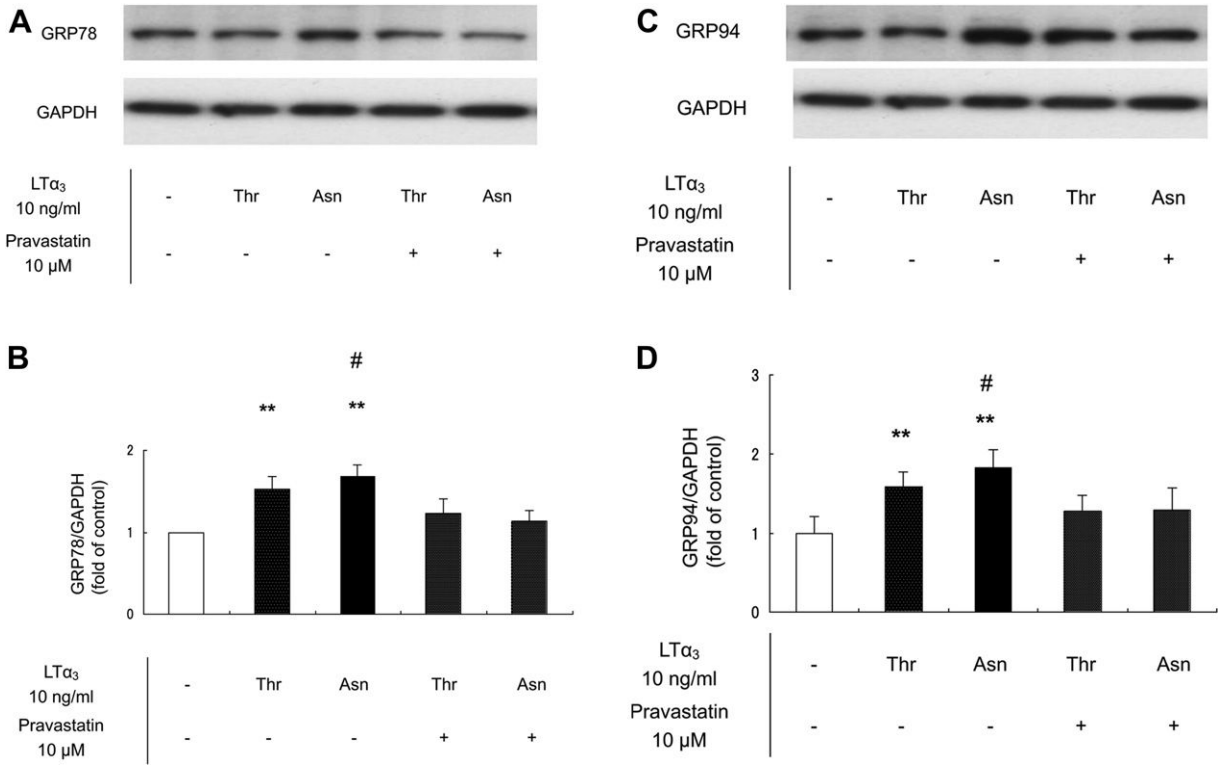

Fig. 3. Effect of LTa C804A polymorphism on the induction of ER stress in rat neonatal cardiomyocytes. The expression levels of glucose-regulated protein (GRP) 78 were increased in rat cardiomyocytes by stimulation with either 26Thr-LTa$_3$ or 26Asn-LTa$_3$ when compared with control cells (**$p < 0.001$) (A and B). 26Asn-LTa$_3$ had a greater effect on GRP78 expression compared to 26Thr-LTa$_3$ (1.68 vs. 1.53 fold when compared with control, #$p < 0.05$), but GRP78 expression induction was attenuated by 10 mM pravastatin pretreatment for both 26Thr-LTa$_3$ and 26Asn-LTa$_3$ ($p = n.s.$). The expression levels of GRP94 were also increased by 26Thr-LTa$_3$ or 26Asn-LTa$_3$ stimulation when compared with control cells (**$p < 0.001$) (C and D), but were higher for 26Asn-LTa$_3$ compared to 26Thr-LTa$_3$ (1.83 vs. 1.59 fold, #$p < 0.05$). The induction of GRP94 expression was also attenuated by the pretreatment of cardiomyocytes with pravastatin ($p = n.s.$).

associated with LTa C804A polymorphism can be lowered by statin treatment, and that the beneficial effects of statins for 804A allele carriers might be attributable to the attenuation of monocyte-endothelial interactions and cardiomyocyte degeneration. Previous experimental studies have revealed that statins attenuate the inflammatory response, including the decreased expression of adhesion molecules triggered by TNFa via the NFkB signaling pathway [22e25]. Considering that LTa shares major receptors (TNF receptors type I and II) with TNFa [11], it is reasonable to speculate that statins attenuate the LTa-induced inflammatory response, thereby preventing atherogenesis and cardiovascular events. Our present experimental data support this idea, as 26Asn-LTa$_3$ stimulation led to greater human monocyte-endothelial adhesion and monocyte migration compared to 26Thr-LTa$_3$, and the effects induced by both 26Asn- and 26Thr-LTa$_3$ were blunted and became comparable following pravastatin treatment.

Inflammation induced by pro-inflammatory cytokines is one of the major causes of ER stress, which is characterized by the accumulation of unfolded proteins induced by stimuli such as oxidative stress and ischemia. As ER stress in cardiomyocytes is followed by cardiac remodeling and heart failure [18,26,27], we evaluated whether LTa polymorphism is associated with the occurrence of ER stress. ER stress triggers the unfolded protein response, which involves a group of signal transduction pathways that ameliorate the accumulation of unfolded proteins in the ER by increasing the expression of ER-resident chaperones, such as GRP78/94. Thus, enhanced expression of GRP78/94 can be used as a marker of ER stress. Here, we found that ER stress in rat cardiomyocytes was significantly elevated by 26Asn-LTa$_3$ stimulation compared with that by 26Thr-LTa$_3$, and that these differences were blunted by pravastatin treatment. These findings may partly explain our observation that LTa 804A allele carriers had higher mortality after MI in the absence of statin treatment.

The preventive effects of statin therapy on cardiovascular events have been demonstrated in many clinical studies and are thought to be mediated, at least in part, by the pleiotropic effects, including anti-inflammatory and lipid-lowering activities [28e30]. However, despite considerable research efforts, the pleiotropic effects of statins remain poorly characterized and have yet to be demonstrated in the clinical setting [15]. In the present study, no significant differences were detected in the average total and HDL-cholesterol level between 804A allele and non-804A allele carriers in both statin(þ) and statin(−) subgroups, suggesting that LTa polymorphism does not modify cardiovascular risk by altering serum cholesterol levels. Therefore, we speculate that statins may mask the adverse effects of LTa polymorphisms via their pleiotropic properties, independently of their lipid-lowering effects.

Several limitations of our study warrant mention. First, the epidemiologic analyses were based on an observational study, and statin prescriptions were not randomized. However, the bias was likely minimal, because statins were prescribed by attending physicians without knowledge of patients' LTa genotype, and as a consequence, statin prescription was naturally "genetically randomized". Second, data on the daily doses, adherence, and discontinuation of statin treatment after discharge were lacking, despite the possibility that these factors may have modified the actual impact of statin therapy on LTa polymorphism. Third, although we found that LTa polymorphism is associated with mortality after the onset of AMI in our patient cohort comprised of Asian people who were predominantly Japanese, further analysis is

needed to verify the results in other ethnic groups. Fourth, the study included only the patients with informed consent, who were in relatively less severity after the onset of MI, which is also a study limitation.

In conclusion, our results demonstrate that the LTa 804A allele is significantly associated with increased mortality in post-AMI patients, a finding that may be attributable to the increased mortality risk of the 804A allele in the absence of statin treatment. Therefore, post-AMI patients with LTa C804A polymorphism may be good candidates for pharmacological intervention with statins to improve long-term mortality. Although further investigations are needed, genetic polymorphisms of LTa, including C804A, may represent suitable therapeutic targets in the near future.

Funding

This work was supported in part by Grants-in-Aid for scientific research from the Ministry of Education, Culture, Sports, Science, and Technology, Japan to Y. Sakata (#19590816) and H. Sato (#19390215).

Conflict of interest

None of the authors have conflicts of interest to declare.

Appendix A. Supplementary data

Supplementary data related to this article can be found at http://dx.doi.org/10.1016/j.atherosclerosis.2013.01.020.

References

[1] Jernberg T, Johanson P, Held C, Svennblad B, Lindback J, Wallentin L. Association between adoption of evidence-based treatment and survival for patients with ST-elevation myocardial infarction. J Am Med Assoc 2011;305:1677e84.
[2] Fox KA, Steg PG, Eagle KA, et al. Decline in rates of death and heart failure in acute coronary syndromes, 1999e2006. J Am Med Assoc 2007;297:1892e900.
[3] Ozaki K, Sato H, Inoue K, et al. SNPs in BRAP associated with risk of myocardial infarction in Asian populations. Nat Genet 2009;41:329e33.
[4] Ozaki K, Sato H, Iida A, et al. A functional SNP in PSMA6 confers risk of myocardial infarction in the Japanese population. Nat Genet 2006;38:921e5.
[5] The PROCARDIS Consortium. A trio family study showing association of the lymphotoxin-alpha N26 (804A) allele with coronary artery disease. Eur J Hum Genet 2004;12:770e4.
[6] Ozaki K, Inoue K, Sato H, et al. Functional variation in LGALS2 confers risk of myocardial infarction and regulates lymphotoxin-alpha secretion in vitro. Nature 2004;429:72e5.
[7] Iwanaga Y, Ono K, Takagi S, et al. Association analysis between polymorphisms of the lymphotoxin-alpha gene and myocardial infarction in a Japanese population. Atherosclerosis 2004;172:197e8.
[8] Ozaki K, Ohnishi Y, Iida A, et al. Functional SNPs in the lymphotoxin-alpha gene that are associated with susceptibility to myocardial infarction. Nat Genet 2002;32:650e4.
[9] Gray PW, Aggarwal BB, Benton CV, et al. Cloning and expression of cDNA for human lymphotoxin, a lymphokine with tumour necrosis activity. Nature 1984;312:721e4.
[10] Granger GA, Williams TW. Lymphocyte cytotoxicity in vitro: activation and release of a cytotoxic factor. Nature 1968;218:1253e4.
[11] Ruddle NH, Waksman BH. Cytotoxic effect of lymphocyte-antigen interaction in delayed hypersensitivity. Science 1967;157:1060e2.
[12] Suna S, Sakata Y, Shimizu M, et al. Lymphotoxin-alpha3 mediates monocyte-endothelial interaction by TNFR I/NF-kappaB signaling. Biochem Biophys Res Commun 2009;379:374e8.
[13] Schreyer SA, Vick CM, LeBoeuf RC. Loss of lymphotoxin-alpha but not tumor necrosis factor-alpha reduces atherosclerosis in mice. J Biol Chem 2002;277:12364e8.
[14] Mizuno H, Sato H, Sakata Y, et al. Impact of atherosclerosis-related gene polymorphisms on mortality and recurrent events after myocardial infarction. Atherosclerosis 2006;185:400e5.
[15] Barber MJ, Mangravite LM, Hyde CL, et al. Genome-wide association of lipid-lowering response to statins in combined study populations. PLoS One 2010;5:e9763.
[16] Kurotobi T, Sato H, Kinjo K, et al. Reduced collateral circulation to the infarct-related artery in elderly patients with acute myocardial infarction. J Am Coll Cardiol 2004;44:28e34.
[17] Yamada Y, Miyauchi A, Takagi Y, Tanaka M, Mizuno M, Harada A. Association of the C-509–>T polymorphism, alone of in combination with the T869–>C polymorphism, of the transforming growth factor-beta1 gene with bone mineral density and genetic susceptibility to osteoporosis in Japanese women. J Mol Med 2001;79:149e56.
[18] Zhao H, Liao Y, Minamino T, et al. Inhibition of cardiac remodeling by pravastatin is associated with amelioration of endoplasmic reticulum stress. Hypertens Res 2008;31:1977e87.
[19] Libby P. Inflammation in atherosclerosis. Nature 2002;420:868e74.
[20] Galkina E, Ley K. Vascular adhesion molecules in atherosclerosis. Arterioscler Thromb Vasc Biol 2007;27:2292e301.
[21] Suna S, Sakata Y, Sato H, et al. Up-regulation of cell adhesion molecule genes in human endothelial cells stimulated by lymphotoxin alpha: DNA microarray analysis. J Atheroscler Thromb 2008;15:160e5.
[22] Wang HR, Li JJ, Huang CX, Jiang H. Fluvastatin inhibits the expression of tumor necrosis factor-alpha and activation of nuclear factor-kappaB in human endothelial cells stimulated by C-reactive protein. Clin Chim Acta 2005;353:53e60.
[23] Planavila A, Laguna JC, Vazquez-Carrera M. Atorvastatin improves peroxisome proliferator-activated receptor signaling in cardiac hypertrophy by preventing nuclear factor-kappa B activation. Biochim Biophys Acta 2005;1687:76e83.
[24] Inoue I, Itoh F, Aoyagi S, et al. Fibrate and statin synergistically increase the transcriptional activities of PPARalpha/RXRalpha and decrease the transactivation of NFkappaB. Biochem Biophys Res Commun 2002;290:131e9.
[25] Rasmussen LM, Hansen PR, Nabipour MT, Olesen P, Kristiansen MT, Ledet T. Diverse effects of inhibition of 3-hydroxy-3-methylglutaryl-CoA reductase on the expression of VCAM-1 and E-selectin in endothelial cells. Biochem J 2001;360:363e70.
[26] Minamino T, Komuro I, Kitakaze M. Endoplasmic reticulum stress as a therapeutic target in cardiovascular disease. Circ Res 2010;107:1071e82.
[27] Okada K, Minamino T, Tsukamoto Y, et al. Prolonged endoplasmic reticulum stress in hypertrophic and failing heart after aortic constriction: possible contribution of endoplasmic reticulum stress to cardiac myocyte apoptosis. Circulation 2004;110:705e12.
[28] Ridker PM, Cannon CP, Morrow D, et al. C-reactive protein levels and outcomes after statin therapy. N Engl J Med 2005;352:20e8.
[29] Wilt TJ, Bloomfield HE, MacDonald R, et al. Effectiveness of statin therapy in adults with coronary heart disease. Arch Intern Med 2004;164:1427e36.
[30] Bonetti PO, Lerman LO, Napoli C, Lerman A. Statin effects beyond lipid loweringeare they clinically relevant? Eur Heart J 2003;24:225e48.

Cardiovasc Drugs Ther (2013) 27:125–132
DOI 10.1007/s10557-012-6437-6

ORIGINAL ARTICLE

Liposomal Amiodarone Augments Anti-arrhythmic Effects and Reduces Hemodynamic Adverse Effects in an Ischemia/Reperfusion Rat Model

Hiroyuki Takahama · Hirokazu Shigematsu · Tomohiro Asai · Takashi Matsuzaki · Shoji Sanada · Hai Ying Fu · Keiji Okuda · Masaki Yamato · Hiroshi Asanuma · Yoshihiro Asano · Masanori Asakura · Naoto Oku · Issei Komuro · Masafumi Kitakaze · Tetsuo Minamino

Published online: 24 January 2013

Abstract

Purpose Although amiodarone is recognized as the most effective anti-arrhythmic drug available, it has negative hemodynamic effects. Nano-sized liposomes can accumulate in and selectively deliver drugs to ischemic/reperfused (I/R) myocardium, which may augment drug effects and reduce side effects. We investigated the effects of liposomal amiodarone on lethal arrhythmias and hemodynamic parameters in an ischemia/reperfusion rat model.

Methods and Results We prepared liposomal amiodarone (mean diameter: 113 ± 8 nm) by a thin-film method. The left coronary artery of experimental rats was occluded for 5 min followed by reperfusion. Ex vivo fluorescent imaging revealed that intravenously administered fluorescent-labeled nano-sized beads accumulated in the I/R myocardium. Amiodarone was measurable in samples from the I/R myocardium when liposomal amiodarone, but not amiodarone, was administered. Although the intravenous administration of amiodarone (3 mg/kg) or liposomal amiodarone (3 mg/kg) reduced heart rate and systolic blood pressure compared with saline, the decrease in heart rate or systolic blood pressure caused by liposomal amiodarone was smaller compared with a corresponding dose of free amiodarone. The intravenous administration of liposomal amiodarone (3 mg/kg), but not free amiodarone (3 mg/kg), 5 min before ischemia showed a significantly reduced duration of lethal arrhythmias (18 ± 9 s) and mortality (0 %) during the reperfusion period compared with saline (195 ± 42 s, 71 %, respectively).

Conclusions Targeting the delivery of liposomal amiodarone to ischemic/reperfused myocardium reduces the mortality due to lethal arrhythmia and the negative hemodynamic changes caused by amiodarone. Nano-size liposomes may be a promising drug delivery system for targeting I/R myocardium with cardioprotective agents.

Keywords Liposome · Amiodarone · Lethal arrhythmia · Ischemia · Reperfusion

T. Matsuzaki · S. Sanada · H. Y. Fu · K. Okuda · M. Yamato · Y. Asano · I. Komuro · T. Minamino (✉)
Department of Cardiovascular Medicine, Osaka University Graduate School of Medicine, 2-2 Yamadaoka, Suita, Osaka 565-0871, Japan
e-mail: minamino@cardiology.med.osaka-u.ac.jp

H. Takahama · M. Asakura · M. Kitakaze
Department of Cardiovascular Medicine, National Cerebral and Cardiovascular Center, Suita 565-8565, Japan

H. Shigematsu · T. Asai · N. Oku
Department of Medical Biochemistry and Global COE, University of Shizuoka Graduate School of Pharmaceutical Sciences, Shizuoka 422-8526 Shizuoka, Japan

H. Asanuma
Department of Cardiovascular Science and Technology, Kyoto Prefectural University School of Medicine, Kyoto 602-8566, Japan

H. Takahama
Division of Cardiovascular Disease, Mayo Clinic, Rochester, MN 55902, USA

Introduction

Therapies for the prevention and treatment of ischemia-induced life-threatening arrhythmias remain an unmet medical need [1]. Amiodarone is currently considered to be the most effective anti-arrhythmic drug available for treating life-threatening arrhythmias [2, 3], despite the fact that this compound has a negative impact on hemodynamic parameters [4, 5]. The intravenous administration of amiodarone is expected

to be beneficial for the immediate treatment of arrhythmias in emergency settings, such as acute myocardial infarction (AMI) [6, 7]. However, in clinical practice, the administration of amiodarone remains problematic for the treatment of AMI [8]. Although lower doses of amiodarone result in fewer incidences of death, high doses of amiodarone can cause hypotension and non-cardiac death, both of which may diminish the positive effects of amiodarone [8, 9]. Therefore, a novel delivery system is strongly desired to enhance the anti-arrhythmic effects of amiodarone without producing severe side effects.

Liposomes are widely used for drug delivery to actively or passively target specific organs and to improve drug stability in cancer and inflammatory diseases [10–12]. In ischemic/reperfused (I/R) myocardium, cellular permeability is enhanced and vascular endothelial integrity is disrupted [13, 14], suggesting that nanoparticles, such as liposomes, may be a promising drug delivery system for targeting I/R myocardium with cardioprotective agents [15]. Indeed, we have recently demonstrated that adenosine encapsulated by liposomes coated with polyethylene glycol (PEG) exhibited enhanced cardioprotective effects and attenuated side effects, such as hypotension and bradycardia, in an ischemia/reperfusion model of rats [16]. In the present study, we prepared liposomal amiodarone and examined 1) the targeted accumulation of liposomal amiodarone in the I/R myocardium, 2) the hemodynamic effects of the intravenous administration of liposomal amiodarone and free amiodarone, and 3) the anti-arrhythmic effects of these preparations in an I/R rat model. We showed that targeting the delivery of liposomal amiodarone to I/R myocardium reduces the mortality due to lethal arrhythmias and the negative hemodynamic changes caused by amiodarone in an I/R rat model.

Methods

Materials

The materials used to prepare PEGylated liposomes, including 1-palmitoyl-2-oleoyl-sn-glycero-3-phosphocholine (POPC), 1,2-dipalmitoyl-sn-glycero-3-phosphocholine (DPPC), cholesterol, and 1,2-distearoyl-sn-glycero-3-phosphoethanolamine-N-poly(ethylene glycol) 2000 (DSPE-PEG2000), were kindly donated by Nippon Fine Chemical Co. (Takasago, Hyogo, Japan). Fluorescent beads (diameter 100 nm) were purchased from Invitrogen. All other materials were obtained from Sigma-Aldrich (St. Louis, MO, USA).

Animals

Male Wistar rats (9 weeks old and weighing 250–310 g; Japan Animals, Osaka, Japan) were used. The animal experiments were approved by the Osaka University Research Committee and were performed according to institutional guidelines. All studies conformed to the Guide for the care and Use of Laboratory Animals published by the US National Institutes of Health (NIH Publication No. 85–23, revised 1996).

Preparation of PEGylated Liposomes

PEGylated liposomes composed of POPC, DPPC, cholesterol, DSPE-PEG2000, and amiodarone were prepared by a thin-film method. Briefly, amiodarone and lipids dissolved in chloroform were evaporated to form a thin lipid film using a rotary evaporator. The lipid film was dried for at least 1 h under reduced pressure and then hydrated with PBS (pH 7.4). The liposome solution was freeze-thawed for 3 cycles with liquid nitrogen. The particle size of the liposomes was adjusted by extrusion through 100-nm-pore polycarbonate filters (Nuclepore, Cambridge, MA, USA). The liposomal solutions were centrifuged at 453,000 g for 15 min (CS120GXL, Hitachi, Japan) to remove the untrapped amiodarone. Then, the liposomes were resuspended in PBS. To determine the efficacy of trapping amiodarone in the liposomes, an aliquot of the liposomal solution was solubilized with 1 % reduced Triton X-100 (Sigma-Aldrich), and the amount of amiodarone was optically determined at 240 nm.

Characterization of PEGylated Liposomes

The particle size and ζ potential of PEGylated liposomes diluted with PBS were measured by dynamic scatter analysis (Zetasizer Nano ZS; Malvern, Worcestershire, UK). The analyses were performed 15 times per sample, and the results represent the analysis of 3 independent experiments.

Experimental Protocol

Targeted Delivery of Fluorescent-labeled Nano-sized Beads to the I/R Myocardium

The rats were anesthetized with intraperitoneal sodium pentobarbital (50 mg/kg). Catheters were advanced into the femoral vein to infuse the drugs. Ischemia/reperfusion was induced by 5 min of left coronary artery occlusion followed by reperfusion [16]. After the hemodynamic parameters became stable, fluorescent-labeled nano-size beads, 100 nm in diameter (FluoSpheres, Invitrogen), were intravenously infused to the rats for 5 min before ischemia or before a sham operation (n = 3, each). Fifteen minutes after reperfusion, the hearts were removed and cut into 5 sections parallel to the axis from the base to the apex. Then, ex vivo fluorescence images were obtained with an Olympus SZX12 stereoscopic microscope equipped with a DP71 digital camera (Olympus, Tokyo, Japan) before and after the hearts were sliced.

Targeted Delivery of Amiodarone and Liposomal Amiodarone to the I/R Myocardium

Catheters were advanced into the femoral artery and vein to measure the systemic blood pressure (BP) and to infuse the drugs into the anesthetized rats, respectively. Electrocardiographic and hemodynamic parameters, such as heart rate (HR) and BP, were continuously monitored during the study using a PowerLab system (ADInstruments, Castle Hill, Australia). After the hemodynamic parameters became stable, to clarify the targeted delivery of amiodarone and liposomal amiodarone to the I/R myocardium, we intravenously administered saline, free amiodarone (3 mg/kg) or liposomal amiodarone (3 mg/kg) to rats for 5 min before the onset of ischemia. Then, we obtained blood samples and myocardium from the I/R area.

Effects of Amiodarone and Liposomal Amiodarone on Lethal Arrhythmias

To evaluate the effects of amiodarone and liposomal amiodarone on lethal arrhythmias, we intravenously administered saline (n = 7), free amiodarone (3.0 or 10.0 mg/kg) (n = 6 each), PEGylated liposomes (empty liposomes) (n = 6), and PEGylated liposomal amiodarone (3.0 mg/kg) (n = 6) for 5 min before ischemia. The dose of amiodarone used in this study was lower than that used in a previous study [17] to clarify whether amiodarone encapsulated by liposomes coated with PEG exhibited enhanced anti-arrhythmic effects. Without any procedure such as electrical conversion or cardiac massage, ventricular tachyarrhythmias (VT/VF) occurred frequently during early period of reperfusion and the mortality of rats reached more than a half of cases in this model [18].

Measurement of Amiodarone Concentration

The concentration of amiodarone in serum and heart tissue from the I/R area was assayed by high-performance liquid chromatography (HPLC) as previously described [19]. The detection limit of the HPLC assay was 50 ng/mL. Blood and myocardial samples were obtained at the end of the experimental protocol. The sample preparation was performed as previously described [19]. Briefly, myocardium was freed from visible blood, thereafter rinsed with 0.9 % sodium chloride and stored at −20 °C until analysis. After that, myocardial tissue samples were finely minced and 100 mg were homogenized with 0.9 % sodium chloride (1 mL) and after centrifugation, the clear supernatant was injected into HPLC.

Quantitative Evaluation of Fluorescent-labeled Nano-sized Beads in the I/R Myocardium

To analyze the quantitative fluorescent intensity, signals from heart slices were quantified by image analysis (Image J; National Institutes of Health, USA) as previously described [20]. The signal intensity from the heart slices was evaluated as the average signals of the whole heart and the left ventricle (LV) (Fig. 2c).

Arrhythmia Analysis

The electrocardiographic tracings were independently analyzed by two of the authors, who were blinded to the treatment assignment. The duration of each spontaneous ventricular tachycardia or fibrillation episode during the I/R protocol was measured using the time scale provided by the recording software. Ventricular tachycardia was defined as 4 or more consecutive ventricular ectopic beats, and ventricular fibrillation was defined as a signal in which the individual QRS deflections could not easily be distinguished from one another. However, distinguishing ventricular tachycardia from fibrillation was often difficult [21]; therefore, we report ventricular tachycardia and fibrillation collectively as ventricular tachyarrhythmias (VT/VF) in this study. VT/VF duration and mortality were evaluated for 5 min of ischemia followed by 15 min of reperfusion.

Statistical Analysis

The parameters of the liposomes are expressed as the mean ± standard deviation (SD). Other data are expressed as the average ± standard error of the mean (SEM). To compare the parameters of the liposomes, unpaired t-tests were performed. We performed the Welch t-test to compare the amiodarone concentration in the plasma and myocardium. For hemodynamic parameters, the data were assessed with the paired t-test for comparisons to the baseline within a group. One-way repeated-measurement ANOVA followed by post-hoc Bonferroni's multiple comparisons were used for comparisons between groups. To address the differences in VT/VF duration among the groups, we performed a non-parametric (Kruskal-Wallis) test followed by evaluation with the Mann–Whitney U test. The mortality rates were compared using the Fisher's exact probability test. In all analyses, $P < 0.05$ was considered to be statistically significant.

Results

Characterization of PEGylated Liposomes

We prepared 5 types of PEGylated liposomes composed of POPC, DPPC, cholesterol, and amiodarone. The ratio of unsaturated lipids (POPC) to saturated lipids (DPPC) varied (Fig. 1). During preparation of the liposomes, the POPC: DPPC:cholesterol:amiodarone molar ratio of 10:0:5:1 exhibited the best encapsulation efficiency for amiodarone compared with the other conditions (Fig. 1).

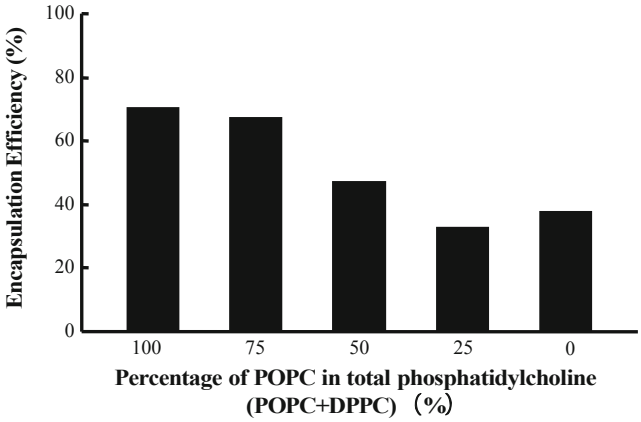

Fig. 1 Encapsulation efficiency of amiodarone in the liposomes. Amiodarone was loaded into liposomes containing POPC, DPPC, or a mixture of POPC and DPPC. The liposomal amiodarone was composed of phosphatidylcholine (POPC + DPPC):cholesterol:amiodarone at a 10:5:1 molar ratio. The percent molar ratio of POPC in total phosphatidylcholine (POPC + DPPC) is indicated in the figure. The encapsulation efficiency of amiodarone was determined as described in the Methods section

The dynamic light scatter analysis showed no significant differences between the mean diameter, polydispersity index, or ζ potential distribution of the empty and amiodarone-loaded PEGylated liposomes (Table 1).

Accumulation of Fluorescence-labeled Nano-sized Beads in the I/R Myocardium

Representative pictures obtained by fluorescence imaging are shown in Fig. 2a (whole heart) and b (sliced hearts). Quantitative analysis revealed that the average fluorescence intensity of the whole heart (Fig. 2c left) or the left ventricle (Fig. 2c right) of the I/R hearts was significantly higher than that in sham-operated hearts.

Amiodarone Concentration in the Blood and I/R Myocardium

The plasma concentration after the administration of liposomal amiodarone was significantly higher than that of free amiodarone (Table 2). Importantly, the amiodarone concentration in the I/R myocardium was detectable after the administration of liposomal, but not free, amiodarone (Table 2).

Hemodynamic Effects of Amiodarone and Liposomal Amiodarone

The baseline heart rates were 411±16, 426±14, 427±12, 409±8 and 414±6 beats/min in the saline, empty liposome, amiodarone (3 mg/kg), amiodarone (10 mg/kg) and liposomal amiodarone (3 mg/kg) groups, respectively. The baseline systolic BP was 113±7, 118±10, 111±5, 90±4 and 104±2 mmHg in the saline, empty liposome, amiodarone (3 mg/kg), amiodarone (10 mg/kg) and liposomal amiodarone (3 mg/kg) groups, respectively. There were no significant differences in the baseline HR or systolic BP among the groups tested. The intravenous administration of amiodarone (3 and 10 mg/kg) or liposomal amiodarone reduced both the HR and systolic BP from the baseline, whereas the saline or empty liposomes did not (Fig. 3). The time-course changes of both the HR and systolic BP were significantly smaller in the liposomal amiodarone group (3 mg/kg) compared with the corresponding dose in the free amiodarone group (3 mg/kg) (Fig. 3). The reductions in HR and systolic BP at 1, but not 3, minutes after liposomal amiodarone administration were significantly smaller compared with those following the corresponding dose of amiodarone.

Antiarrhythmic Effects of Amiodarone and Liposomal Amiodarone

Representative electrocardiograms of the rats that received saline, free amiodarone or liposomal amiodarone are shown in Fig. 4. The intravenous administration of liposomal amiodarone (3 mg/kg), but not amiodarone (3 mg/kg), significantly reduced the duration of VT/VF compared with saline (Table 3). Furthermore, the mortality in the group that received liposomal amiodarone (3 mg/kg), but not the corresponding dose of amiodarone (3 mg/kg), was significantly lower than that in the saline group. In the group of rats that received a high dose of amiodarone (10 mg/kg), the VT/VF duration was 36±12 s, and none of the rats died (Table 3), which was similar to the low dose of liposomal amiodarone group (3 mg/kg).

Discussion

In this study, we revealed that 1) liposomal amiodarone was successfully prepared using a thin-film method, 2) the

Table 1 Characterization of liposomes by dynamic light scatter analysis

	Mean diameter (nm)	Polydispersity index	ζ Potential (mV)
PEGylated liposomes (empty liposomes)	111±14	0.124±0.027	−2.1
PEGylated liposomal amiodarone	113±8	0.128±0.040	−3.7

Results represent 4 independent experiments. The values are expressed as the mean ± SD. PEG polyethylene glycol

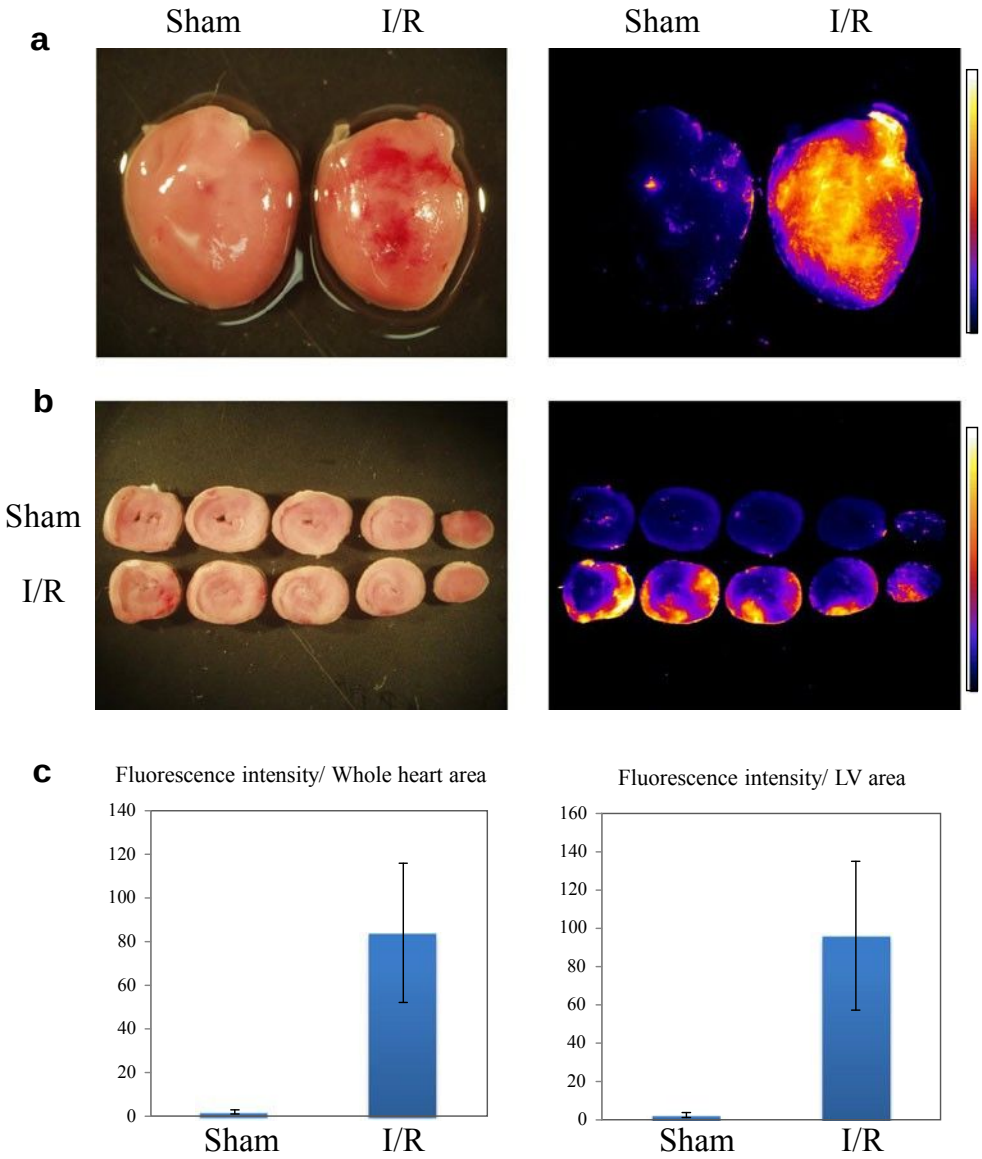

Fig. 2 Representative pictures of ischemia/reperfused myocardium with and without fluorescence-labeled nano-sized beads. Representative pictures obtained by fluorescent imaging are shown in a (whole heart) and b (sliced hearts). Quantitative analysis revealed that the average fluorescence intensity of the whole heart (c left) or the left ventricle (c right) of the I/R hearts was significantly higher than that of the sham-operated hearts

accumulation of nano-sized beads was observed in the I/R myocardium, 3) liposomal amiodarone showed a smaller reduction in the HR and systolic BP compared with free amiodarone, and 4) liposomal amiodarone, but not amiodarone, reduced the VT/VF duration and mortality during the reperfusion period compared with saline.

Table 2 Amiodarone concentration in the blood and I/R myocardium

Groups	Plasma, ng/mL	Myocardium, ng/mL
Saline	N.D.	N.D.
Free amiodarone	472±147	N.D.
Liposomal amiodarone	3872±378*	71±7*

Data are expressed as the mean ± SEM. N.D. not detected. n = 3 rats in each group. * $p<0.05$ versus free amiodarone

Preparation of Liposomal Amiodarone

This study is the first to encapsulate amiodarone in PEGylated liposomes, although it has been previously encapsulated in other liposomes [22] and micelles [23]. We demonstrated that lipid bilayers composed of unsaturated lipids are more suitable for encapsulating amiodarone in PEGylated liposomes compared with those composed of saturated lipids. PEGylated liposomes have a long circulating time in the bloodstream because PEG endows a steric barrier to liposomes, allowing them to avoid interactions with opsonins and cells of the mononuclear phagocytic system [24]. Thus, they have been used to increase drug stability, safety, and bioavailability in clinical applications. In this study, we found that a higher concentration of amiodarone was retained in the blood when we administered liposomal amiodarone compared with the administration of

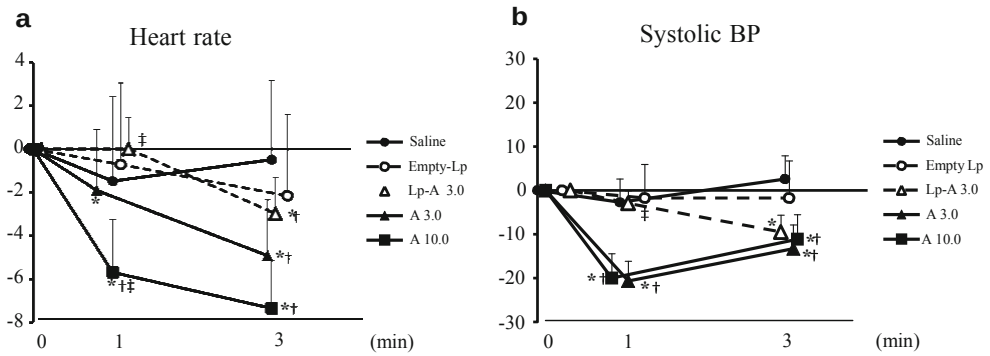

Fig. 3 Time-course changes in HR and systolic BP after drug administration. Shows the percent change from baseline for HR (a) and systolic BP (b) after intravenous administration of the tested drugs. The data are expressed as the mean ± SEM. *P < 0.05 versus baseline, paired t-test. P=0.0009 (HR), 0.0002 (systolic BP) between amiodarone (3 mg/kg) and liposomal amiodarone (3 mg/kg), 1-way repeated-measurement ANOVA. †P < 0.05 versus saline, ‡P < 0.05 versus amiodarone (3 mg/kg), 1-way repeated-measurement ANOVA with Bonferroni's multiple comparison

free amiodarone, suggesting that encapsulation of amiodarone in PEGylated liposomes enhances the stability of amiodarone in the blood.

Targeted Delivery to the I/R Myocardium by Liposomal Amiodarone

Ex vivo fluorescence imaging revealed that fluorescence-labeled nano-sized beads accumulated in the I/R myocardium, suggesting that myocardial permeability can be enhanced in the I/R myocardium. Consistent with this finding, we observed that the amiodarone concentration in the I/R myocardium in the liposomal amiodarone group was much higher compared with that in the amiodarone group. Enhanced permeability in the I/R myocardium and the prolonged presence of amiodarone in PEGylated liposomes in the blood represent a possible mechanism for increased amiodarone concentrations in the I/R myocardium. Amiodarone will be released from accumulated liposomal amiodarone in I/R myocardium due to the natural decay and concentration gradient. These findings suggest that the I/R myocardium is a promising passive target for liposomal drug delivery.

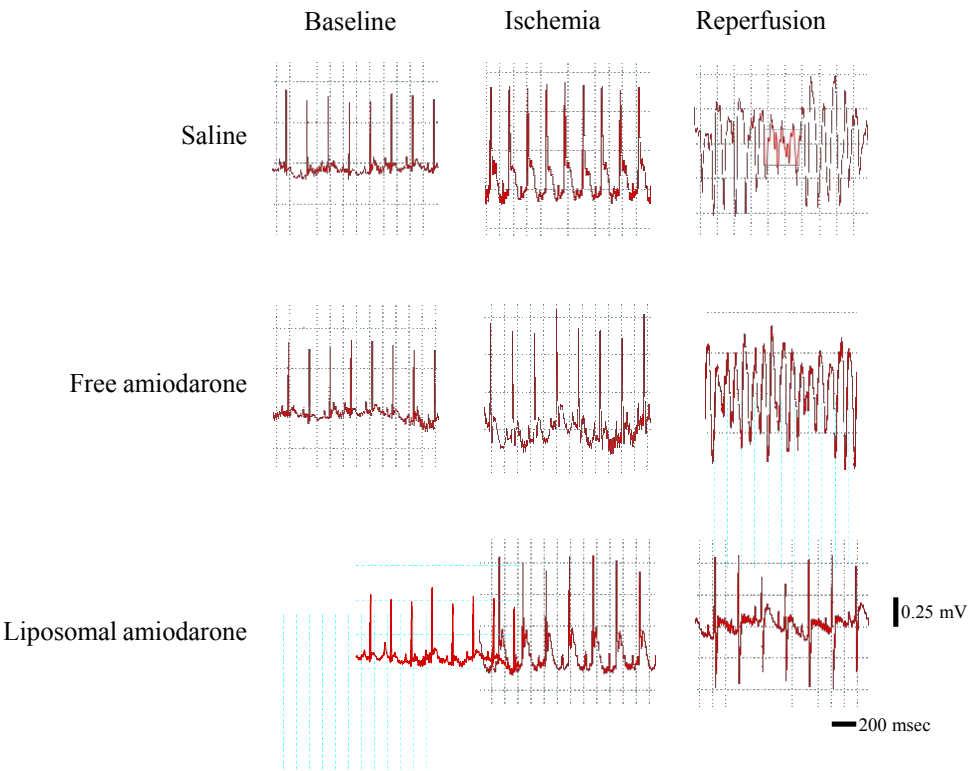

Fig. 4 Representative electrocardiograms. The upper, middle and lower panels show representative electrocardiograms under baseline conditions during ischemia and at the onset of reperfusion for rats that received saline, free amiodarone (3 mg/kg) and liposomal amiodarone (3 mg/kg), respectively

Table 3 Lethal arrhythmias and mortality in an I/R rat model

	Number	VT/VF duration (sec)	Mortality (%)
Saline	7	195±42	71
Empty liposomes	6	162±31	50
Amiodarone (3 mg/kg)	6	167±78	33
Amiodarone (10 mg/kg)	6	36±12*	0#
Liposomal Amiodarone (3 mg/kg)	6	18±9*	0#

*$p<0.05$ versus saline (VT/VF duration). # $p<0.05$ versus saline group (mortality). VT ventricular tachycardia, VF ventricular fibrillation

Minimal Negative Hemodynamic Effects of Liposomal Amiodarone

Amiodarone causes hypotension and bradycardia in clinical settings [4, 5]. In this study, both free and liposomal amiodarone significantly reduced the HR and systolic BP; however, the time-course changes for both the HR and systolic BP in the liposomal amiodarone group were significantly smaller compared with those following the corresponding dose of free amiodarone. Importantly, the reductions in HR and systolic BP at 1, but not 3, minutes after liposomal amiodarone administration were significantly smaller compared with those following the corresponding dose of amiodarone. These findings suggest that liposomal amiodarone may minimize the negative effects on systemic hemodynamics immediately after the administration of amiodarone. One possible mechanism to explain this finding is that amiodarone on the surface of the liposome membrane is covered with PEG so that amiodarone cannot act directly on cardiovascular cells. Gradual release of amiodarone from liposome may minimize the rapid hemodynamic changes, because systemic hemodynamic effects of liposomal amiodarone were significantly attenuated in liposomal amiodarone group than free amiodarone group.

Augmented Anti-arrhythmic Effects of Liposomal Amiodarone

In this study, liposomal amiodarone (3 mg/kg), but not the corresponding dose of free amiodarone (3 mg/kg), significantly reduced the VT/VF duration and mortality compared with saline in an I/R rat model. Because the acute effects of amiodarone are known to be attributable to blockade of Na^+, Ca^{2+} and dose-dependent K^+ channels [2, 25], increasing the concentration of amiodarone in the I/R myocardium may augment its anti-arrhythmic effects through its tonic effects on cardiomyocytes caused by blocking cardiac ionic currents. Kishida et al. reported that amiodarone enhances nitric oxide production in cultured human endothelial cells [26]. Furthermore, amiodarone protects cardiac myocytes against oxidative injury by scavenging free radicals [27]. These pleiotropic effects of amiodarone are also enhanced by its increased concentration in the I/R myocardium via PEGylated liposomes, which may contribute to the reduction of lethal arrhythmias during reperfusion followed by ischemia. In the present study, since we did not do any procedure such as electrical conversion or cardiac massage for VT/VF, the mortality was higher than in our previous report [16].

Clinical Implications

In clinical settings, higher doses of amiodarone cause hypotension and non-cardiac death or induce worsening heart failure through negative inotropic effects [28]. These effects often diminish the beneficial effects of amiodarone for patients with AMI or heart failure [8, 9]. The present study demonstrated that liposomal amiodarone (3 mg/kg) exerts anti-arrhythmic effects similar to a high dose of free amiodarone (10 mg/kg) while reducing the extent of bradycardia and hypotension, suggesting that encapsulating amiodarone in liposomes augments its anti-arrhythmic effects and reduces its negative effects on hemodynamic parameters with reducing administrative dose. These findings can have a great impact on preventing lethal arrhythmias during reperfusion in AMI patients.

Study Limitations

There are several limitations in this study. We used a brief period of I/R without myocardial infarction in rats. Sakamoto et al. demonstrated that the incidence of VT/VF in a rodent model was 'bell-shaped' with a maximum at 5 min of ischemia and that most lethal arrhythmias occurred within first 20 s after the onset of reperfusion [29]. Consistently, our data showed that the mean time at which the lethal arrhythmia occurred after the onset of reperfusion was 3.3+/−1.6 s. Therefore, we chose the 5 min of ischemia followed by 15 min of reperfusion model. We also chose the timing of drug administration before the onset of ischemia to clarify whether liposomal-amiodarone could prevent the lethal arrhythmia that occurs in the early period of reperfusion. In addition, in clinical practice lethal arrhythmias often occur after a brief period of I/R without any irreversible damage to the heart, indicating that the anti-arrhythmic effects of liposomal amiodarone during a brief period of ischemia model could have clinical relevance [30]. However, careful interpretation is necessary when using liposomal amiodarone in acute myocardial infarction with irreversible damage to confirm the beneficial effects of liposomal amiodarone. Furthermore, because the electrophysiology of rats differs from that of humans and drug administration in our study started before the onset of

ischemia, additional pre-clinical studies including a longer period of I/R model to consider the timing of drug administration are needed using large animal models. We should also take into account that the potential side effects of amiodarone such as bradycardia are minimal in the left coronary artery occlusion model used in the present study.

Conclusion

In conclusion, the targeted delivery of liposomal amiodarone to the I/R myocardium exerted strong anti-arrhythmic effects and reduced the negative impact on systemic hemodynamics. Nano-sized liposomes may be a promising drug delivery system for targeting the I/R myocardium with cardioprotective agents.

Acknowledgments The authors thank Takaki Hayakawa for her technical assistance, Takeshi Aiba for his special advice about data analysis. This research was supported by Grants-in-Aid from the Ministry of Health, Labor, and Welfare of Japan; Grants-in-Aid from the Ministry of Education, Culture, Sports, Science, and Technology of Japan; grants from the Japan Heart Foundation; and grants from the Japan Cardiovascular Research Foundation.

References

1. Di Diego JM, Antzelevitch C. Ischemic ventricular arrhythmias: experimental models and their clinical relevance. Hear Rhythm. 2011;8:1963–8.
2. Kodama I, Kamiya K, Toyama J. Cellular electropharmacology of amiodarone. Cardiovasc Res. 1997;35:13–29.
3. Vassallo P, Trohman RG. Prescribing amiodarone: an evidence-based review of clinical indications. JAMA. 2007;298:1312–22.
4. Scheinman MM, Levine JH, Cannom DS, et al. Dose-ranging study of intravenous amiodarone in patients life-threatening ventricular tachyarrhythmias. The Intravenous Amiodarone Muticenter Investigators Group. Circulation. 1995;92:3264–72.
5. Podrid PJ. Amiodarone; reevaluation of an old drug. Ann Intern Med. 1995;122:689–700.
6. Shiga T, Tanaka T, Irie S, Hagiwara N, Kasanuki H. Pharmacokinetics of intravenous amiodarone and its electrocardiographic effects on healthy Japanese subjects. Hear Vessel. 2011;26:274–81.
7. Wenzel V, Russo SG, Arntz HR, et al. [Comments on the 2010 guidelines on cardiopulmonary resuscitation of the European Resuscitation Council.]. Anaesthesist. 2010.
8. Elizari MV, Martínez JM, Belziti C, et al. Morbidity and mortality following early administration of amiodarone in acute myocardial infarction. GEMICA study investigators, GEMA Group, Buenos Aires, Argentina. Grupo de Estudios Multicentricos en Argentina. Eur Heart J. 2000;21:198–205.
9. Hu K, Gaudron P, Ertl G. Effects of high- and low-dose amiodarone on mortality, left ventricular remodeling, and hemodynamics in rats with experimental myocardial infarction. J Cardiovasc Pharmacol. 2004;44:627–30.
10. Semalty A, Semalty M, Rawat BS, Singh D, Rawat MS. Pharmacosomes: the lipid-based new drug delivery system. Expert Opin Drug Deliv. 2009;6:599–612.
11. Whitehead KA, Langer R, Anderson DG. Knocking down barriers: advances in siRNA delivery. Nat Rev Drug Discov. 2009;8:129–38.
12. Malam Y, Loizidou M, Seifalian AM. Liposomes and nanoparticles: nanosized vehicles for drug delivery in cancer. Trends Pharmacol Sci. 2009;30:592–9.
13. Horwitz LD, Kaufman D, Keller MW, Kong Y. Time course of coronary endothelial healing after injury due to ischemia and reperfusion. Circulation. 1994;90:2439–47.
14. Dauber IM, VanBenthuysen KM, McMurtry IF, et al. Functional coronary microvascular injury evident as increased permeability due to brief ischemia and reperfusion. Circ Res. 1990;66:986–98.
15. Galagudza MM, Korolev DV, Sonin DL, et al. Targeted drug delivery into reversibly injured myocardium with silica nanoparticles: surface functionalization, natural biodistribution, and acute toxicity. Int J Nanomedicine. 2010;5:231–7.
16. Takahama H, Minamino T, Asanuma H, et al. Prolonged targeting of ischemic/reperfused myocardium by liposomal adenosine augments cardioprotection in rats. J Am Coll Cardiol. 2009;53:709–17.
17. Riva E, Hearse DJ. Anti-arrhythmic effects of amiodarone and desethylamiodarone on malignant ventricular arrhythmias arising as a consequence of ischaemia and reperfusion in the anaesthetised rat. Cardiovasc Res. 1989;23:331–9.
18. Canyon SJ, Dobson GP. Protection against ventricular arrhythmias and cardiac death using adenosine and lidocaine during regional ischemia in the in vivo rat. Am J Physiol Heart Circ Physiol. 2004;287:H1286–95.
19. Plomp TA, Wiersinga WM, Maes RA. Tissue distribution of amiodarone and desethylamiodarone in rats after repeated oral administration of various amiodarone dosages. Arzneimittelforschung. 1985;35:1805–10.
20. Feige JN, Sage D, Wahli W, Desvergne B, Gelman L. PixFRET, an ImageJ plug-in for FRET calculation that can accommodate variations in spectral bleed-trhoughs. Microsc Res Tech. 2005;68:51–8.
21. Opitz CF, Mitchell GF, Pfeffer MA, Pfeffer JM. Arrhythmias and death after coronary artery occlusion in the rat. Continuous telemetric ECG monitoring in conscious, untethered rats. Circulation. 1995;92:253–61.
22. Klibanov AL, Maruyama K, Torchilin VP, Huang L. Amphipathic polyethyleneglycols effectively prolong the circulation time of liposomes. FEBS Lett. 1990;268:235–7.
23. Theodossiou TA, Galanou MC, Paleos CM. Novel amiodarone-doxorubicin cocktail liposomes enhance doxorubicin retention and cytotoxicity in DU145 human prostate carcinoma cells. J Med Chem. 2008;51:6067–74.
24. Elhasi S, Astaneh R, Lavasanifar A. Solubilization of an amphiphilic drug by poly(ethylene oxide)-block-poly(ester) micelles. Eur J Pharm Biopharm. 2007;65:406–13.
25. Kamiya K, Nishiyama A, Yasui K, Hojo M, Sanguinetti MC, Kodama I. Short- and long-term effects of amiodarone on the two components of cardiac delayed rectifier K(+) current. Circulation. 2001;9:1317–24.
26. Kishida S, Nakajima T, Ma J, et al. Amiodarone and N-desethylamiodarone enhance endothelial nitric oxide production in human endothelial cells. Int Heart J. 2006;47:85–93.
27. Ide T, Tsutsui H, Kinugawa S, Utsumi H, Takeshita A. Amiodarone protects cardiac myocytes against oxidative injury by its free radical scavenging action. Circulation. 1999;100:690–2.
28. Freedman MD, Somberg JC. Pharmacology and pharmacokinetics of amiodarone. J Clin Pharamacol. 1991;31:1061–9.
29. Sakamoto J, Miura T, Tsuchida A, Fukuma T, Hasegawa T, Shimamoto K. Reperfusion arrhythmias in the murine heart: their characteristics and alteration after ischemic preconditioning. Basic Res Cardiol. 1999;94:489–95.
30. Tzivoni D, Keren A, Granot H, Gottlieb S, Benhorin J, Stern S. Ventricular fibrillation caused by myocardial reperfusion in Prinzmetal's angina. Am Heart J. 1983;105:323–5.

Treatment of cerebral ischemia-reperfusion injury with PEGylated liposomes encapsulating FK506

Takayuki Ishii,* Tomohiro Asai,* Dai Oyama,* Yurika Agato,* Nodoka Yasuda,* Tatsuya Fukuta,* Kosuke Shimizu,* Tetsuo Minamino,† and Naoto Oku*,[1]

*Department of Medical Biochemistry, School of Pharmaceutical Sciences, University of Shizuoka, Shizuoka, Japan; and †Department of Cardiovascular Medicine, Osaka University Graduate School of Medicine, Osaka, Japan

ABSTRACT **FK506 (Tacrolimus) has the potential to decrease cerebral ischemia-reperfusion injury. However, the clinical trial of FK506 as a neuroprotectant failed due to adverse side effects. This present study aimed to conduct the selective delivery of FK506 to damaged regions, while at the same time reducing the dosage of FK506, by using a liposomal drug delivery system. First, the cytoprotective effect of polyethylene glycol-modified liposomes encapsulating FK506 (FK506-liposomes) on neuron-like pheochromocytoma PC12 cells was examined. FK506-liposomes protected these cells from H_2O_2-induced toxicity in a dose-dependent manner. Next, we investigated the usefulness of FK506-liposomes in transient middle cerebral artery occlusion (t-MCAO) rats. FK506-liposomes accumulated in the brain parenchyma by passing through the disrupted blood-brain barrier at an early stage after reperfusion had been initiated. Histological analysis showed that FK506-liposomes strongly suppressed neutrophil invasion and apoptotic cell death, events that lead to a poor stroke outcome. Corresponding to these results, a single injection of FK506-liposomes at a low dosage significantly reduced cerebral cell death and ameliorated motor function deficits in t-MCAO rats. These results suggest that liposomalization of FK506 could reduce the administration dose by enhancing the therapeutic efficacy; hence, FK506-liposomes should be a promising neuroprotectant after cerebral stroke.—Ishii, T., Asai, T., Oyama, D., Agato, Y., Yasuda, N., Fukuta, T., Shimizu, K., Minamino, T., Oku, N. Treatment of cerebral ischemia-reperfusion injury with PEGylated liposomes encapsulating FK506. *FASEB J.* 27, 1362–1370 (2013). www.fasebj.org**

Key Words: neuroprotectant · tacrolimus · apoptosis · inflammation · motor function

After restoration of blood flow in cerebral stroke patients, cerebral ischemia-reperfusion (I/R) injury often occurs, resulting in neurological deficits (1, 2). Hence, the development of neuroprotective therapy for this type of injury has been awaited for a better outcome after a cerebral stroke. Although >1000 candidate compounds have shown potency as a neuroprotectant, and >100 of them have been tested in clinical studies in the past, none of them have passed these trials due to insufficiency of medicinal efficacy and to adverse side effects (3, 4). To overcome the present situation, we previously applied the liposomal drug delivery system (DDS) to the treatment of cerebral I/R injury (5). When 100 nm liposomes were intravenously injected immediately after the start of reperfusion, they selectively accumulated in the I/R region, suggesting that drug delivery using liposomes is applicable for treatment of I/R injuries. Moreover, liposomes modified with the antiapoptotic protein asialoerythropoietin significantly suppressed cerebral cell death and improved motor functional deficits induced by I/R injury in transient middle cerebral artery occlusion (t-MCAO) rats by increasing the accumulation of the protein in the injured region compared with the outcome for the free asialoerythropoietin-treated group. This finding offers the possibility that liposomal DDS could be a useful strategy for the treatment of cerebral I/R injury. However, the efficacy of liposomal DDS for treatment of cerebral I/R injuries has been proven for just a single protein, *i.e.*, asialoerythropoietin. Accordingly, more study is needed to reinforce the utility of this therapeu-

Abbreviations: DDS, drug delivery system; DiI-C_{18}, 1,1=-dioctadecyl-3,3,3=,3=-tetramethylindocarbocyanine; DPPC, dipalmitoylphosphatidylcholine; DSPE, distearoylphosphatidylethanolamine; FK506-liposome, polyethylene glycol-modified liposomes encapsulating FK506; HCO-60, polyoxyethylene (60) hydrogenated castor oil; HS, horse serum; ICA, internal carotid artery; I/R, ischemia-reperfusion; IVIS, *in vivo* imaging system; MCA, middle cerebral artery; MPO, myeloperoxidase; NGF, nerve growth factor; PEG, polyethylene glycol; t-MCAO, transient middle cerebral artery occlusion; TTC, 2,3,5-triphenyltetrazolium chloride; TTW, therapeutic time window; TUNEL, terminal deoxyribonucleotidyl transferase (TDT)-mediated dUTP-digoxigenin nick end labeling

[1] Correspondence: Department of Medical Biochemistry, School of Pharmaceutical Sciences, University of Shizuoka, 52-1 Yada, Suruga-ku, Shizuoka 422-8526, Japan. E-mail: oku@u-shizuoka-ken.ac.jp

doi: 10.1096/fj.12-221325

This article includes supplemental data. Please visit *http://www.fasebj.org* to obtain this information.

0892-6638/13/0027-1362 © FASEB

tic strategy. The therapeutic effect of liposomes encapsulating a neuroprotective chemodrug on I/R injury has not been examined yet. Therefore, in this study designed for achieving this purpose and developing a novel neuroprotectant, we prepared polyethylene glycol (PEG)-modified liposomes encapsulating FK506 (FK506-liposomes).

The immunosuppressant FK506 has been widely used to prevent allograft rejections in clinical organ transplantation, and was also recently reported to be a drug candidate for the treatment of acute stroke in animal studies (6 – 8). Calcineurin is activated by excessive influx of Ca^{2+} into cerebral cells after a cerebral ischemic event, resulting in the induction of nitric oxide, generation of inflammatory cytokines, and the release of cytochrome *c* (9 –12). FK506 inhibits the activation of calcineurin by associating with the FK506-binding protein (FKBP) in neuronal cells and glial cells; hence, it shows a neuroprotective effect on experimental stroke models. However, the frequent administration of FK506 required to achieve a good outcome has the risk of developing side effects such as heart deficits and nephrotoxicity. The liposomalization of FK506 is a promising approach for changing the biodistribution and negating the problem of poor water solubility (13, 14). The liposomal formulation of FK506 is as effective as an equal dose of commercial FK506 in preventing the rejection of transplant grafts, but with considerably less nephrotoxicity (14). The efficient delivery of FK506 to ischemic regions by using liposomes might potentially reduce the administration dosage without changing neuroprotective efficacy. In the present study, we assessed the potential of FK506-liposomes as a neuroprotectant against cerebral I/R injury by investigating their cerebral distribution, pharmacological activity, therapeutic effect, and therapeutic time window in t-MCAO rats.

MATERIALS AND METHODS

Animals

Male Wistar rats (170 –210 g) were purchased from Japan SLC, Inc. (Shizuoka, Japan). The animals were cared for according to the Animal Facility Guidelines of the University of Shizuoka. All animal procedures were approved by the Animal and Ethics Review Committee of the University of Shizuoka.

Preparation of FK506-liposomes

The lipid composition of FK506-liposomes was dipalmitoylphosphatidylcholine (DPPC) and distearoylphosphatidylethanolamine (DSPE)-PEG (molecular weight of PEG was 2000) in a 20:1 molar ratio. FK506-liposomes were prepared by the following freeze-drying method: FK506 was dissolved in methanol and added to a flask containing the above lipids dissolved in *tert*-butylalcohol. The molar ratio of FK506 to DPPC was 1:50. The solution was lyophilized, and then the lyophilizate was hydrated with PBS (pH 7.4) at 50°C. The liposome solution was freeze-thawed for 3 cycles with liquid nitrogen. Then the particle size of the liposomes was adjusted by extrusion through 100-nm pore-size polycarbonate filters (Nuclepore, Cambridge, MA, USA). Unencapsulated FK506 was removed by ultracentrifugation at 604,000 *g* for 15 min (Hitachi, Tokyo, Japan), and the concentration of FK506 in the liposomes was determined by HPLC (Hitachi). Final liposomal concentration was 10 mM as DSPC. FK506-liposomes were dissolved in tetrahydrofuran, and 20 j.Ll of the solution was injected into an octadecylsilane (ODS) column (TSK gel ODS-80TM, 4.6×150 mm, Tosoh, Tokyo, Japan). The mobile phase consisted of acetonitrile and water (3:2, v/v). HPLC analysis was performed at 60°C and a flow rate of 1 ml/min with UV detection at 214 nm. For the cerebral distribution study, 1,1=-dioctadecyl-3,3,3=,3=-tetramethylindocarbocyanine (DiI-C_{18}; Molecular Probes Inc., Eugene, OR, USA) was mixed with the initial lipid solution for fluorescence labeling of the liposomes.

Cell culture

Pheochromocytoma cells [PC12 cells; European Collection of Cell Cultures (ECACC), Porton Down, UK] were cultured in high-glucose DME medium (Wako, Osaka, Japan) supplemented with streptomycin (100 j.Lg/ml), penicillin (100 U/ml), heat-inactivated 5% fetal bovine serum (FBS; Japan Bioserum, Tokyo, Japan), and 10% horse serum (HS; MP Biomedicals, Solon, OH, USA) at 37°C in a humidified chamber with 5% CO_2. PC12 cells were plated on poly-d-lysine-coated 24-well plates for the WST (viability) assay. These cells were caused to differentiate into nerve-like cells by adding nerve growth factor (NGF) at 100 ng/ml to DME medium containing 0.5% HS. Five days after incubation with NGF, these cells were used for subsequent experiments.

Cell proliferation assays

FK506-liposomes (0.01, 0.1, or 1.0 j.LM as FK506 dosage) or free FK506 (1.0 j.LM) were added to differentiated PC12 cells in 24-well plates. H_2O_2 was added to each well to a final concentration of 75 j.LM at 30 min after addition of the samples. The number of viable cells was measured by using TetraColor One (Seikagaku, Tokyo, Japan). Briefly, TetraColar One solution was added to each well, and the cells were then incubated at 37°C for 3 h in a humidified atmosphere containing 5% CO_2. Absorbance at 450 nm was measured by using a Tecan Infinite M200 microplate reader (Tecan, Männedorf, Switzerland). FK506 was dissolved in ethanol, and the final concentration of ethanol was 0.1% in medium.

t-MCAO rats

Preparation of t-MCAO rats was performed as described previously (15). Briefly, anesthesia was induced with 3% isoflurane and maintained with 1.5% isoflurane during surgery. During surgery, the body temperature of the rats was maintained at 37°C with a heating pad. After a median incision of the neck skin had been made, the right carotid artery, external carotid artery, and internal carotid artery (ICA) were isolated with careful conservation of the vagal nerve. An ◆18 mm 4-0 monofilament nylon suture coated with silicon was introduced into the right ICA and advanced to the origin of the MCA to occlude it. Silk thread was used for ligation to keep the filament at the site of insertion into the MCA. After the surgery, the neck was closed; anesthesia was then discontinued. MCAO was performed for 1 h. Success of the surgery was judged by the appearance of hemiparesis and an increase in body temperature (>37.8°C). Reperfusion was started by withdrawing the filament ◆10 mm at 1 h after the start of occlusion under isoflurane anesthesia.

Drug administration

Polyoxyethylene (60) hydrogenated castor oil (HCO-60; 200 mg/ml), including 10% ethanol was used as vehicle for free FK506. FK506 or FK506-liposomes were intravenously injected at a single dose of 30, 100, or 300 μg/kg body weight (0.5 ml/rat) immediately after the start of reperfusion. In the therapeutic time window study, the injection time was shifted as indicated in the legend of **Fig. 6**. It was reported earlier that the vehicle has no effect on the outcome of ischemia (6, 16, 17).

Cerebral distribution of FK506-liposomes

PEGylated liposomes and FK506-liposomes were fluorescently labeled with DiI-C_{18} as described above. They were intravenously injected into the t-MCAO rats at the start of reperfusion. The rats were euthanized at 3 or 24 h after the injection, and their brains were sliced into 2-mm-thick coronal sections with a rat brain slicer (Muromachi Kikai, Tokyo, Japan). All sections were put on glass slides, and the fluorescence of DiI was measured with an *in vivo* imaging system (IVIS; Xenogen Corp., Alameda, CA, USA). Thereafter, these sections were embedded in optical cutting temperature (OCT) compound (Sakura, Finetech., CO Ltd., Tokyo, Japan) and then frozen in a dry ice/ethanol bath. These frozen sections were cut into 10-μm ones with a cryostat (HM505E; Microm, Walldorf, Germany) for subsequent immunostaining experiments. Average photon counts in I/R region were calculated from 4 rats at each time.

Immunostaining for CD31

The sections were incubated with 1% bovine serum albumin in PBS for 10 min at room temperature for blocking, and then with biotinylated anti-mouse CD31 rat monoclonal antibody (BD Pharmingen, Franklin Lakes, NJ, USA) for 18 h at 4°C, and thereafter with streptavidin-Alexa fluor 488 conjugates (Molecular Probes Inc.) for 30 min at room temperature. Finally, the sections were mounted with Perma Fluor Aqueous Mounting Medium (Thermo Shandon, Pittsburgh, PA, USA) and observed for fluorescence in the striatum with an LSM microscope system (Carl Zeiss Co., Ltd., Oberkochen, Germany).

Terminal deoxyribonucleotidyl transferase (TDT)-mediated dUTP-digoxigenin nick end labeling (TUNEL) staining

Brains of t-MCAO rats were dissected at 24 h after the injection of FK506-liposomes (100 μg/kg as FK506 dosage), free FK506 (100 μg/kg), PEGylated liposomes (same lipid concentration as FK506-liposomes), or PBS; embedded in optimal cutting temperature (OCT) compound (Sakura Finetek, Torrance, CA, USA); and then frozen in dry ice/ethanol. Frozen sections (10 μm) were prepared by using a cryostatic microtome (HM 505E, Microm, Walldorf, Germany) and were stained with TUNEL reagents supplied in an ApopTag Plus fluorescein *in situ* apoptosis detection kit (Chemicon International, Inc., Temecula, CA, USA), as described below. For fixation of the sections, they were incubated in 4% paraformaldehyde for 15 min at room temperature, and then in ethanol/acetic acid (2:1) solution for 5 min at −20°C. DNA strand breaks were labeled with the digoxigenin-conjugated terminal deoxynucleotidyl transferase enzyme by incubation for 1 h at 37°C. Then, the sections were incubated in antidigoxigenin-fluorescein solution for 30 min at room temperature. Finally, the sections were mounted with Perma Fluor aqueous mounting medium including DAPI (1.0 μg/ml) and observed for fluorescence with the LSM system. The observed area in the striatum was similar to the imaged region in **Fig. 2C, D**. For quantitative evaluation, the number of TUNEL-positive cells was counted in 4 sections/rat. Five rats were used to obtain the quantitative data.

Histological analysis of neutrophil influx

Frozen sections (7 μm) were prepared as described above. For fixation of these sections, they were incubated in acetone for 1 min at room temperature, and then in 0.3% H_2O_2 solution for 30 min at room temperature. After having been blocked with fetal bovine serum for 20 min at room temperature, the sections were incubated with anti-myeloperoxidase (MPO) rabbit polyclonal antibody (Thermo Fisher Scientific, Rockford, IL, USA) for 30 min at room temperature. A Vectastain ABC rabbit IgG kit and DAB peroxidase substrate kit (both from Vector Laboratories, Inc., Burlingame, CA, USA) were used for identification of neutrophils in the sections. Finally, the sections were counterstained with hematoxylin and observed microscopically (BX51; Olympus, Tokyo, Japan). The observed area in the striatum was similar to the imaged region in Fig. 2*C*, *D*.

Therapeutic experiment

FK506-liposomes (30 or 100 μg/kg as FK506 dosage), PBS, free FK506 (30, 100, or 300 μg/kg), or vehicle (200 mg/ml HCO-60 including 10% ethanol in PBS) for FK506 were intravenously injected into t-MCAO rats immediately after the start of reperfusion. The volume of damaged region, the degree of brain swelling, and the functional outcome of rats were assessed at 24 h after the injection. For the functional outcome study, the rats underwent a 21-point neurological score analysis prior to sacrifice, as described previously (18). All of the normal and sham-operated rats received 21 points in this test. After this study, the brains of t-MCAO rats were sliced into 2-mm-thick coronal sections by using a rat brain slicer (Muromachi Kikai) and stained with 2,3,5-triphenyltetrazolium chloride (TTC; Wako) for the detection of cerebral cell death. The volume of the damaged regions was calculated by using an image-analysis system (Image J; U.S. National Institutes of Health, Bethesda, MD, USA). The damaged regions were considered to be those appearing completely white. Brain swelling was calculated as the ratio of volumes between ipsilateral and contralateral hemisphere sections.

Assessment of therapeutic time window

t-MCAO rats were intravenously injected with FK506-liposomes (30 or 100 μg/kg as FK506 dosage) or PBS at various times after the start of reperfusion. The volume of damaged regions was assessed at 24 h after injection by using TTC staining as described above.

Statistical analysis

Statistical analysis was performed by 1-way analysis of variance (ANOVA) followed by Dunnett's multiple comparison tests. Data are presented as means ±SD.

RESULTS

FK506-liposomes protected differentiated PC12 cells from H_2O_2-induced toxicity

The particle size and ζ-potential of FK506 liposomes were 109 ±4.3 nm and −7.2 ±0.7 mV, respectively. To

assess the pharmacological activity of FK506-liposomes, we examined the cytoprotective effect of them on differentiated PC12 cells treated with H_2O_2. The number of live PC12 cells was decreased to ~40% by exposure to H_2O_2 (**Fig. 1**). FK506-liposomes suppressed this cell death induced by H_2O_2 in a dose-dependent manner, whereas empty-liposomes (PEGylated liposomes) showed no cytoprotective effect against the H_2O_2-induced toxicity.

FK506-liposomes diffused into the brain parenchyma only in the ischemic hemisphere

The intracerebral distribution of FK506-liposomes given immediately after the start of reperfusion to t-MCAO rats was observed at 3 h (Fig. 2*A*) and 24 h (Fig. 2*B*) after the injection. The fluorescence of DiI-labeled FK506-liposomes was observed only in the ischemic hemisphere at both time points. Immunohistological analysis revealed that the FK506-liposomes had leaked into the brain parenchyma from cerebral vessels in the ipsilateral hemisphere (Fig. 2*C*, *D*). Moreover, higher DiI fluorescence intensity was detected in the brain sections prepared at 24 h after the injection than in those prepared at 3 h (Fig. 2*E*) after it, which suggests that the accumulation of FK506-liposomes in the brain parenchyma gradually increased by continuous leakage from cerebral vessels according to enhanced permeability and the retention effect. In contrast, no leakage of them into the cerebral parenchyma of the contralateral hemisphere occurred.

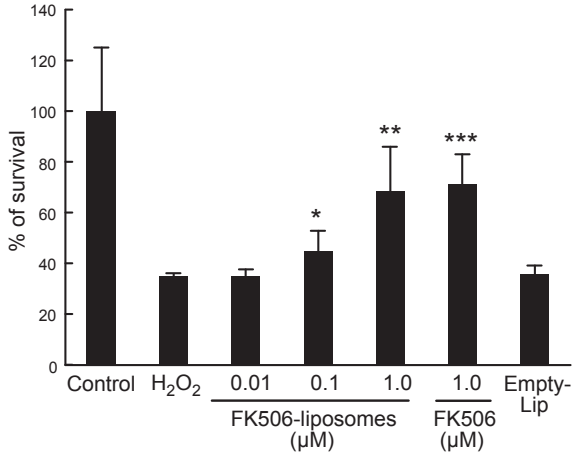

Figure 1. FK506-liposome-mediated attenuation of H_2O_2-induced cytotoxicity toward differentiated PC12 cells. PC12 cells were caused to differentiate by the addition of NGF at 100 ng/ml to culture medium supplemented with 0.5% HS. After 5 d in culture for differentiation, FK506-liposomes, free FK506, or empty liposomes (Empty-Lip) were added to the culture medium, and then H_2O_2 was added to each well. After 24 h, viable cell numbers were determined by performing the WST assay. Final lipid concentration of empty liposomes was same as that of FK506-liposomes. Data are presented as means ± sd (n = 6). *P < 0.05, **P < 0.01, ***P < 0.001 *vs.* H_2O_2-treated group.

FK506-liposomes showed antiapoptotic effect in t-MCAO rats

At 24 h after the injection of each sample, apoptosis of the cerebral cells in t-MCAO rats was identified by TUNEL staining (**Fig. 3**). TUNEL-positive cells were detected in neither the striatum nor the cerebral cortex in the nonischemic hemisphere (data not shown). A number of apoptotic cells were observed in the control group and free FK506-treated group (Fig. 3*A*, *B*). This dosage (100 μg/kg) of free FK506 was too low to exert an antiapoptotic effect in t-MCAO rats. However, FK506-liposomes obviously reduced the number of TUNEL-positive cells despite the same dosage as free FK506. Quantitative analysis of TUNEL-positive cells elucidated the difference between each group (Fig. 3*C*). In the FK506-liposome-treated group, the number of apoptotic cells in the striatum was significantly reduced compared with that in the other groups. In contrast to this result, there was no significant difference in the cortex between FK506-liposome-treated group and other groups, even though this treatment tended to suppress the cerebral apoptosis. Empty liposomes had no effect on apoptosis induced by I/R injury.

FK506-liposomes suppressed neutrophil invasion induced by I/R

To evaluate anti-inflammatory effect of FK506-liposomes, we examined neutrophil invasion into I/R regions as an indicator of intracerebral inflammation (**Fig. 4**). In the nonischemic hemisphere of all groups, almost no MPO-stained cells were identified (data not shown). Conversely, a number of neutrophils that had infiltrated were detected in the striatum and the cortex of the ischemic hemisphere (Fig. 4*A*, control). In the FK506-liposome-treated group, few MPO-positive cells were observed in the striatum, whereas they were more numerous in the cortex. The quantitative analysis revealed that FK506-liposomes reduced the number of infiltrating neutrophils in the striatum by ~80%, and significantly suppressed neutrophil invasion compared with the treatment with the same dosage of free FK506 (Fig. 4*B*).

FK506-liposomes ameliorated cerebral I/R injury in t-MCAO rats

t-MCAO caused cerebral cell death and brain swelling in these experimental model rats. Treatment with free FK506 at 30 or 100 μg/kg hardly affected the damaged region and brain swelling induced by I/R, whereas FK506-liposomes at these same dosages as the free drug significantly reduced the amount of brain damage (**Fig. 5A, B**). Furthermore, administration of FK506-liposomes at 100 μg/kg showed therapeutic efficacy quite similar to that obtained with the free drug at 300 μg/kg. These results suggest that liposomalization of FK506 enhanced its cytoprotective

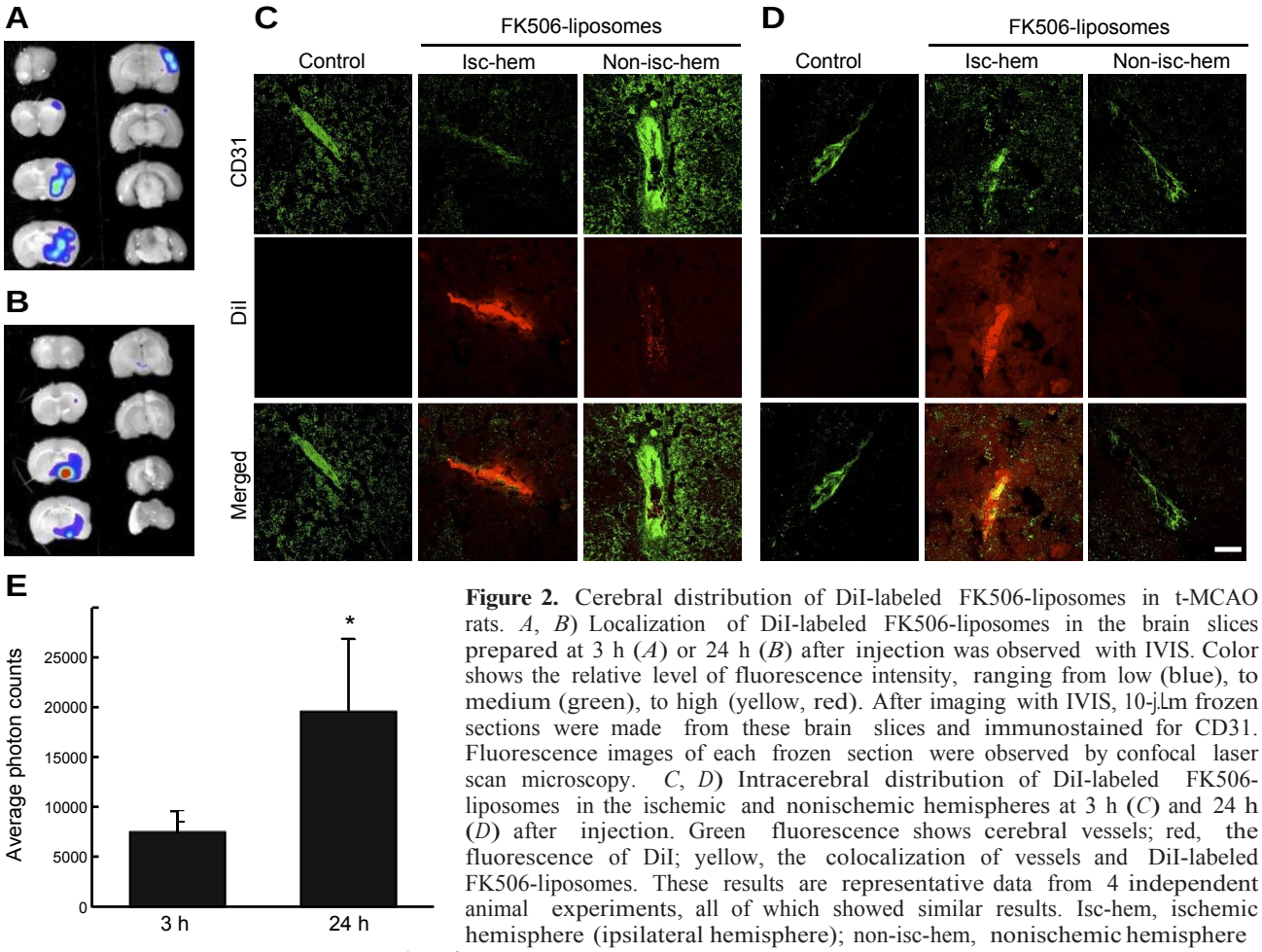

Figure 2. Cerebral distribution of DiI-labeled FK506-liposomes in t-MCAO rats. *A*, *B*) Localization of DiI-labeled FK506-liposomes in the brain slices prepared at 3 h (*A*) or 24 h (*B*) after injection was observed with IVIS. Color shows the relative level of fluorescence intensity, ranging from low (blue), to medium (green), to high (yellow, red). After imaging with IVIS, 10-j.Lm frozen sections were made from these brain slices and immunostained for CD31. Fluorescence images of each frozen section were observed by confocal laser scan microscopy. *C*, *D*) Intracerebral distribution of DiI-labeled FK506-liposomes in the ischemic and nonischemic hemispheres at 3 h (*C*) and 24 h (*D*) after injection. Green fluorescence shows cerebral vessels; red, the fluorescence of DiI; yellow, the colocalization of vessels and DiI-labeled FK506-liposomes. These results are representative data from 4 independent animal experiments, all of which showed similar results. Isc-hem, ischemic hemisphere (ipsilateral hemisphere); non-isc-hem, nonischemic hemisphere (contralateral hemisphere). Scale bar = 20 j.Lm. *E*) Average photon counts in the ischemic hemisphere were determined by the image of brain slices with IVIS ($n=4$). *$P < 0.05$.

effect due to improved biodistribution. In accordance with several reports, the extent of cerebral cell death, as indicated by reduced brain volume (Fig. 5*A*), and that of brain swelling (Fig. 5*B*) were similar in both control (PBS-injected) and vehicle-injected groups.

The therapeutic time window (TTW) of agents is critical information for developing neuroprotectants, particularly in designing the clinical trial. The TTW of FK506-liposomes was estimated by altering the time of injection after the commencement of reperfusion (Fig. 6). The volume of brain damage in the t-MCAO rats was significantly decreased by the dose of FK506-liposomes administered at 30 j.Lg/kg as FK506 up through 2 h after reperfusion had begun. However, the treatment with the same dose of FK506-liposomes given at 3 h after the start of reperfusion or later had almost no effect on cerebral cell death, as judged by the results of TTC staining. Moreover, a higher amount of FK506-liposomes (100 j.Lg/kg as FK506) injected at 3 h after reperfusion had begun also scarcely suppressed the brain damage. Taken together, these data indicate that the therapeutic time window for FK506-liposomes was up to 2 h after MCAO/reperfusion in this experimental model rat, and suggest that the injection of them at an early time would result in a good outcome.

The motor ability of the t-MCAO rats was evaluated based on the 21-point motor score (**Fig. 7**). In the control group, hemiparesis was observed at 24 h after the start of reperfusion, resulting in a low score. On the other hand, t-MCAO rats treated with FK506-liposomes showed alleviated hemiparesis, especially in their hind legs. This recovery probably contributed to the high scores on the inclined platform test, horizontal bar test (forepaws placed on ribbed bar), and circling test obtained for the FK506-liposome-treated animals (Supplemental Table S1). The administration of free FK506 at 300 j.Lg/kg also significantly improved motor function deficit. These results correlated well with the extent of cerebral cell death and swelling.

DISCUSSION

The present study showed that FK506-liposomes significantly suppressed neutrophil invasion and apoptotic cell death, and ameliorated neurological deficits in t-MCAO rats compared with free FK506. The liposomalization of FK506 might lead to an increase in the amount of drug accumulation in I/R regions. The disruption of blood-brain barrier is induced at an early

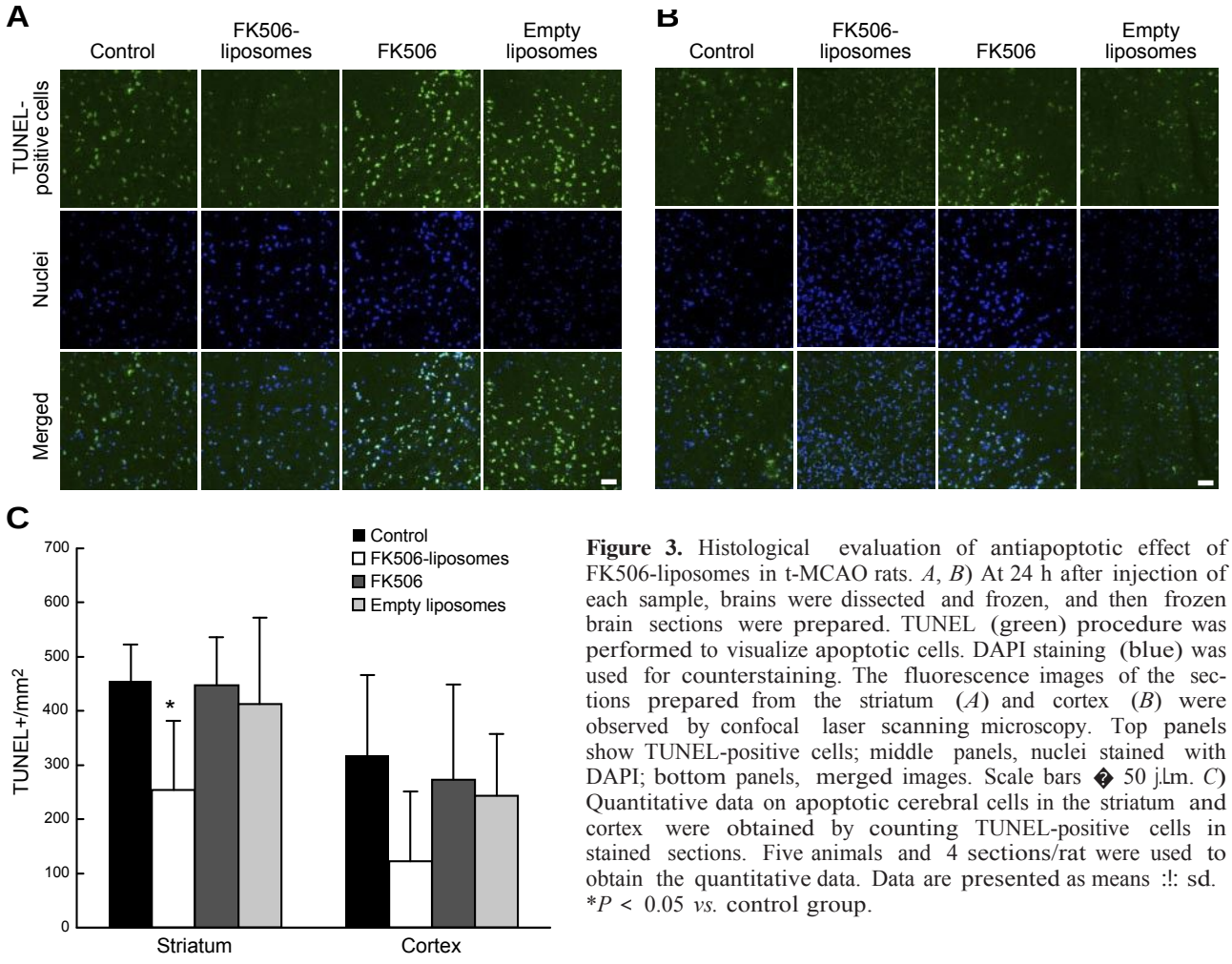

Figure 3. Histological evaluation of antiapoptotic effect of FK506-liposomes in t-MCAO rats. *A*, *B*) At 24 h after injection of each sample, brains were dissected and frozen, and then frozen brain sections were prepared. TUNEL (green) procedure was performed to visualize apoptotic cells. DAPI staining (blue) was used for counterstaining. The fluorescence images of the sections prepared from the striatum (*A*) and cortex (*B*) were observed by confocal laser scanning microscopy. Top panels show TUNEL-positive cells; middle panels, nuclei stained with DAPI; bottom panels, merged images. Scale bars = 50 μm. *C*) Quantitative data on apoptotic cerebral cells in the striatum and cortex were obtained by counting TUNEL-positive cells in stained sections. Five animals and 4 sections/rat were used to obtain the quantitative data. Data are presented as means ± sd. $^{*}P < 0.05$ *vs.* control group.

stage in the ischemic core region after cerebral ischemia (19, 20). Moreover, a previous report demonstrated that the area in which macromolecules accumulate expands as time passes after I/R in t-MCAO rats (21). Hence, the concept of passive targeting, as constructed for cancer treatment, could be a promising scheme for efficient drug delivery to I/R regions. In the present study, a higher extent of localization of FK506-liposomes in the ischemic hemisphere was observed at 24 h than at 3 h after the injection. This result suggests that the accumulation amount of FK506-liposomes given at the start of reperfusion gradually increased in

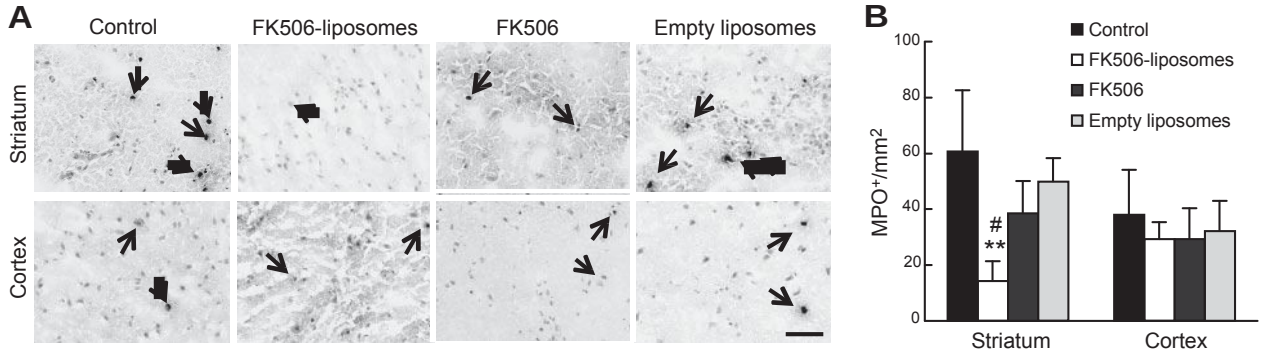

Figure 4. Invasion of neutrophils into the brain parenchyma of t-MCAO rats. At 24 h after injection of each sample, brains were dissected and frozen; and then frozen brain sections were prepared. MPO immunostaining was performed to visualize neutrophils (brown). Hematoxylin staining (blue) was used for counterstaining. *A*) Stained sections were observed by microscopy. Arrows indicate neutrophils that had infiltrated the brain parenchyma. Scale bar = 50 μm. *B*) Quantitative data on neutrophil invasion analysis were obtained by counting MPO-positive cells in stained sections. Data are presented as means ± sd ($n=6$). $^{**}P < 0.01$ *vs.* control group; $^{\#}P < 0.05$ *vs.* free FK506-treated group.

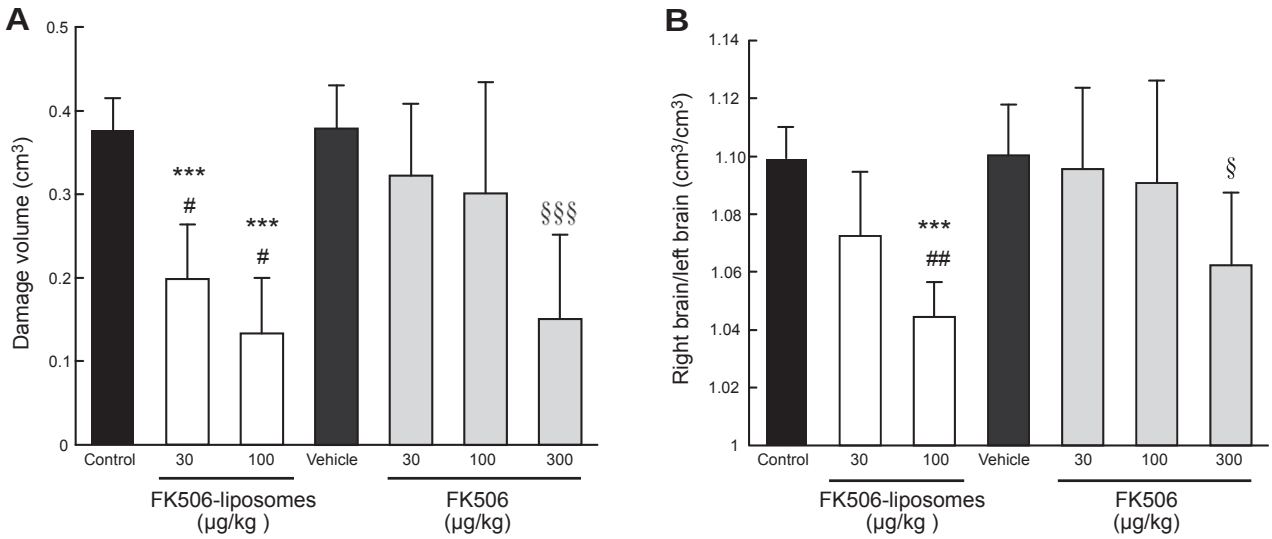

Figure 5. Suppression of cerebral cell death and brain swelling by the treatment with FK506-liposomes. t-MCAO rats were injected *via* a tail vein with PBS, FK506-liposomes, vehicle for free FK506 or free FK506 immediately after the start of reperfusion at dosages indicated as FK506. At 24 h after injection, brains were dissected and stained with TTC. Damage volume (*A*) and degree of brain swelling (*B*) were calculated by using Image J. Data are means ±sd (n=7). ***P < 0.001 *vs.* control group; $^{\#}P$ < 0.05, $^{\#\#}P$ < 0.01 *vs.* free FK506-treated group at the same dose; $^{\S}P$ < 0.05, $^{\S\S\S}P$ < 0.001 *vs.* vehicle-treated group.

a time-dependent manner, as in the case of enhanced permeability and retention effect. However, the half-life of free FK506 is extremely short, and FK506 administered intravenously is almost totally metabolized by the liver, primarily by cytochrome P450 3A (22, 23). The change in biodistribution afforded by liposomalization would be expected to be closely related to the therapeutic outcome.

Fatal damage in the striatum, the region assumed to be the ischemic core in the present experimental model, occurs at an early stage after an I/R event (21). In this study, FK506-liposomes substantially reduced the cerebral cell death and inflammation induced by I/R in this region. Thus, FK506-liposomes spreading into the brain parenchyma quickly showed pharmacological activity. Although PEG-modification of liposomes prolongs their circulation in the blood, it causes a decrease in cellular uptake of liposomes (24, 25). Therefore, FK506-liposomes reaching I/R regions might have released FK506 into the brain parenchyma, and the released drugs then acted on the cerebral cells.

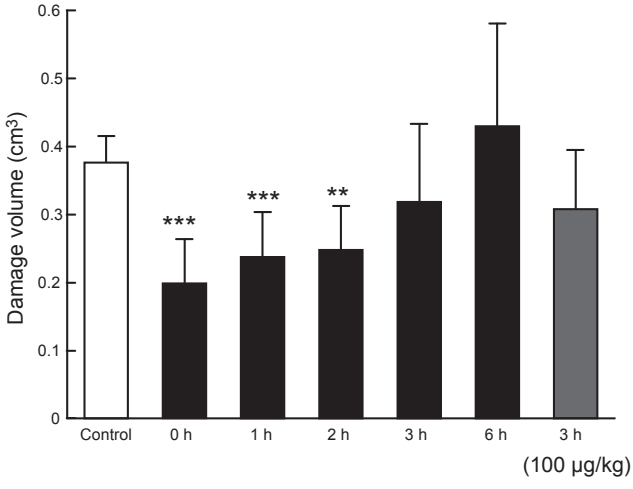

Figure 6. Therapeutic time window of FK506-liposomes in t-MCAO rats. t-MCAO rats were intravenously injected *via* a tail vein with FK506-liposomes (30 or 100 j.lg/kg as FK506 dosage) at the indicated times (0, 1, 2, 3, or 6 h) after the start of reperfusion. At 24 h after reperfusion had begun, brain was dissected and stained with TTC. Damage volume was calculated by using Image J. Data are presented as means ±sd (n=6–7). **P < 0.01, ***P < 0.001 *vs.* control.

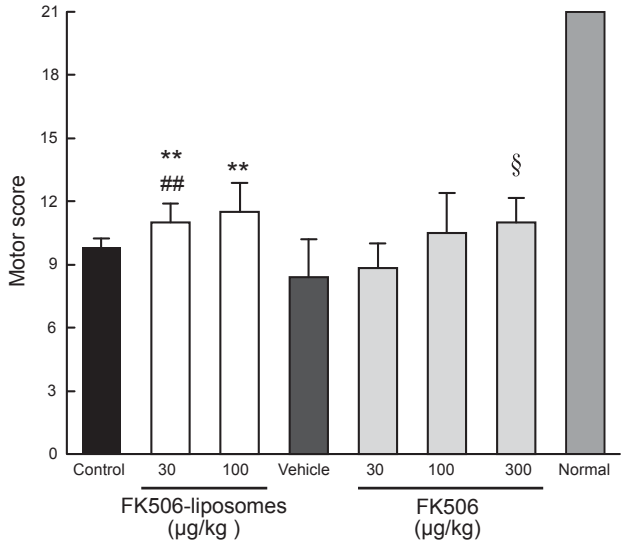

Figure 7. Motor activity score of t-MCAO rats. t-MCAO rats were treated with each sample as described in the legend of Fig. 5, and these rats were then assessed for motor function in a 21-point neuropathological scoring system. Data are presented as means ±sd (n=7). **P < 0.01 *vs.* control group; $^{\#\#}P$ < 0.01 *vs.* free FK506-treated group at the same dose; $^{\S}P$ < 0.05 *vs.* vehicle-treated group.

Neutrophils generate cytotoxic substances such as hypochlorous acid in inflammation sites, resulting in progressive inflammation. These cells normally do not exist in the brain, but they do invade into the cerebral parenchyma *via* brain endothelial cells after a cerebral ischemic event. This invasion induced by intracerebral inflammation occurs during the period of 9 to 24 h after the start of reperfusion in t-MCAO rats (26). Therefore, the observation of neutrophil invasion is one way to assess the extent of cerebral inflammation after I/R. In the present study, FK506-liposomes significantly suppressed the neutrophil invasion induced by cerebral I/R. A past study showed that FK506 inhibits the expression of adhesion molecules in the cerebral vasculature by reducing the production of inflammatory cytokines by neuronal cells and glia cells (26). Accordingly, we suggest that FK506-liposomes administered after the start of reperfusion inhibited the inflammatory response by affecting neuronal cells and glia cells in the t-MCAO rats.

FK506 directly suppresses apoptotic cell death induced by cerebral I/R through the inhibition of Bad dephosphorylation and subsequent cytochrome *c* release (27, 28). In addition, the prevention of reactive oxygen species production is related to its antiapoptotic effect on cerebral cells injured by I/R (29). The present study demonstrated that FK506-liposomes markedly reduced the number of apoptotic cells in t-MCAO rats. These multifunctional mechanisms, including the anti-inflammatory effect of FK506-liposomes, probably effectively acted on the neurovascular unit to bring about the good outcome in the t-MCAO rats.

A large number of small molecules as neuroprotectants have failed in clinical trials (30). Based on our present data, we propose that liposomalization of small molecular neuroprotectants should overcome their insufficiency of medicinal efficacy and adverse side effects. Liposomes can encapsulate many kinds of drugs regardless of their being hydrophilic or hydrophobic. Furthermore, liposomes can be modified with functional molecules, resulting in improved biodistribution, controlled release of drugs, increase in drug accumulation in targeted cells, regulation of intracellular distribution, and so on (31–34). Therefore, liposomal DDS has a great potential to be a novel strategy for the treatment of cerebral I/R injury.

In summary, our data demonstrate the usefulness of FK506-liposomes for the treatment of cerebral ischemia/reperfusion injury. FK506-liposomes intravenously injected immediately after the start of reperfusion significantly suppressed neutrophil invasion, apoptotic cell death, and infarct volume compared with free FK506 in t-MCAO rats. In addition, the motor function deficits induced by ischemia/reperfusion in these rats were ameliorated to a greater extent by the treatment with FK506-liposomes than by that with free FK506. Therefore, liposomalization of FK506 should permit a reduction in the dosage of FK506 without a decrease in the therapeutic efficacy of the drug. Taken together, our present findings indicate that FK506-liposomes have a clear potential to be a neuroprotectant if administered quickly after a cerebral stroke. FJ

The authors thank Astellas Pharmaceutical Co., Ltd. (Tokyo, Japan) for the gift of the FK506. This research was supported by a grant-in-aid for scientific research from the Japan Society for the Promotion of Science.

REFERENCES

1. Wong, C. H., and Crack, P. J. (2008) Modulation of neuro-inflammation and vascular response by oxidative stress following cerebral ischemia-reperfusion injury. *Curr. Med. Chem.* **15,** 1–14
2. Eltzschig, H. K., and Eckle, T. (2011) Ischemia and reperfusion–from mechanism to translation. *Nat. Med.* **17,** 1391–1401
3. Tuma, R. F., and Steffens, S. (2012) Targeting the endocannabinod system to limit myocardial and cerebral ischemic and reperfusion injury. *Curr. Pharm. Biotechnol.* **13,** 46–58
4. Ginsberg, M. D. (2009) Current status of neuroprotection for cerebral ischemia: synoptic overview. *Stroke* **40,** S111–114
5. Ishii, T., Asai, T., Oyama, D., Fukuta, T., Yasuda, N., Shimizu, K., Minamino, T., and Oku, N. (2012) Amelioration of cerebral ischemia-reperfusion injury based on liposomal drug delivery system with asialo-erythropoietin. *J. Control. Release* **160,** 81–87
6. Sharkey, J., and Butcher, S. P. (1994) Immunophilins mediate the neuroprotective effects of FK506 in focal cerebral ischaemia. *Nature* **371,** 336–339
7. Furuichi, Y., Maeda, M., Moriguchi, A., Sawamoto, T., Kawamura, A., Matsuoka, N., Mutoh, S., and Yanagihara, T. (2003) Tacrolimus, a potential neuroprotective agent, ameliorates ischemic brain damage and neurologic deficits after focal cerebral ischemia in nonhuman primates. *J. Cereb. Blood Flow Metab.* **23,** 1183–1194
8. Szydlowska, K., Zawadzka, M., and Kaminska, B. (2006) Neuroprotectant FK506 inhibits glutamate-induced apoptosis of astrocytes in vitro and in vivo. *J. Neurochem.* **99,** 965–975
9. Morioka, M., Hamada, J., Ushio, Y., and Miyamoto, E. (1999) Potential role of calcineurin for brain ischemia and traumatic injury. *Prog. Neurobiol.* **58,** 1–30
10. Wang, H. G., Pathan, N., Ethell, I. M., Krajewski, S., Yamaguchi, Y., Shibasaki, F., McKeon, F., Bobo, T., Franke, T. F., and Reed, J. C. (1999) Ca2+-induced apoptosis through calcineurin dephosphorylation of BAD. *Science* **284,** 339–343
11. Hashiguchi, A., Kawano, T., Yano, S., Morioka, M., Hamada, J., Sato, T., Shirasaki, Y., Ushio, Y., and Fukunaga, K. (2003) The neuroprotective effect of a novel calmodulin antagonist, 3-[2-[4-(3-chloro-2-methylphenyl)-1-piperazinyl]ethyl]-5,6-dimethoxy-1-(4-imidazolylmethyl)-1H-indazole dihydrochloride 3.5 hydrate, in transient forebrain ischemia. *Neuroscience* **121,** 379–386
12. Kaminska, B., Gaweda-Walerych, K., and Zawadzka, M. (2004) Molecular mechanisms of neuroprotective action of immunosuppressants–facts and hypotheses. *J. Cell. Mol. Med.* **8,** 45–58
13. Chuang, Y. C., Tyagi, P., Huang, H. Y., Yoshimura, N., Wu, M., Kaufman, J., and Chancellor, M. B. (2011) Intravesical immune suppression by liposomal tacrolimus in cyclophosphamide-induced inflammatory cystitis. *Neurourol. Urodyn.* **30,** 421–427
14. Moffatt, S. D., McAlister, V., Calne, R. Y., and Metcalfe, S. M. (1999) Potential for improved therapeutic index of FK506 in liposomal formulation demonstrated in a mouse cardiac allograft model. *Transplantation* **67,** 1205–1208
15. Longa, E. Z., Weinstein, P. R., Carlson, S., and Cummins, R. (1989) Reversible middle cerebral artery occlusion without craniectomy in rats. *Stroke* **20,** 84–91
16. Zhang, N., Komine-Kobayashi, M., Tanaka, R., Liu, M., Mizuno, Y., and Urabe, T. (2005) Edaravone reduces early accumulation of oxidative products and sequential inflammatory responses after transient focal ischemia in mice brain. *Stroke* **36,** 2220–2225
17. Toung, T. J., Bhardwaj, A., Dawson, V. L., Dawson, T. M., Traystman, R. J., and Hurn, P. D. (1999) Neuroprotective FK506 does not alter in vivo nitric oxide production during ischemia and early reperfusion in rats. *Stroke* **30,** 1279–1285

18. Hunter, A. J., Hatcher, J., Virley, D., Nelson, P., Irving, E., Hadingham, S. J., and Parsons, A. A. (2000) Functional assessments in mice and rats after focal stroke. *Neuropharmacology* **39,** 806–816
19. Rosenberg, G. A., Estrada, E. Y., and Dencoff, J. E. (1998) Matrix metalloproteinases and TIMPs are associated with blood-brain barrier opening after reperfusion in rat brain. *Stroke* **29,** 2189–2195
20. Dirnagl, U., Iadecola, C., and Moskowitz, M. A. (1999) Pathobiology of ischaemic stroke: an integrated view. *Trends Neurosci.* **22,** 391–397
21. Ishii, T., Asai, T., Urakami, T., and Oku, N. (2010) Accumulation of macromolecules in brain parenchyma in acute phase of cerebral infarction/reperfusion. *Brain Res.* **1321,** 164–168
22. Yura, H., Yoshimura, N., Hamashima, T., Akamatsu, K., Nishikawa, M., Takakura, Y., and Hashida, M. (1999) Synthesis and pharmacokinetics of a novel macromolecular prodrug of Tacrolimus (FK506), FK506-dextran conjugate. *J. Control. Release* **57,** 87–99
23. Shiraga, T., Matsuda, H., Nagase, K., Iwasaki, K., Noda, K., Yamazaki, H., Shimada, T., and Funae, Y. (1994) Metabolism of FK506, a potent immunosuppressive agent, by cytochrome P450 3A enzymes in rat, dog and human liver microsomes. *Biochem. Pharmacol.* **47,** 727–735
24. Duzgune, scedil, and Nir, S. (1999) Mechanisms and kinetics of liposome-cell interactions. *Adv. Drug Deliv. Rev.* **40,** 3–18
25. Vertut-Doi, A., Ishiwata, H., and Miyajima, K. (1996) Binding and uptake of liposomes containing a poly(ethylene glycol) derivative of cholesterol (stealth liposomes) by the macrophage cell line J774: influence of PEG content and its molecular weight. *Biochim. Biophys. Acta* **1278,** 19–28
26. Noto, T., Furuichi, Y., Ishiye, M., Matsuoka, N., Aramori, I., Mutoh, S., and Yanagihara, T. (2007) Tacrolimus (FK506) limits accumulation of granulocytes and platelets and protects against brain damage after transient focal cerebral ischemia in rat. *Biol. Pharm. Bull.* **30,** 313–317
27. Li, J. Y., Furuichi, Y., Matsuoka, N., Mutoh, S., and Yanagihara, T. (2006) Tacrolimus (FK506) attenuates biphasic cytochrome c release and Bad phosphorylation following transient cerebral ischemia in mice. *Neuroscience* **142,** 789–797
28. Shichinohe, H., Kuroda, S., Abumiya, T., Ikeda, J., Kobayashi, T., Yoshimoto, T., and Iwasaki, Y. (2004) FK506 reduces infarct volume due to permanent focal cerebral ischemia by maintaining BAD turnover and inhibiting cytochrome c release. *Brain Res.* **1001,** 51–59
29. Dawson, T. M., Steiner, J. P., Dawson, V. L., Dinerman, J. L., Uhl, G. R., and Snyder, S. H. (1993) Immunosuppressant FK506 enhances phosphorylation of nitric oxide synthase and protects against glutamate neurotoxicity. *Proc. Natl. Acad. Sci. U.|S.|A.* **90,** 9808–9812
30. Sahota, P., and Savitz, S. I. (2011) Investigational therapies for ischemic stroke: neuroprotection and neurorecovery. *Neurotherapeutics* **8,** 434–451
31. Asai, T., Matsushita, S., Kenjo, E., Tsuzuku, T., Yonenaga, N., Koide, H., Hatanaka, K., Dewa, T., Nango, M., Maeda, N., Kikuchi, H., and Oku, N. (2011) Dicetyl phosphate-tetraethylenepentamine-based liposomes for systemic siRNA delivery. *Bioconjug. Chem.* **22,** 429–435
32. Tan, M. L., Choong, P. F., and Dass, C. R. (2010) Recent developments in liposomes, microparticles and nanoparticles for protein and peptide drug delivery. *Peptides* **31,** 184–193
33. Torres, E., Mainini, F., Napolitano, R., Fedeli, F., Cavalli, R., Aime, S., and Terreno, E. (2011) Improved paramagnetic liposomes for MRI visualization of pH triggered release. *J. Control. Release* **154,** 196–202
34. Micheli, M. R., Bova, R., Magini, A., Polidoro, M., and Emiliani, C. (2012) Lipid-based nanocarriers for CNS-targeted drug delivery. *Recent Pat. CNS Drug Discov.* **7,** 71–86

Received for publication October 1, 2012.
Accepted for publication December 4, 2012.

Am J Physiol Heart Circ Physiol 304: H1361–H1369, 2013.
First published March 15, 2013; doi:10.1152/ajpheart.00454.2012.

Dipeptidyl-peptidase IV inhibition improves pathophysiology of heart failure and increases survival rate in pressure-overloaded mice

Ayako Takahashi,[1,4] Masanori Asakura,[2] Shin Ito,[1] Kyung-Duk Min,[1] Kazuhiro Shindo,[1,4] Yi Yan,[4] Yulin Liao,[6] Satoru Yamazaki,[1] Shoji Sanada,[5] Yoshihiro Asano,[4,5] Hatsue Ishibashi-Ueda,[3] Seiji Takashima,[4,5] Tetsuo Minamino,[5] Hiroshi Asanuma,[7] Naoki Mochizuki,[1] and Masafumi Kitakaze[2]

[1]*Department of Cell Biology,* [2]*Department of Clinical Research and Development, and* [3]*Division of Pathology, National Cerebral and Cardiovascular Center, Osaka, Japan;* [4]*Department of Molecular Cardiology and* [5]*Department of Cardiovascular Medicine, Osaka University Graduate School of Medicine, Osaka, Japan;* [6]*Department of Cardiology, Nanfang Hospital, Southern Medical University, Guangzhou, China; and* [7]*Department of Cardiology, Kyoto Prefectural University School of Medicine, Kyoto, Japan*

Submitted 12 June 2012; accepted in final form 25 January 2013

Takahashi A, Asakura M, Ito S, Min KD, Shindo K, Yan Y, Liao Y, Yamazaki S, Sanada S, Asano Y, Ishibashi-Ueda H, Takashima S, Minamino T, Asanuma H, Mochizuki N, Kitakaze M. Dipeptidyl-peptidase IV inhibition improves pathophysiology of heart failure and increases survival rate in pressure-overloaded mice. *Am J Physiol Heart Circ Physiol* 304: H1361–H1369, 2013. First published March 15, 2013; doi:10.1152/ajpheart.00454.2012.—Incretin hormones, including glucagon-like peptide-1 (GLP-1), a target for diabetes mellitus (DM) treatment, are associated with cardioprotection. As dipeptidyl-peptidase IV (DPP-IV) inhibition increases plasma GLP-1 levels in vivo, we investigated the cardioprotective effects of the DPP-IV inhibitor vildagliptin in a murine heart failure (HF) model. We induced transverse aortic constriction (TAC) in C57BL/6J mice, simulating pressure-overloaded cardiac hypertrophy and HF. TAC or sham-operated mice were treated with or without vildagliptin. An intraperitoneal glucose tolerance test revealed that blood glucose levels were higher in the TAC than in sham-operated mice, and these levels improved with vildagliptin administration in both groups. Vildagliptin increased plasma GLP-1 levels in the TAC mice and ameliorated TAC-induced left ventricular enlargement and dysfunction. Vildagliptin palliated both myocardial apoptosis and fibrosis in TAC mice, demonstrated by histological, gene and protein expression analyses, and improved survival rate on *day 28* (TAC with vildagliptin, 67.5%; TAC without vildagliptin, 41.5%; $P < 0.05$). Vildagliptin improved cardiac dysfunction and overall survival in the TAC mice, both by improving impaired glucose tolerance and by increasing GLP-1 levels. DPP-IV inhibitors represent a candidate treatment for HF patients with or without DM.

heart failure; impaired glucose tolerance; dipeptidyl-peptidase IV inhibitor

HEART FAILURE (HF) is a leading causes of death in humans worldwide (1, 20, 37, 56), and is often linked to impaired glucose tolerance or diabetes mellitus (DM) (21, 53). DM is a major risk factor for cardiac dysfunction; Lind et al. (28) reported that poor glycemic control among patients with type 1 DM led to a high incidence of cardiovascular events. The energetic substrate utilization of cardiomyocytes under hyperglycemic conditions shifts from glucose to fatty acid oxidation, leading to HF (38). In DM, oxidative stress also causes endothelial dysfunction and decreases endothelial NO release, inducing microangiopathy (13, 31). Either glucose abnormalities or diabetes commonly exists in patients with HF, but as previously reported, patients with diabetes have no worse outcome of HF (50). Our previous clinical study revealed that ~90% of patients with chronic HF had impaired glucose tolerance (21).

Incretin hormones have recently been proposed as new targets for DM treatment. Glucagon-like peptide-1 (GLP-1) is an incretin hormone secreted from the lower intestines and colon, which stimulates insulin secretion from pancreatic beta cells. Its receptors are ubiquitously expressed, including in the cardiovascular system (8). GLP-1 is thought to possess cardioprotective properties because of the following three reasons: *1*) GLP-1 receptors localize to cardiomyocytes and endothelial cells (3, 57); *2*) activation of GLP-1 receptors increases phosphoinositide 3 (PI3)-kinase, serine/threonine protein kinase Akt (Akt), and extracellular signal-regulated kinase phosphorylation, potentially mediating cardioprotection (6, 19); and *3*) activation of GLP-1 receptors stimulates p38 mitogen-activated protein (MAP) kinase and endothelial nitric oxide synthase via protein kinase A activation, putatively affecting cardioprotection (5, 59) and plasma glucose normalization (16). As dipeptidyl-peptidase IV (DPP-IV) rapidly degrades GLP-1, which has a biological half-life of approximately 1.5–5 min (11, 18), both GLP-1 analogs and DPP-IV inhibitors have been developed as new drugs to treat type 2 DM. GLP-1 analogs reportedly ameliorate not only DM but also HF and myocardial ischemia (15, 33, 34, 48, 59), suggesting that DPP-IV inhibitors function cardioprotectively. Indeed, DPP-IV inhibitors are reportedly effective against myocardial infarction in mice and pacing-induced heart failure in pigs (14, 42, 59), suggesting that DPP-IV inhibitors may also affect the survival rate. However, the effects of DPP-IV inhibitors on the pathophysiology of pressure-overloaded HF and survival after HF are unknown.

We aimed to clarify whether vildagliptin, a DPP-IV inhibitor, improves the pathophysiology of HF and increases survival rate in pressure-overloaded mice.

METHODS

All of the animal care procedures were performed according to the American Physiological Society "Guiding Principles in the Care and Use of Vertebrate Animals in Research and Training" and with the approval of the ethical committee of Osaka University.

Address for reprint requests and other correspondence: M. Asakura, Dept. of Clinical Research and Development, National Cerebral and Cardiovascular Center, 5-7-1, Fujishirodai, Suita, Osaka, 565-8565 Japan (e-mail: masakura@ncvc.go.jp).

Animal preparation. Male C57BL/6J mice (8 wk old, weighing 22–24 g) were purchased from CLEA Japan, (Tokyo, Japan). After 1 wk of observation, either transverse aortic constriction (TAC) or a sham operation was performed as previously described (24). In brief, the transverse aorta was isolated between the carotid arteries and constricted by a 7-0 silk suture ligature tied firmly against a 30-gauge needle. Sham-operated mice underwent a similar surgical procedure without aortic constriction. The needle was promptly removed, and the chest was closed with a 5-0 silk suture. Each surgical procedure was completed within 30 min to maintain the body temperature at 37°C.

Experimental protocol. Vildagliptin was gifted by Novartis Pharmaceuticals (Basel, Switzerland). The sham-operated or TAC mice were randomly divided into two subgroups; the sham-operated group with ($n = 10$) or without vildagliptin ($n = 10$) and TAC with ($n = 40$) or without vildagliptin ($n = 41$). The vildagliptin treatment subgroups were provided with drinking water containing vildagliptin (10 mg·kg body wt^{-1}·day^{-1}) (39, 58), and the other groups received unsupplemented drinking water from 1 day postsurgery. The mice were allowed to drink ad libitum, and the drinking volumes were measured. The mice were fed a normal chow diet for 4 wk.

Echocardiography. Transthoracic echocardiography was performed before euthanasia as previously described (24). In brief, at 4 wk postsurgery, the mice were placed in a supine position without anesthesia. Short-axis, two-dimensional guided M-mode Doppler echocardiograms were captured and analyzed offline using a Vevo 770 High-Resolution in vivo Micro-Imaging System (VisualSonics, Toronto, Canada) equipped with a 15- to 45-MHz transducer. Left ventricular (LV) end-diastolic diameter (Dd), end-systolic diameter (Ds), and fractional shortening (FS) were measured. All measurements were made from leading edge to leading edge, according to the American Society of Echocardiography guidelines (22). Percentage FS was calculated as follows: $\%FS = [(LVDd - LVDs)/LVDd] \times 100$. The investigator performing and interpreting the echocardiograms was blinded to the subgroups.

Hemodynamic assessment. To confirm pressure overload, four to five mice in each group were randomly selected for LV pressure measurement, as previously described (27). In brief, under pentobarbital anesthesia, an endotracheal tube was inserted and connected to a volume-cycled rodent ventilator. A 1.4-Fr micromanometer-tipped catheter (Millar Instruments, Houston, TX) was inserted into the right carotid artery, blood pressure and heart rate were measured simultaneously, and data were acquired using the PowerLab Data Acquisition System (AD Instruments, Bella Vista, NSW, Australia).

Analysis of intraperitoneal glucose tolerance test. Four weeks after either TAC or sham operation, about half of the surviving mice, namely five mice in each sham-operated group and 12 and 8 mice in TAC with and without vildagliptin groups, were randomly selected for an intraperitoneal glucose tolerance test following overnight fasting (12–16 h). As overnight fasting and glucose injection might be stressful, we enrolled only half of the surviving mice to reduce the effect on additional deaths. Glucose (1 mg/kg body wt) was injected into the intraperitoneal cavity, as previously described (54). Blood was sampled from the tail prior to and at 30, 60, 90, and 120 min after glucose administration. Blood glucose concentrations were measured by a glucose meter using the glucose oxidase method (Glutest Ace R; Sanwa Kagaku Kenkyusho, Nagoya, Japan).

GLP-1 measurement [ELISA]. Four weeks after treatment, their chests were opened under anesthesia 1 h after feeding following overnight fasting for GLP-1 measurement by enzyme-linked immunosorbent assay (ELISA). Blood samples were obtained from the hearts and immediately collected in BD P700 tubes (Becton Dickinson, Franklin Lakes, NJ) containing EDTA and DPP-IV protease inhibitor cocktail. The tubes were centrifuged at 1,200 *g* for 10 min to extract plasma. The plasma samples were then stored at −80°C in a freezer until GLP-1 assay. Plasma GLP-1 levels were measured using a Glucagon-Like Peptide-1 (Active) ELISA Kit (Millipore, Billerica, MA) according to the manufacturer's instructions (52). The GLP-1 ELISA measures biologically active GLP-1-(7–37) and GLP-1-(7–36)-NH_2 but does not cross-react with glucagon, GLP-2, inactive GLP-1-(9–37) or GLP-1-(9–37)-NH_2.

Histology and immunohistochemistry. Histochemical analysis was performed as previously described (25). Briefly, the surviving mice were euthanized after 4 wk of observation. The hearts were harvested, and cardiac tissues were fixed with 4% paraformaldehyde. The fixed samples were embedded in paraffin and sectioned at 4-!Lm thickness for picrosirius red staining. The extent of myocardial collagen was analyzed in five hearts from each group (30). The original images were digitized and transformed into binary images, and each area was calculated using ImageJ software (NIH, Bethesda, MD). The total myocardial collagen index was defined as the total area of collagen content in the entire microscopic field divided by the total connective tissue area plus the myocardial area. The terminal deoxynucleotidyl transferase dUTP nick-end labeling (TUNEL) assay was performed using an ApopTag Peroxidase In Situ Apoptosis Detection Kit (Millipore), according to the manufacturer's instructions. The number of TUNEL-positive cells was expressed as a percentage of total cells, as previously described (35).

Real-time quantitative polymerase chain reaction. Four weeks after TAC, murine ventricles were processed for total RNA isolation using TRIzol reagent (Invitrogen, Carlsbad, CA) according to the manufacturer's instructions. First-strand cDNA was synthesized from 1 !Lg total RNA using the High-Capacity cDNA Reverse Transcription Kit (Applied Biosystems, Foster City, CA). The primers and probes used to quantify *transforming growth factor-1*13 *(Tgf-1*13*)* and *glyceraldehyde 3-phosphate dehydrogenase (Gapdh)* were recommended by the manufacturer (Applied Biosystems). Real-time quantitative reverse transcriptase polymerase chain reaction (RT-PCR) was performed in a StepOne Real-Time PCR System (Applied Biosystems). From each amplification plot, a threshold cycle (Ct) value was calculated, representing the PCR cycle number at which fluorescence was detectable above an arbitrary threshold. Each sample was analyzed in duplicate, and the results were systematically normalized to GAPDH expression using the LILICt method (29).

Western blot analysis. LV samples frozen at −80°C were placed on ice, homogenized, and lysed with lysis buffer [1% NP-40, 150 mM NaCl, 20 mM Tris pH 7.5, 2 mM EDTA, 50 mM NaF, 1 mM Na_3VO_4, plus protease inhibitor cocktail (Nacalai tesque, Kyoto, Japan)]. The supernatant was loaded onto 10%–15% sodium dodecyl sulfate-polyacrylamide gel electrophoresis gels. Immunoblotting was performed as previously described (41). The ChemiDoc XRS System (Bio-Rad Laboratories, Hercules, CA) was used for chemiluminescence imaging. Primary antibodies against phospho-Smad2 (p-Smad2), p-Smad3, caspase-3, and cleaved caspase-3 primary antibodies were purchased from Cell Signaling Technology (Beverly, MA); anti-Smad2/3 primary antibody was purchased from BD Transduction Laboratories (Franklin Lakes, NJ); and anti-GAPDH (used as a loading control) primary antibody was purchased from Millipore. Target bands were identified using ECL prime and ECL Select Western blotting reagents (GE Healthcare, Little Chalfont, Buckinghamshire, UK). Protein bands were quantified by densitometry.

Statistical analysis. All of the data are expressed as means + SE and were analyzed by repeated-measures analysis of variance (ANOVA) followed by Bonferroni test and Student's *t*-test for paired and nonpaired data as appropriate. The differences in the number of surviving mice were analyzed by Kaplan-Meier method. *P* values of <0.05 were considered significant using JMP 8.0.1 software (SAS Institute, Cary, NC).

RESULTS

Hemodynamic measurements. The blood pressures and heart rates 4 wk after TAC were similar in the sham-operated groups with and without vildagliptin (71.2 + 3.1 vs. 74.5 + 3.2

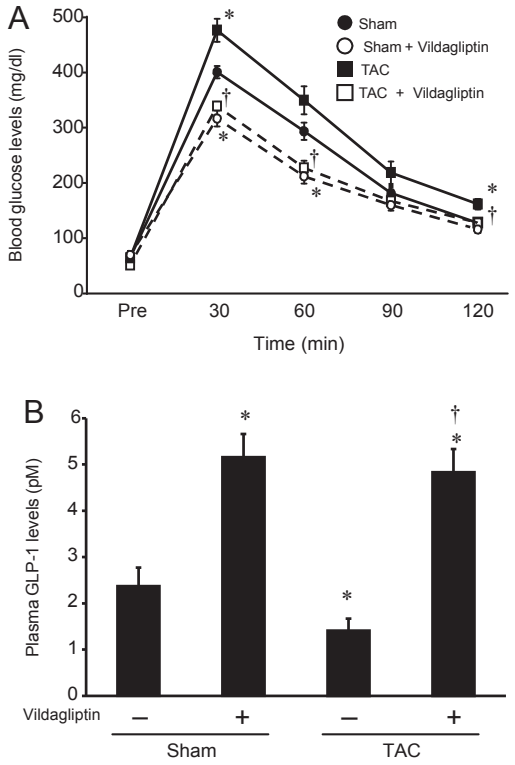

Fig. 1. *A*: plasma glucose levels measured by intraperitoneal glucose tolerance test. Sham-operated mice (n = 5), sham-operated mice with vildagliptin (n = 5), mice with transverse aortic constriction (TAC) (n = 8), and TAC mice with vildagliptin (n = 12) were enrolled. *B*: plasma levels of glucagon-like peptide-1 (GLP-1) 4 wk after TAC or sham operation. All blood samples were collected 1 h after feeding following overnight fasting. Sham-operated (n = 8), sham-operated mice with vildagliptin (n = 10), TAC mice (n = 15), and TAC mice with vildagliptin (n = 21) were measured. The data shown are means + SE. *P < 0.05 vs. sham operated, †P < 0.05 vs. TAC.

mmHg; 459 + 36 vs. 451 + 22 beats/min; P = 0.482 and P = 0.830, respectively; n = 5 in each group), and in the TAC groups with and without vildagliptin (101.4 + 9 vs. 121.4 + 10 mmHg; 394 + 80 vs. 463 + 27 beats/min; P = 0.193 and P = 0.400; n = 5 and n = 4, respectively).

Intraperitoneal glucose tolerance test and plasma GLP-1 levels. Figure 1*A* shows the results of the intraperitoneal glucose tolerance test. Blood glucose levels at 30 and 120 min after intraperitoneal glucose injections were higher in the TAC mice than in the sham-operated mice (TAC vs. sham operated: 476.4 + 20.9 vs. 400.5 + 11.2 mg/dl at 30 min, and 161.5 + 9.4 vs. 127.3 + 8.3 mg/dl at 120 min, n = 8 and 5; P < 0.05). This was consistent with our previous report (27) in which TAC mice exhibited impaired glucose tolerance. Vildagliptin administration decreased blood glucose levels at each time point after glucose injection in TAC mice (with vs. without vildagliptin: 345.1 + 7.9 vs. 476.4 + 20.9 mg/dl at 30 min, 245.5 + 13.1 vs. 349.6 + 25.3 mg/dl at 60 min, and 127.9 + 8.5 vs. 161.5 + 9.4 mg/dl at 120 min, n = 12 and 8; P < 0.05).

We evaluated the GLP-1 levels in the TAC mice with or without vildagliptin. Because ad libitum feeding could have affected the plasma GLP-1 levels, we conducted a preliminary experiment to identify the optimal conditions for GLP-1 measurement. Nine-week-old C57BL6/J mice were fed a normal chow diet, divided into two groups, and treated with or without vildagliptin for 4 wk, as described above. To evaluate whether feeding affected the plasma GLP-1 levels, the mice were fasted 12 h before blood sampling. We randomly separated each group into two subgroups; the two subgroups were fasted further, and the others were allowed to feed 1 h before sampling. Under fasting conditions, vildagliptin produced a statistically insignificant increase in GLP-1 levels (with vs. without vildagliptin: 5.19 + 1.04 vs. 3.93 + 0.70 pM, n = 5 each; P > 0.05). In the mice sampled 1 h after feeding, GLP-1 levels were elevated with in the vildagliptin group (with vs. without vildagliptin: 9.13 + 2.35 vs. 4.47 + 0.87 pM, n = 4 and 5; P < 0.05), suggesting that this sampling time schedule, i.e., 1 h after food intake, was suitable for plasma GLP-1 measurement. Figure 1*B* shows the plasma GLP-1 levels under this time schedule. The GLP-1 levels were decreased in the TAC mice (sham operated vs. TAC: 2.37 + 0.40 vs. 1.41 + 0.26 pM, n = 8 and 15; P < 0.05), but elevated in TAC mice with vildagliptin to the levels of sham-operated mice with vildagliptin (with vs. without vildagliptin: 4.83 + 0.50 vs. 1.41 + 0.26 pM, n = 21 and 15; P < 0.05).

Echocardiography. Representative echocardiographic images are shown in Fig. 2. Echocardiographic analysis revealed enlarged Dd and Ds in the TAC mice both with and without vildagliptin (n = 27 and 17). Both LV dilatation and dysfunction in the TAC group were ameliorated by vildagliptin treatment (Fig. 3).

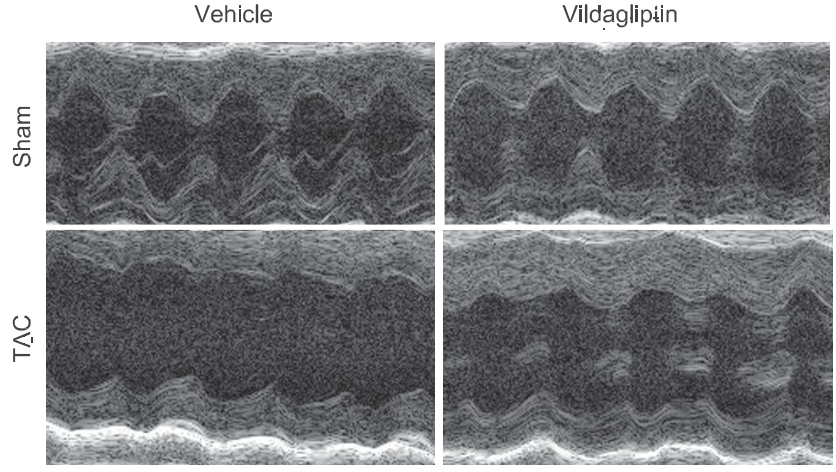

Fig. 2. Representative M-mode echocardiograms of mice 4 wk after TAC or sham operation. Top left, sham operated; top right, sham operated with vildagliptin; bottom left, TAC; bottom right, TAC with vildagliptin.

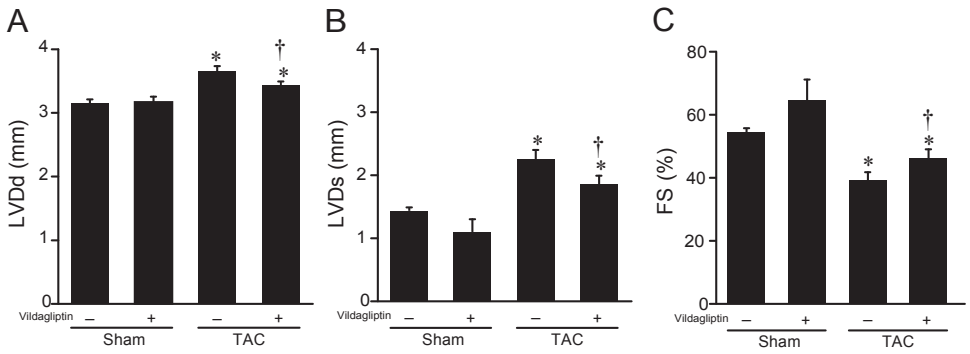

Fig. 3. *A* and *B*: left ventricular (LV) dimensions. *C*: fractional shortening (FS) 4 wk after TAC or sham operation. LV end-diastolic diameter (Dd), end-systolic diameter (Ds), and FS measured by echocardiography at 4 wk after TAC or sham operation. Echocardiographic analysis revealed enlarged LV end-diastolic and end-systolic diameters in both of the TAC groups compared with the sham-operated mice. Both LV dilatation and dysfunction in the TAC group were ameliorated by vildagliptin treatment. Sham-operated mice (n = 5), sham-operated mice with vildagliptin (n = 5), TAC mice (n = 17), and TAC mice with vildagliptin (n = 27) were examined. LVDd, LV end-diastolic dimension; LVDs, LV end-systolic dimension. Data shown are means + SE. *P < 0.05 vs. sham operated, †P < 0.05 vs. TAC.

Water uptake and heart weight. Body weight was not statistically different between the groups: 24.3 + 1.7 g and 23.4 + 1.4 g in the sham-operated and TAC mice without vildagliptin (n = 10 and 17), 25.8 + 1.7 g and 25.2 + 2.4 g in the sham-operated and TAC mice with vildagliptin (n =10 and 27). Heart weight-to-body weight ratio (HW/BW) markedly increased in the TAC group compared with the sham-operated group (4.9 + 0.1 vs. 9.3 + 0.5 for sham-operated and TAC mice without vildagliptin, respectively; P < 0.05), and vildagliptin did not attenuate HW/BW (9.2 + 0.4 for TAC with vildagliptin; Fig. 4). Volumes of vildagliptin solution or water consumed were similar in all of the groups (5.2 + 0.2, 4.9 + 0.5, 4.4 + 0.9, and 4.5 + 1.3 ml/day for sham-operated with and without vildagliptin and TAC with and without vildagliptin, respectively; P > 0.05 for all).

Apoptosis and fibrosis. We performed TUNEL staining to clarify the degree of apoptosis in the murine hearts. Apoptosis in the myocardium of the TAC mice was increased compared with the sham-operated mice, and this increase in apoptotic cell death was largely attenuated by vildagliptin (Fig. 5, *A* and *B*, n = 4 per each group). Next we performed immunoblotting to confirm apoptotic changes in protein levels. We observed increased cleaved caspase-3 protein in pressure-overloaded murine hearts, which was partially ameliorated by vildagliptin (Fig. 5, *C* and *D*, n = 4 per each group). These findings indicate that vildagliptin partly reduces myocardial apoptosis in pressure-overloaded murine hearts.

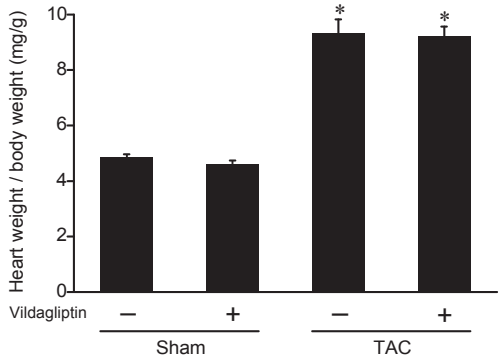

Fig. 4. Heart weight (mg)/body wt (g) ratio 4 wk after the TAC or sham operation. Sham-operated mice (n = 10), sham-operated mice with vildagliptin (n = 10), TAC mice (n = 17), and TAC mice with vildagliptin (n = 27) mice were measured. The values shown are means + SE. *P < 0.05 vs. sham operated.

Figure 6*A* shows increases in myocardial collagen in the TAC group, also ameliorated by vildagliptin. Figures 6*B* shows fibrotic areas identified by picrosirius red staining. The total myocardial interstitial collagen area significantly increased in the TAC group compared with the sham-operated groups (P < 0.05 vs. sham operated, n = 5 per each group) but was decreased in the TAC with vildagliptin group (P < 0.05 vs. TAC) (sham operated, 1.79 + 0.22%; sham operated with vildagliptin, 1.77 + 0.20%; TAC, 12.12 + 0.27%; TAC with vildagliptin, 8.02 + 1.84%). We next analyzed expression of *Tgf-1*13, a fibrosis-related gene, using RT-PCR. Myocardial *Tgf-1*13 expression significantly increased in the TAC group compared with that in the sham-operated group (P < 0.05 vs. sham operated) but significantly decreased in the groups with vildagliptin (P < 0.05 vs. TAC; sham operated, 1 + 0.08; sham operated with vildagliptin, 0.98 + 0.11; TAC, 1.85 + 0.12; TAC with vildagliptin, 1.55 + 0.06; Fig. 6*C*, n = 3 per each group).

Finally, we performed immunoblotting to verify the fibrotic changes that arose through increased levels of TGF-β pathway proteins. We observed increased p-Smad2 and p-Smad3 protein levels in the pressure-overloaded murine hearts, which were partially restored by vildagliptin (Fig. 7, n = 4 per each group). These findings indicate that vildagliptin reverses myocardial fibrosis via the TGF-β pathway in murine pressure-overloaded hearts.

Survival analysis. The number of TAC mice without vildagliptin was 41 and the number of those with vildagliptin was 40. Only 17 (41.5%) TAC mice without vildagliptin survived 28 days, whereas 27 (67.5%) TAC mice with vildagliptin survived 28 days (Fig. 8; P < 0.05). These data indicate that vildagliptin treatment is strongly protective. Vildagliptin did not affect the survival rate in the sham-operated mice.

DISCUSSION

This study was the first to demonstrate that a DPP-IV inhibitor improved survival rate in mice with pressure-overloaded HF. We presented the following experimental evidence: *1*) TAC exacerbated the development of impaired glucose

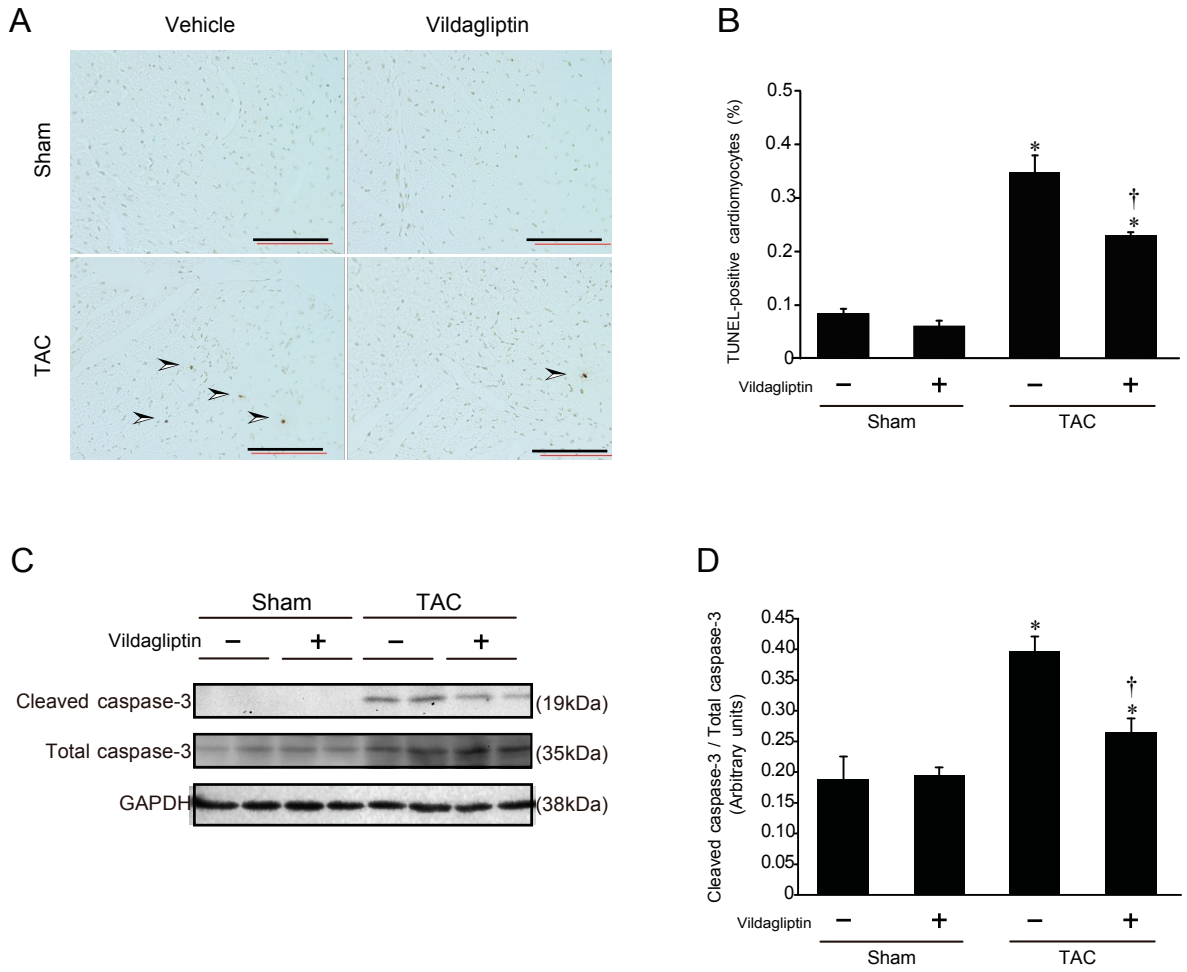

Fig. 5. *A*: representative images of the terminal deoxynucleotidyl transferase dUTP nick-end labeling (TUNEL)-positive cells in murine hearts. Top left, sham operated; top right, sham operated with vildagliptin; bottom left, TAC; bottom right, TAC with vildagliptin. Evidence of apoptosis, including chromatin condensation, is indicated with arrowheads. The proportion of TAC-induced apoptotic cells was decreased by vildagliptin. Bar = 200 !Lm; original magnification, ×200. *B*: quantitative analysis of murine apoptotic cardiomyocytes. TAC increased the number of apoptotic cells in the myocardium compared with the sham-operated group, and vildagliptin attenuated the increase in apoptosis. $n = 4$ for each group. *C*: representative immunoblotting analysis of cleaved/total caspase-3 and GAPDH in the hearts of sham-operated and TAC mice with or without vildagliptin. *D*: intensity of bands was quantified from four independent experiments by densitometry. Cleaved/total caspase-3 protein levels were increased by pressure overload in the hearts of TAC mice, which were reversed in TAC mice with vildagliptin. $n = 4$ for each group. The values shown are means + SE. $*P < 0.05$ vs. sham operated, $\dagger P < 0.05$ vs. TAC.

tolerance, which was attenuated by vildagliptin with an attendant increase in total GLP-1 levels; *2*) TAC induced myocardial apoptosis and fibrosis, which were attenuated by vildagliptin; *3*) TAC increased LVDd and LVDs, leading to FS decline, while vildagliptin attenuated increased LVDd and LVDs and increased LVFS. These effects may contribute to the improvement in survival rate generated by vildagliptin in mice with pressure overload-induced HF.

We demonstrated that TAC exacerbated the development of impaired glucose tolerance, which was attenuated by vildagliptin. This result implies that HF causes impaired glucose tolerance and improvement of impaired glucose tolerance may ameliorate HF severity. Glycemic control independently correlates with reduced LV contractile reserve and positivity for HF in diabetic patients (12, 28). We previously reported that HF is associated with impaired glucose tolerance in mice and dogs, and that correction of impaired glucose tolerance with voglibose or metformin reduces HF severity (26, 27, 41). Shimizu et al. (46) reported that systolic dysfunction induced by pressure overload exacerbates plasma glucose and hepatic insulin resistance via Akt and insulin signaling in rodents. In humans, chronic HF is associated with hyperinsulinemia (36, 51). Insulin resistance observed in HF is partly due to the lack of activity and increase in weight gain/fat redistribution. Stolen et al. (49) showed that exercise training improved insulin-stimulated myocardial glucose uptake in patients with dilated cardiomyopathy. Ashrafian et al. (2) proposed the other mechanism of HF-induced insulin resistance. Hyperadrenergic state of HF initiates the elevation of plasma free fatty acids (FFAs). The elevation of plasma FFAs induces insulin resistance due to increased triglycerides, increased cellular FFAs, and increased cytoplasmic fatty acid metabolites in hearts and skeletal muscle (43).

To our knowledge, this is the first study to evaluate an improvement in impaired glucose tolerance in animals with HF in the presence of DPP-IV inhibitors. Indeed, vildagliptin increased the plasma GLP-1 levels in animals with TAC-induced HF, suggesting that HF is attenuated by the correction

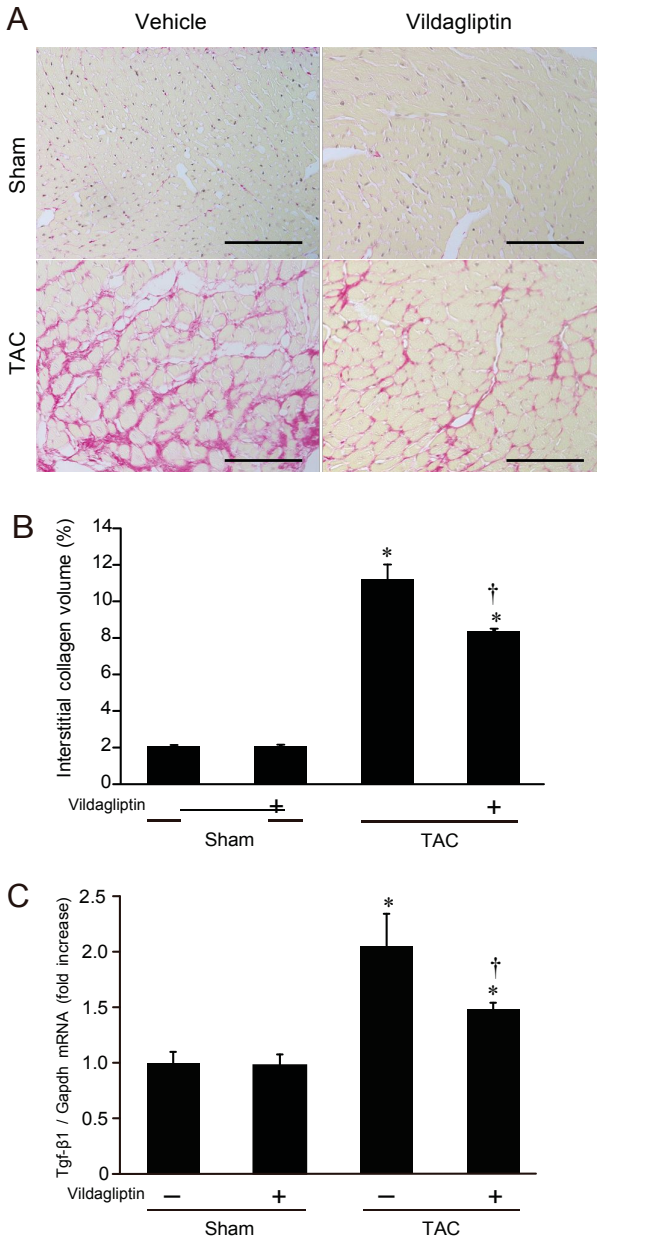

Fig. 6. *A*: representative images of the murine myocardium stained by picrosirius red. Collagen accumulation induced by TAC was regressed with vildagliptin. Top left, sham operated; top right, sham operated with vildagliptin; bottom left, TAC; bottom right, TAC with vildagliptin. Bar = 100 !Lm; original magnification, ×400. *B*: quantitative analysis shows that vildagliptin ameliorated myocardial collagen deposition resulting from pressure overload. $n = 5$ for each group. *C*: quantitative analysis of *transforming growth factor-1 13 (Tgf13)* in murine hearts: the expression level (normalized to *Gapdh*) in TAC group was increased compared with that in sham operated, which was alleviated in TAC with vildagliptin. $n = 3$ for each group. Data are presented as the relative change vs. sham operated. The values shown are means + SE. *$P < 0.05$ vs. sham operated, †$P < 0.05$ vs. TAC.

of glucose intolerance by DPP-IV inhibitors. This hypothesis is supported by our findings that vildagliptin attenuates LV apoptosis and fibrosis in the TAC mice, which may explain the amelioration of LV dilatation and dysfunction. This evidence is consistent with previous studies in which sitagliptin was shown to attenuate HF severity induced by rapid pacing in pigs (14), ameliorate myocardial fibrosis in diabetic ($db/db^{-/-}$) mice (23), and improve diastolic dysfunction without altering ejection fraction in a rat model of uremic cardiomyopathy (9).

Intriguingly, GLP-1 reportedly has cardioprotective properties besides its ability to correct glucose intolerance in HF. GLP-1 receptors are expressed in the heart and activate PI3 kinase and Akt in addition to cyclic AMP (6, 19). Protein kinase A activation via accumulation of cyclic AMP may activate p38 MAP kinase, which may in turn mediate cardio-

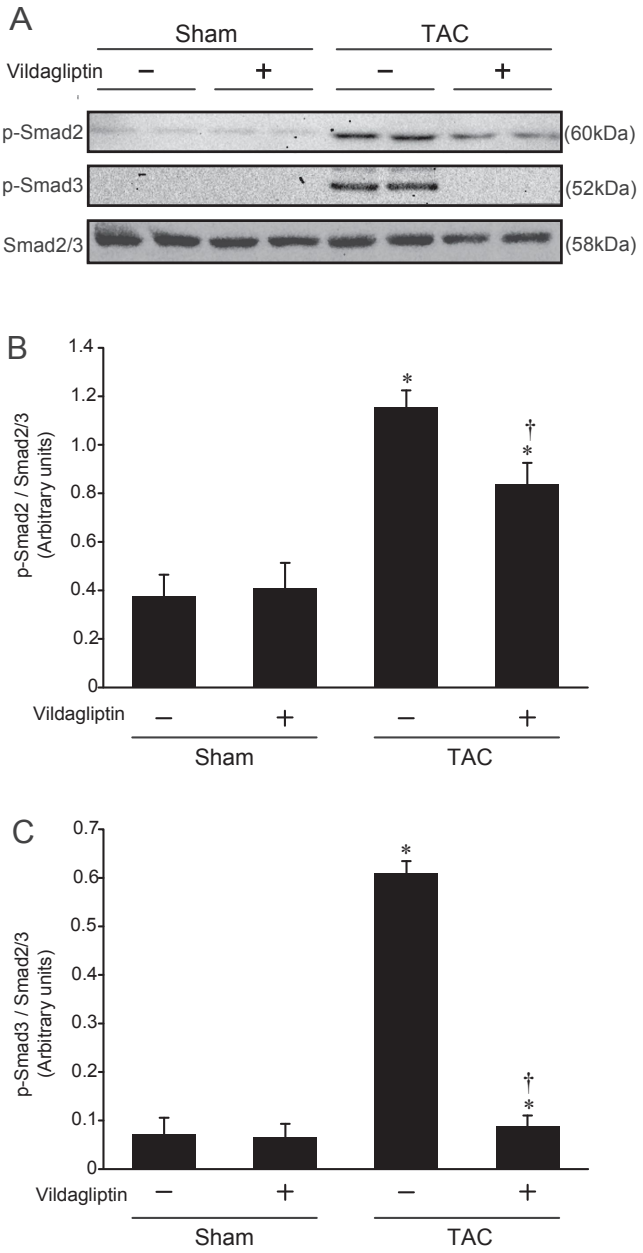

Fig. 7. *A*: representative immunoblotting analysis of phosphorylated Smad2 (p-Smad2), p-Smad3, and Smad2/3 in the hearts of sham-operated and TAC mice with or without vildagliptin. *B*: band intensity quantified by densitometry. p-Smad2/Smad2/3 protein levels increased as a result of pressure overload in the hearts of TAC mice, but recovered in TAC mice with vildagliptin. *C*: band intensity quantified by densitometry. p-Smad3/Smad2/3 protein levels increased as a result of pressure overload in the hearts of the TAC mice, but recovered in the TAC mice with vildagliptin. $n = 4$ for each group. The values shown are means + SE. *$P < 0.05$ vs. sham operated, †$P < 0.05$ vs. TAC.

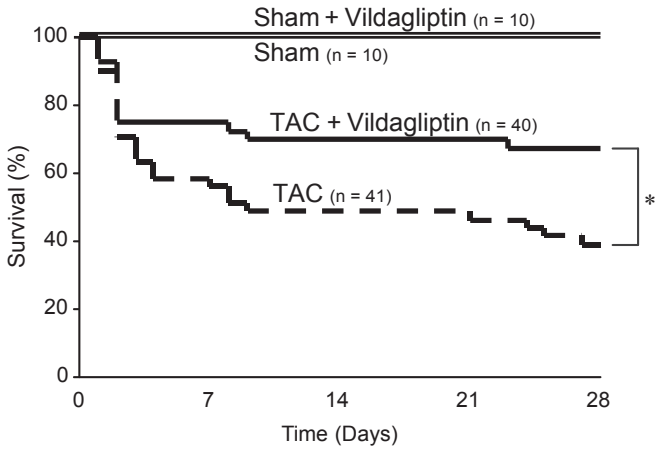

Fig. 8. The Kaplan-Meier curve analysis shows that the TAC group with vildagliptin exhibited improved survival compared with the TAC group without vildagliptin. We enrolled 41 mice in the TAC and 40 mice in the TAC with vildagliptin groups, respectively. The survival rates at 28 days after the TAC operation were 41.5% (17/41) in the TAC and 67.5% (27/40) in the TAC with vildagliptin groups, respectively. *$P < 0.05$ vs. TAC; *n*, number of mice.

protection (40, 59), and activation of PI3 kinase and Akt may further enhance these cardioprotective effects. A recent report (55) demonstrated amelioration of nonalcoholic steatohepatitis in mice by an analog of exenatide, a GLP-1 receptor agonist, supporting the antifibrotic effect of GLP-1 in murine hearts. Indeed, GLP-1 administration in patients with HF decreased the HF severity with or without DM, suggesting that GLP-1 may have cardioprotective properties independent of its effects on blood glucose levels (48). However, GLP-1 levels were elevated ~10-fold (17), significantly higher than the GLP-1 levels observed with DPP-IV inhibitors (4), suggesting that even a 1-pM increase in GLP-1 may be sufficient for cardioprotection. Moreover, in a large meta-analysis, vildagliptin was not associated with an increased risk of adjudicated cardio- and cerebrovascular events relative to all comparators in the patients with type 2 diabetes, including increased cerebrovascular risks (44). Chaykovska et al. (9) showed that increased *Tgf-β1*, *collagen type I* d*1*, and *collagen type III* d*1* expression in uremic rat hearts, compared with the sham-operated rat hearts, was significantly reduced by linagliptin, a DPP-IV inhibitor, supporting our observations. Importantly, DPP-IV inhibitors impact cardioprotection independently of GLP-1; DPP-IV also reportedly degrades peptides tyrosine-tyrosine, stromal cell-derived factor-1, and B-type natriuretic peptide (BNP) (7, 32, 45, 47). Taken together, these data suggest that DPP-IV inhibitors are cardioprotective, suggesting that they may also be beneficial for patients with HF. However, this hypothesis is limited because we used 8-wk-old mice with TAC as a model of HF in this study. Although this model is one of established animal models for HF, this model is not the universal model for the patients with HF, or does not mimic the background of the HF patients (e.g., age, dyslipidemia, ischemia, etc.). Further basic and preclinical studies are needed to apply DPP-IV inhibitors to HF patients.

The most important issue in this study was to determine whether DPP-IV inhibitors increase the survival rate because improvements in HF do not necessarily increase the survival rate. Indeed, inotropic agents such as phosphodiesterase III inhibitors (e.g., vesnarinone) improved pathophysiological parameters of HF in basic studies, even improving symptoms and cardiac function in patients with HF in clinical studies, but these drugs actually decreased the patient survival rate in large-scale clinical trials (10). This unexpected finding is attributable to the fact that the effect of these drugs on survival rate was never tested in experimental models of chronic HF. Yin et al. (60) reported the rat models with the administration of vildagliptin 2 days before or 3 wk after acute myocardial infarction surgery. They did not show the cardiac contractility and survival or any change in glucose metabolism with vildagliptin treatment. Compared with their protocol, we administered vildagliptin from 1 day postsurgery of murine TAC, which finally reversed the survival rate. These discrepancies between the study of Yin et al. and our present study may be attributable to the manner of HF induction (e.g., models and species), their glucose levels, and the dosage of vildagliptin. Their echocardiographic data seem to show worse HF than ours, which was too severe to treat with their dose set. In addition, although they did not mention any condition of the feeding (e.g., fasting or ad libitum feeding) during sampling, no difference in their blood glucose levels may suggest that the dosage was not enough to be cardioprotective. We observed that vildagliptin increased survival rate in the context of pressure overload-induced HF in mice, indicating that an adequate dose of DPP-IV inhibitors is ultimately cardioprotective against HF.

This study includes the limitations. Since TAC animals are fragile, especially when using the narrower size of needle (30 gauge) to create severe HF, the procedures of the examination such as glucose tolerance test may worsen the HF of the TAC mice. Indeed, in the preliminary study, we tried to perform oral glucose tolerance test at first, but 2 of 6 died because of the onset of acute severe HF (pulmonary edema shown by dissection). This is the reason that we shifted to the intraperitoneal glucose tolerance test, which did not cause severe HF leading to death. Importantly, the timing and number of procedures were identical in the groups with or without vildagliptin, suggesting that these additional stresses of examination to TAC do not largely affect the present results and conclusions.

In conclusion, vildagliptin, a DPP-IV inhibitor, improved the pathophysiology of HF in pressure-overloaded mice. This effect was mediated partly by improved glucose tolerance and partly by the cardioprotective effects of GLP-1, both of which ultimately improved survival following HF.

ACKNOWLEDGMENTS

We are thankful to Akiko Ogai, Chizuko Kimura, and Nobuyoshi Imai for excellent technical assistance. Vildagliptin was a gift from Novartis.

GRANTS

This work was supported by grants-in-aid from the Ministry of Health, Labor, and Welfare of Japan and the Ministry of Education, Culture, Sports, Science and Technology of Japan.

DISCLOSURES

No conflicts of interest, financial or otherwise, are declared by the author(s).

AUTHOR CONTRIBUTIONS

Author contributions: A.T., M.A., and M.K. conception and design of research; A.T., S.I., Y.Y., and Y.L. performed experiments; A.T., S.Y., and M.K. analyzed data; A.T., S.I., K.-D.M., K.S., and Y.Y. prepared figures; A.T. drafted manuscript; A.T., S.I., K.-D.M., K.S., S.S., Y.A., S.T., T.M., and H.A.

edited and revised manuscript; S.I., K.-D.M., Y.L., H.I.-U., and M.K. interpreted results of experiments; N.M. and M.K. approved final version of manuscript.

REFERENCES

1. **Abhayaratna WP, Marwick TH, Smith WT, Becker NG.** Characteristics of left ventricular diastolic dysfunction in the community: an echocardiographic survey. *Heart* 92: 1259–1264, 2006.
2. **Ashrafian H, Frenneaux MP, Opie LH.** Metabolic mechanisms in heart failure. *Circulation* 116: 434–448, 2007.
3. **Ban K, Noyan-Ashraf MH, Hoefer J, Bolz SS, Drucker DJ, Husain M.** Cardioprotective and vasodilatory actions of glucagon-like peptide 1 receptor are mediated through both glucagon-like peptide 1 receptor-dependent and -independent pathways. *Circulation* 117: 2340–2350, 2008.
4. **Bergman AJ, Stevens C, Zhou Y, Yi B, Laethem M, De Smet M, Snyder K, Hilliard D, Tanaka W, Zeng W, Tanen M, Wang AQ, Chen L, Winchell G, Davies MJ, Ramael S, Wagner JA, Herman GA.** Pharmacokinetic and pharmacodynamic properties of multiple oral doses of sitagliptin, a dipeptidyl peptidase-IV inhibitor: a double-blind, randomized, placebo-controlled study in healthy male volunteers. *Clin Ther* 28: 55–72, 2006.
5. **Bhashyam S, Fields AV, Patterson B, Testani JM, Chen L, Shen YT, Shannon RP.** Glucagon-like peptide-1 increases myocardial glucose uptake via p38alpha MAP kinase-mediated, nitric oxide-dependent mechanisms in conscious dogs with dilated cardiomyopathy. *Circ Heart Fail* 3: 512–521, 2010.
6. **Bose AK, Mocanu MM, Carr RD, Brand CL, Yellon DM.** Glucagon-like peptide 1 can directly protect the heart against ischemia/reperfusion injury. *Diabetes* 54: 146–151, 2005.
7. **Brandt I, Lambeir AM, Ketelslegers JM, Vanderheyden M, Scharpe S, De Meester I.** Dipeptidyl-peptidase IV converts intact B-type natriuretic peptide into its des-SerPro form. *Clin Chem* 52: 82–87, 2006.
8. **Bullock BP, Heller RS, Habener JF.** Tissue distribution of messenger ribonucleic acid encoding the rat glucagon-like peptide-1 receptor. *Endocrinology* 137: 2968–2978, 1996.
9. **Chaykovska L, von Websky K, Rahnenfuhrer J, Alter M, Heiden S, Fuchs H, Runge F, Klein T, Hocher B.** Effects of DPP-4 inhibitors on the heart in a rat model of uremic cardiomyopathy. *PloS One* 6: e27861, 2011.
10. **Cohn JN, Goldstein SO, Greenberg BH, Lorell BH, Bourge RC, Jaski BE, Gottlieb SO, McGrew F, 3rd DeMets DL, White BG.** A dose-dependent increase in mortality with vesnarinone among patients with severe heart failure. Vesnarinone Trial Investigators. *N Engl J Med* 339: 1810–1816, 1998.
11. **Deacon CF, Nauck MA, Toft-Nielsen M, Pridal L, Willms B, Holst JJ.** Both subcutaneously and intravenously administered glucagon-like peptide I are rapidly degraded from the NH2-terminus in type II diabetic patients and in healthy subjects. *Diabetes* 44: 1126–1131, 1995.
12. **Egstrup M, Kistorp CN, Schou M, Hofsten DE, Moller JE, Tuxen CD, Gustafsson I.** Abnormal glucose metabolism is associated with reduced left ventricular contractile reserve and exercise intolerance in patients with chronic heart failure. *Eur Heart J Cardiovasc Imaging* 14: 349–357, 2013.
13. **Falcao-Pires I, Hamdani N, Borbely A, Gavina C, Schalkwijk CG, van der Velden J, van Heerebeek L, Stienen GJ, Niessen HW, Leite-Moreira AF, Paulus WJ.** Diabetes mellitus worsens diastolic left ventricular dysfunction in aortic stenosis through altered myocardial structure and cardiomyocyte stiffness. *Circulation* 124: 1151–1159, 2011.
14. **Gomez N, Touihri K, Matheeussen V, Mendes Da Costa A, Mahmoud-abady M, Mathieu M, Baerts L, Peace A, Lybaert P, Scharpe S, De Meester I, Bartunek J, Vanderheyden M, McEntee K.** Dipeptidyl peptidase IV inhibition improves cardiorenal function in overpacing-induced heart failure. *Eur J Heart Fail* 14: 14–21, 2012.
15. **Greig NH, Holloway HW, De Ore KA, Jani D, Wang Y, Zhou J, Garant MJ, Egan JM.** Once daily injection of exendin-4 to diabetic mice achieves long-term beneficial effects on blood glucose concentrations. *Diabetologia* 42: 45–50, 1999.
16. **Gutzwiller JP, Drewe J, Goke B, Schmidt H, Rohrer B, Lareida J, Beglinger C.** Glucagon-like peptide-1 promotes satiety and reduces food intake in patients with diabetes mellitus type 2. *Am J Physiol Regul Integr Comp Physiol* 276: R1541–R1544, 1999.
17. **Halbirk M, Norrelund H, Moller N, Holst JJ, Schmitz O, Nielsen R, Nielsen-Kudsk JE, Nielsen SS, Nielsen TT, Eiskjaer H, Botker HE, Wiggers H.** Cardiovascular and metabolic effects of 48-h glucagon-like peptide-1 infusion in compensated chronic patients with heart failure. *Am J Physiol Heart Circ Physiol* 298: H1096–H1102, 2010.
18. **Hui H, Farilla L, Merkel P, Perfetti R.** The short half-life of glucagon-like peptide-1 in plasma does not reflect its long-lasting beneficial effects. *Eur J Endocrinol* 146: 863–869, 2002.
19. **Hui H, Nourparvar A, Zhao X, Perfetti R.** Glucagon-like peptide-1 inhibits apoptosis of insulin-secreting cells via a cyclic 5=-adenosine monophosphate-dependent protein kinase A- and a phosphatidylinositol 3-kinase-dependent pathway. *Endocrinology* 144: 1444–1455, 2003.
20. **Kane GC, Karon BL, Mahoney DW, Redfield MM, Roger VL, Burnett JC Jr, Jacobsen SJ, Rodeheffer RJ.** Progression of left ventricular diastolic dysfunction and risk of heart failure. *JAMA* 306: 856–863, 2011.
21. **Kim J, Nakatani S, Hashimura K, Komamura K, Kanzaki H, Asakura M, Asanuma H, Kokubo Y, Tomoike H, Kitakaze M.** Abnormal glucose tolerance contributes to the progression of chronic heart failure in patients with dilated cardiomyopathy. *Hypertens Res* 29: 775–782, 2006.
22. **Lang RM, Bierig M, Devereux RB, Flachskampf FA, Foster E, Pellikka PA, Picard MH, Roman MJ, Seward J, Shanewise JS, Solomon SD, Spencer KT, Sutton MS, Stewart WJ.** Recommendations for chamber quantification: a report from the American Society of Echocardiography's Guidelines and Standards Committee and the Chamber Quantification Writing Group, developed in conjunction with the European Association of Echocardiography, a branch of the European Society of Cardiology. *J Am Soc Echocardiogr* 18: 1440–1463, 2005.
23. **Lenski M, Kazakov A, Marx N, Bohm M, Laufs U.** Effects of DPP-4 inhibition on cardiac metabolism and function in mice. *J Mol Cell Cardiol* 51: 906–918, 2011.
24. **Liao Y, Ishikura F, Beppu S, Asakura M, Takashima S, Asanuma H, Sanada S, Kim J, Ogita H, Kuzuya T, Node K, Kitakaze M, Hori M.** Echocardiographic assessment of LV hypertrophy and function in aortic-banded mice: necropsy validation. *Am J Physiol Heart Circ Physiol* 282: H1703–H1708, 2002.
25. **Liao Y, Takashima S, Asano Y, Asakura M, Ogai A, Shintani Y, Minamino T, Asanuma H, Sanada S, Kim J, Ogita H, Tomoike H, Hori M, Kitakaze M.** Activation of adenosine A1 receptor attenuates cardiac hypertrophy and prevents heart failure in murine left ventricular pressure-overload model. *Circ Res* 93: 759–766, 2003.
26. **Liao Y, Takashima S, Maeda N, Ouchi N, Komamura K, Shimomura I, Hori M, Matsuzawa Y, Funahashi T, Kitakaze M.** Exacerbation of heart failure in adiponectin-deficient mice due to impaired regulation of AMPK and glucose metabolism. *Cardiovasc Res* 67: 705–713, 2005.
27. **Liao Y, Takashima S, Zhao H, Asano Y, Shintani Y, Minamino T, Kim J, Fujita M, Hori M, Kitakaze M.** Control of plasma glucose with alpha-glucosidase inhibitor attenuates oxidative stress and slows the progression of heart failure in mice. *Cardiovasc Res* 70: 107–116, 2006.
28. **Lind M, Bounias I, Olsson M, Gudbjornsdottir S, Svensson AM, Rosengren A.** Glycaemic control and incidence of heart failure in 20,985 patients with type 1 diabetes: an observational study. *Lancet* 378: 140–146, 2011.
29. **Livak KJ, Schmittgen TD.** Analysis of relative gene expression data using real-time quantitative PCR and the 2[−Delta Delta C(T)] method. *Methods* 25: 402–408, 2001.
30. **Lucas JA, Zhang Y, Li P, Gong K, Miller AP, Hassan E, Hage F, Xing D, Wells B, Oparil S, Chen YF.** Inhibition of transforming growth factor-beta signaling induces left ventricular dilation and dysfunction in the pressure-overloaded heart. *Am J Physiol Heart Circ Physiol* 298: H424–H432, 2010.
31. **Mariappan N, Elks CM, Sriramula S, Guggilam A, Liu Z, Borkhsenious O, Francis J.** NF-kappaB-induced oxidative stress contributes to mitochondrial and cardiac dysfunction in type II diabetes. *Cardiovasc Res* 85: 473–483, 2010.
32. **Mentlein R, Dahms P, Grandt D, Kruger R.** Proteolytic processing of neuropeptide Y and peptide YY by dipeptidyl peptidase IV. *Regul Pept* 49: 133–144, 1993.
33. **Nikolaidis LA, Doverspike A, Hentosz T, Zourelias L, Shen YT, Elahi D, Shannon RP.** Glucagon-like peptide-1 limits myocardial stunning following brief coronary occlusion and reperfusion in conscious canines. *J Pharmacol Exper Ther* 312: 303–308, 2005.
34. **Nikolaidis LA, Elahi D, Hentosz T, Doverspike A, Huerbin R, Zourelias L, Stolarski C, Shen YT, Shannon RP.** Recombinant glucagon-like peptide-1 increases myocardial glucose uptake and improves left ventricular performance in conscious dogs with pacing-induced dilated cardiomyopathy. *Circulation* 110: 955–961, 2004.

35. **Okada K, Minamino T, Tsukamoto Y, Liao Y, Tsukamoto O, Takashima S, Hirata A, Fujita M, Nagamachi Y, Nakatani T, Yutani C, Ozawa K, Ogawa S, Tomoike H, Hori M, Kitakaze M.** Prolonged endoplasmic reticulum stress in hypertrophic and failing heart after aortic constriction: possible contribution of endoplasmic reticulum stress to cardiac myocyte apoptosis. *Circulation* 110: 705–712, 2004.
36. **Paolisso G, Tagliamonte MR, Rizzo MR, Gambardella A, Gualdiero P, Lama D, Varricchio G, Gentile S, Varricchio M.** Prognostic importance of insulin-mediated glucose uptake in aged patients with congestive heart failure secondary to mitral and/or aortic valve disease. *Am J Cardiol* 83: 1338–1344, 1999.
37. **Redfield MM, Jacobsen SJ, Burnett JC Jr, Mahoney DW, Bailey KR, Rodeheffer RJ.** Burden of systolic and diastolic ventricular dysfunction in the community: appreciating the scope of the heart failure epidemic. *JAMA* 289: 194–202, 2003.
38. **Rijzewijk LJ, van der Meer RW, Lamb HJ, de Jong HW, Lubberink M, Romijn JA, Bax JJ, de Roos A, Twisk JW, Heine RJ, Lammertsma AA, Smit JW, Diamant M.** Altered myocardial substrate metabolism and decreased diastolic function in nonischemic human diabetic cardiomyopathy: studies with cardiac positron emission tomography and magnetic resonance imaging. *J Am Coll Cardiol* 54: 1524–1532, 2009.
39. **Roy S, Khanna V, Mittra S, Dhar A, Singh S, Mahajan DC, Priyadarsiny P, Davis JA, Sattigeri J, Saini KS, Bansal VS.** Combination of dipeptidylpeptidase IV inhibitor and low dose thiazolidinedione: preclinical efficacy and safety in *db/db* mice. *Life Sci* 81: 72–79, 2007.
40. **Sanada S, Kitakaze M, Papst PJ, Asanuma H, Node K, Takashima S, Asakura M, Ogita H, Liao Y, Sakata Y, Ogai A, Fukushima T, Yamada J, Shinozaki Y, Kuzuya T, Mori H, Terada N, Hori M.** Cardioprotective effect afforded by transient exposure to phosphodiesterase III inhibitors: the role of protein kinase A and p38 mitogen-activated protein kinase. *Circulation* 104: 705–710, 2001.
41. **Sasaki H, Asanuma H, Fujita M, Takahama H, Wakeno M, Ito S, Ogai A, Asakura M, Kim J, Minamino T, Takashima S, Sanada S, Sugimachi M, Komamura K, Mochizuki N, Kitakaze M.** Metformin prevents progression of heart failure in dogs: role of AMP-activated protein kinase. *Circulation* 119: 2568–2577, 2009.
42. **Sauve M, Ban K, Momen MA, Zhou YQ, Henkelman RM, Husain M, Drucker DJ.** Genetic deletion or pharmacological inhibition of dipeptidyl peptidase-4 improves cardiovascular outcomes after myocardial infarction in mice. *Diabetes* 59: 1063–1073, 2010.
43. **Savage DB, Petersen KF, Shulman GI.** Mechanisms of insulin resistance in humans and possible links with inflammation. *Hypertension* 45: 828–833, 2005.
44. **Schweizer A, Dejager S, Foley JE, Couturier A, Ligueros-Saylan M, Kothny W.** Assessing the cardio-cerebrovascular safety of vildagliptin: meta-analysis of adjudicated events from a large Phase III type 2 diabetes population. *Diabetes Obesity Metab* 12: 485–494, 2010.
45. **Shigeta T, Aoyama M, Bando YK, Monji A, Mitsui T, Takatsu M, Cheng XW, Okumura T, Hirashiki A, Nagata K, Murohara T.** Dipeptidyl peptidase-4 modulates left ventricular dysfunction in chronic heart failure via angiogenesis-dependent and -independent actions. *Circulation* 126: 1838–1851, 2012.
46. **Shimizu I, Minamino T, Toko H, Okada S, Ikeda H, Yasuda N, Tateno K, Moriya J, Yokoyama M, Nojima A, Koh GY, Akazawa H, Shiojima I, Kahn CR, Abel ED, Komuro I.** Excessive cardiac insulin signaling exacerbates systolic dysfunction induced by pressure overload in rodents. *J Clin Invest* 120: 1506–1514, 2010.
47. **Shioda T, Kato H, Ohnishi Y, Tashiro K, Ikegawa M, Nakayama EE, Hu H, Kato A, Sakai Y, Liu H, Honjo T, Nomoto A, Iwamoto A, Morimoto C, Nagai Y.** Anti-HIV-1 and chemotactic activities of human stromal cell-derived factor 1alpha (SDF-1alpha) and SDF-1beta are abolished by CD26/dipeptidyl peptidase IV-mediated cleavage. *Proc Natl Acad Sci USA* 95: 6331–6336, 1998.
48. **Sokos GG, Nikolaidis LA, Mankad S, Elahi D, Shannon RP.** Glucagon-like peptide-1 infusion improves left ventricular ejection fraction and functional status in patients with chronic heart failure. *J Card Fail* 12: 694–699, 2006.
49. **Stolen KQ, Kemppainen J, Kalliokoski KK, Luotolahti M, Viljanen T, Nuutila P, Knuuti J.** Exercise training improves insulin-stimulated myocardial glucose uptake in patients with dilated cardiomyopathy. *J Nucl Cardiol* 10: 447–455, 2003.
50. **Suskin N, McKelvie RS, Burns RJ, Latini R, Pericak D, Probstfield J, Rouleau JL, Sigouin C, Solymoss CB, Tsuyuki R, White M, Yusuf S.** Glucose and insulin abnormalities relate to functional capacity in patients with congestive heart failure. *Eur Heart J* 21: 1368–1375, 2000.
51. **Swan JW, Anker SD, Walton C, Godsland IF, Clark AL, Leyva F, Stevenson JC, Coats AJ.** Insulin resistance in chronic heart failure: relation to severity and etiology of heart failure. *J Am Coll Cardiol* 30: 527–532, 1997.
52. **Szeto IM, Aziz A, Das PJ, Taha AY, Okubo N, Reza-Lopez S, Giacca A, Anderson GH.** High multivitamin intake by Wistar rats during pregnancy results in increased food intake and components of the metabolic syndrome in male offspring. *Am J Physiol Regul Integr Comp Physiol* 295: R575–R582, 2008.
53. **Thrainsdottir IS, Aspelund T, Thorgeirsson G, Gudnason V, Hardarson T, Malmberg K, Sigurdsson G, Ryden L.** The association between glucose abnormalities and heart failure in the population-based Reykjavik study. *Diabetes Care* 28: 612–616, 2005.
54. **Toye AA, Lippiat JD, Proks P, Shimomura K, Bentley L, Hugill A, Mijat V, Goldsworthy M, Moir L, Haynes A, Quarterman J, Freeman HC, Ashcroft FM, Cox RD.** A genetic and physiological study of impaired glucose homeostasis control in C57BL/6J mice. *Diabetologia* 48: 675–686, 2005.
55. **Trevaskis JL, Griffin PS, Wittmer C, Neuschwander-Tetri BA, Brunt EM, Dolman CS, Erickson MR, Napora J, Parkes DG, Roth JD.** Glucagon-like peptide-1 receptor agonism improves metabolic, biochemical, and histopathological indices of nonalcoholic steatohepatitis in mice. *Am J Physiol Gastrointest Liver Physiol* 302: G762–G772, 2012.
56. **Vasan RS, Larson MG, Benjamin EJ, Evans JC, Reiss CK, Levy D.** Congestive heart failure in subjects with normal versus reduced left ventricular ejection fraction: prevalence and mortality in a population-based cohort. *J Am Coll Cardiol* 33: 1948–1955, 1999.
57. **Wei Y, Mojsov S.** Tissue-specific expression of the human receptor for glucagon-like peptide-I: brain, heart and pancreatic forms have the same deduced amino acid sequences. *FEBS Lett* 358: 219–224, 1995.
58. **Winzell MS, Ahren B.** The high-fat diet-fed mouse: a model for studying mechanisms and treatment of impaired glucose tolerance and type 2 diabetes. *Diabetes* 53, *Suppl* 3: S215–S219, 2004.
59. **Ye Y, Keyes KT, Zhang C, Perez-Polo JR, Lin Y, Birnbaum Y.** The myocardial infarct size-limiting effect of sitagliptin is PKA-dependent, whereas the protective effect of pioglitazone is partially dependent on PKA. *Am J Physiol Heart Circ Physiol* 298: H1454–H1465, 2010.
60. **Yin M, Sillje HH, Meissner M, van Gilst WH, de Boer RA.** Early and late effects of the DPP-4 inhibitor vildagliptin in a rat model of post-myocardial infarction heart failure. *Cardiovasc Diabetol* 10: 85, 2011.